European Journal of Medicinal Chemistry 315 (2026) 118882

Contents lists available at ScienceDirect

European Journal of Medicinal Chemistry

journal homepage: www.elsevier.com/locate/ejmech

Research paper

Copper(II) complexes of indolo[2,3-*c*]quinoline-derived Schiff bases: Insight into the mechanism of their antiproliferative activity

Felix Bacher [a,*], Christian Madejski [a], Irina Kuznetcova [a], Orsolya Dömötör [b], Béla Gyurcsik [b], Zeyad H. Nafaee [b,c], Nóra Igaz [d], Csenge Bocz [d], Bálint Péntek [d], Mónika Kiricsi [d], Petra Raptova [e], Alexandru-Constantin Stoica [f], Michaela Hejl [a], Michael A. Jakupec [a], Samah Mutasim Alfadul [g], Maria V. Babak [g], Peter Rapta [h], Jóhannes Reynisson [i], Lenka Sindlerova [e], Éva A. Enyedy [b,**], Ernest Hamel [j], Vladimir B. Arion [a,f,***]

[a] *Institute of Inorganic Chemistry, Faculty of Chemistry, University of Vienna, Währinger Strasse 42, Vienna, A-1090, Austria*
[b] *Department of Molecular and Analytical Chemistry, Interdisciplinary Excellence Centre, University of Szeged, Dóm tér 7-8, Szeged, H-6720, Hungary*
[c] *College of Pharmacy, University of Babylon, Hillah, 51001, Iraq*
[d] *Department of Biochemistry and Molecular Biology, University of Szeged, Közép Fasor 52, Szeged, H-6726, Hungary*
[e] *Institute of Biophysics, Academy of Sciences of the Czech Republic, v.v.i., Department of Biophysics of Immune System, Kralovopolska 135, Brno, CZ-61200, Czech Republic*
[f] *Department of Inorganic Polymers, "Petru Poni" Institute of Macromolecular Chemistry, Aleea Gr. Ghica Voda 41 A, Iasi, 700487, Romania*
[g] *Drug Discovery Lab, Department of Chemistry, City University of Hong Kong, 83 Tat Chee Avenue, 999077, Hong Kong Special Administrative Region*
[h] *Institute of Physical Chemistry and Chemical Physics, Faculty of Chemical and Food Technology, Slovak University of Technology in Bratislava, Radlinského 9, Bratislava, SK-81237, Slovakia*
[i] *School of Allied Health Professions and Pharmacy, Keele University, Hornbeam Building, Staffordshire, ST5 5BG, United Kingdom*
[j] *Molecular Pharmacology Branch, Developmental Therapeutics Program, Division of Cancer Treatment and Diagnosis, National Cancer Institute, Frederick National Laboratory for Cancer Research, National Institutes of Health, Frederick, MD, 21702, United States*

A B S T R A C T

Indoloquinolines are potent anticancer agents, but their poor aqueous solubility prevents clinical development. Indoloquinoline-based metal complexes offer an opportunity to circumvent this drawback. A series of new indolo[2,3-*c*]quinoline derivatives **HL^{1}**–**HL^{8}** and their copper(II) complexes were synthesized, comprehensively characterized and tested for antiproliferative activity against MDA-MB-231, MCF-7, MCF-7 KCR, A549 and DU-145 cancer cells and compared to known isomeric indolo[3,2-*c*]quinolines (**HL^{11}**–**HL^{14}** and **11**–**14**). The Cu(II) complexes were generally as active, or slightly more so, than the proligands. Lead compounds **HL^{8}** and **8** showed superior anticancer activity compared to isomers **HL^{14}** and **14**, respectively. Complex **8** was superior to **HL^{8}** in ROS generation in A549 cells, induced mitochondrial dysfunction as evidenced by JC-1 staining, induced lactate dehydrogenase release in medium, inhibited DNA synthesis and triggered apoptosis. DNA-binding studies, supported by molecular docking calculations, showed strong affinity of the compounds for double stranded DNA, to which they bind by intercalation.

1. Introduction

Indoloquinolines are plant alkaloids occurring in the West African shrub *Cryptolepis sanguinolenta*. These compounds exhibit antimalarial and anticancer activity [1–3]. In terms of molecular structure of the main scaffold, these fused four-ring heterocycles can be divided into 6*H*-indolo[2,3-*b*]quinoline, 7*H*-indolo[2,3-*c*]quinoline, 10*H*-indolo[3,2-*b*]quinoline and 11*H*-indolo[3,2-*c*]quinoline isomers (see Chart 1) [4–6]. It is assumed that the anticancer activity of indoloquinolines is due to their ability to intercalate into DNA, resulting in the inhibition of the enzyme topoisomerase II, thus preventing cell division and ultimately leading to apoptosis [7–9].

One prominent example is 5,11-dimethyl-5*H*-indolo[2,3-*b*]quinoline (DiMIQ), which showed promising anticancer activity *in vivo* against mice bearing P388 or L1210 leukemia [8–10]. However, this compound proved to be poorly water soluble, limiting its clinical value. A liposomal

* Corresponding author.
** Corresponding author.
*** Corresponding author. Institute of Inorganic Chemistry, Faculty of Chemistry, University of Vienna, Währinger Strasse 42, A-1090, Vienna, Austria.
E-mail addresses: felix.bacher@univie.ac.at (F. Bacher), enyedy@chem.u-szeged.hu (É.A. Enyedy), vladimir.arion@univie.ac.at (V.B. Arion).

https://doi.org/10.1016/j.ejmech.2026.118882
Received 7 March 2026; Received in revised form 10 April 2026; Accepted 19 April 2026
Available online 21 April 2026

formulation of DiMIQ was found to overcome this drawback [11]. This example demonstrates a general problem, when it comes to the development of novel indoloquinolines as potential drugs. Alternative efforts to enhance aqueous solubility and thereby the pharmacological profile of indoloquinolines led to the attachment of an amino acid, peptide or guanidine moiety at the indoloquinoline backbone [12–15]. The aqueous solubility of indoloquinolines can also be improved by complex formation with transition metals. Since the indoloquinoline backbone itself is not able to chelate metal ions, it was chemically modified to install binding sites for a variety of metals, e.g., copper(II), zinc(II), ruthenium(II), or osmium(II) (Chart S1, Supplementary Material) [16–23]. Some copper(II) complexes based on the indolo[3,2-*c*]quinoline scaffold modified at the $N^5{=}C^6$ bond (Chart 1) were highly cytotoxic against A549, SW480 and CH1 cancer cells, with IC_{50} values in the low micromolar to nanomolar range [16]. Similar structural modifications could be performed only with the indolo[2,3-*c*]quinoline scaffold from those shown in Chart 1. Even though copper(II) complexes as anticancer drugs are still unavailable on the market, their clinical application has advanced significantly [24–28]. A series of mixed-ligand copper(II) complexes, known as Cassiopeínas, and copper(II) bis(thiohydrazide) amide complex called Elesclomol (ELC) reached clinical trials showing potential for the treatment of colorectal cancer and acute myeloid leukemia [29–31]. In addition, some copper(II) thiosemicarbazonates have reached clinical trials and confirmed their efficacy for diagnostic and theranostic applications [27,32,33].

The angular indolo[2,3-*c*]quinoline backbone is also the only molecular structure of the four indoloquinoline isomers that was not yet found in nature, and, as a result, less explored with regard to its biological activity [34,35]. Recent studies revealed potent anticancer activity of several indolo[2,3-*c*]quinoline derivatives and their Cu(II) complexes (see also Chart S1 in the Supplementary Material) [36–38], offering an opportunity for disclosure of novel bioactivity with unexpected advantages. Therefore, we decided (i) to apply the procedures developed previously for the indolo[3,2-*c*]quinoline scaffold and create a metal binding site at the $N^5{=}C^6$ bond of indolo[2,3-*c*]quinoline with the potential to act as a tridentate ligand, (ii) to extend the number of such proligands by modifying the substitution pattern at the core scaffold, (iii) to synthesize the Cu(II) complexes with the small library of potentially tridentate ligands, (iv) to perform antiproliferative activity assays both in cancer cell lines and in non-cancer cells, (v) to elucidate structure-activity relationships by comparison with isomeric compounds reported previously, and (vi) to get initial insight into their mechanism of antiproliferative action.

Herein we report on the synthesis and full characterization of eight novel indolo[2,3-*c*]quinoline based ligands and their copper(II) complexes (Scheme 1) by ESI mass spectrometry, ^{1}H and ^{13}C NMR spectroscopy (**HL^1**–**HL^8**) and single crystal X-ray diffraction (SC-XRD) (**HL^2**, **1**, **2**, **9** and **10**). Solution speciation studies were performed and antiproliferative activity in both cancer cell lines (MDA-MB-231, MCF-7, MCF-7 KCR, A549 and DU-145) and normal cells (MRC-5) was determined. New structure-antiproliferative activity relationships were obtained by modifying the indoloquinoline backbone and by installation of a bromo substituent at position 8, 9 or 10 of the indolo[2,3-*c*]quinoline backbone.

In addition, for comparison, we prepared four proligands (**HL^{11}**–**HL^{14}**) and four Cu(II) complexes (**11**–**14**) based on isomeric indolo[3,2-*c*]quinolines (see Chart 2) reported previously [16] and tested them for antiproliferative activity. We used 2-formylpyridine and 2-acetylpyridine to create two sets of Schiff bases. Reaction of these potentially tridentate proligands with copper(II) chloride afforded distorted square-pyramidal complexes of the type **[Cu(HL^n)Cl$_2$]**, where n = 1–8 (**1**–**8**). Moreover, the ligands can be easily deprotonated under basic conditions to give distorted square-planar complexes of the type **[Cu(L^n)Cl]**, of which we synthesized two (**9**, **10**), also for comparative studies.

Finally, the interaction of lead drug candidates with biological reductants, DNA in both cell-free medium and in the cells was investigated, along with their ability to produce oxidative stress, mitochondrial dysfunction and induce apoptosis.

2. Results and discussion

2.1. Synthesis and characterization of the proligands HL^1–HL^8

The synthesis of the indolo[2,3-*c*]quinoline backbone and proligands **HL^1**—**HL^8** was performed starting from the corresponding aminobenzophenones **3a–3d** by adapting protocols reported previously [16,39], as shown in Scheme 1. Since 2-bromo- and 3-bromo-aminobenzophenones (**3b** and **3c**) are not commercially available, they were synthesized in two steps by known procedures [40,41]. Aminobenzophenones **3a–3d** were reacted with chloroacetyl chloride to give acetylated compounds **4a–4d** in 68–95% yields. In the next step, the chloro-substituent was replaced by an azido functional group to give **5a–5d** in 78–89% yields. Base catalyzed cyclization of **5a–5d** led to azido-phenylquinolinones **6a–6c** in 83–86% yields. The presence of a bromo-substituent in positions 3 and 4 slowed down the reaction rate, and, therefore, the reaction time was prolonged from 1 to 5–6 h for a complete conversion. Compound **5b**, with a bromo-substituent in position 2, did not undergo the desired cyclization. Attempts to extend the reaction time, increase temperature or the amount of base led to undesired side reactions. Most likely the bulkier bromo-substituent in the *ortho* position prevented nucleophilic attack at the carbonyl carbon atom. Thus, the desired 11-bromo-5,7-dihydro-6*H*-indolo[2,3-*c*]quinolin-6-one was not accessible by this synthetic pathway, but the synthesis of precursors is described in the Supplementary Material. The obtained azido-phenylquinolinones **6a–6c** were not stable at high temperature and were converted into the desired indolo[2,3-*c*]quinolinones in a second cyclization step, accompanied by the release of nitrogen, simply by refluxing them in toluene to afford indoloquinolines **7a**, **7c**, as well as **7b** and **7d** (as an isomeric mixture), in excellent yields (96–99%). 3-Azido-4-(3-bromophenyl)quinolin-2(1*H*)-one **6b** gave rise to two isomers (8- and 10-bromo-5,7-dihydro-(6*H*)-indolo[2,3-*c*]quinolin-6-one, **7b** and **7d**) in a ratio of ca. 0.7 : 1. This is due to the rotation of the bromo substituted phenyl ring in **6b**. The isomers proved to be difficult to separate, due to their low solubility in solvents commonly used in column chromatography. However, separation was possible after the next step in which the indolo[2,3-*c*]quinolinones **7a–7d** were reacted with phosphorus oxychloride to give 6-chloro-substituded indolo[2,3-*c*]quinolines **8a–8d** in good yields. Then 6-chloro derivatives **8a–8d** were reacted with hydrazine monohydrate to give 6-hydrazin-yl derivatives

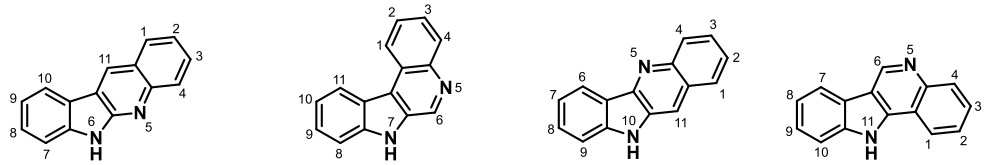

Chart 1. Indoloquinoline isomers with atom numbering schemes.

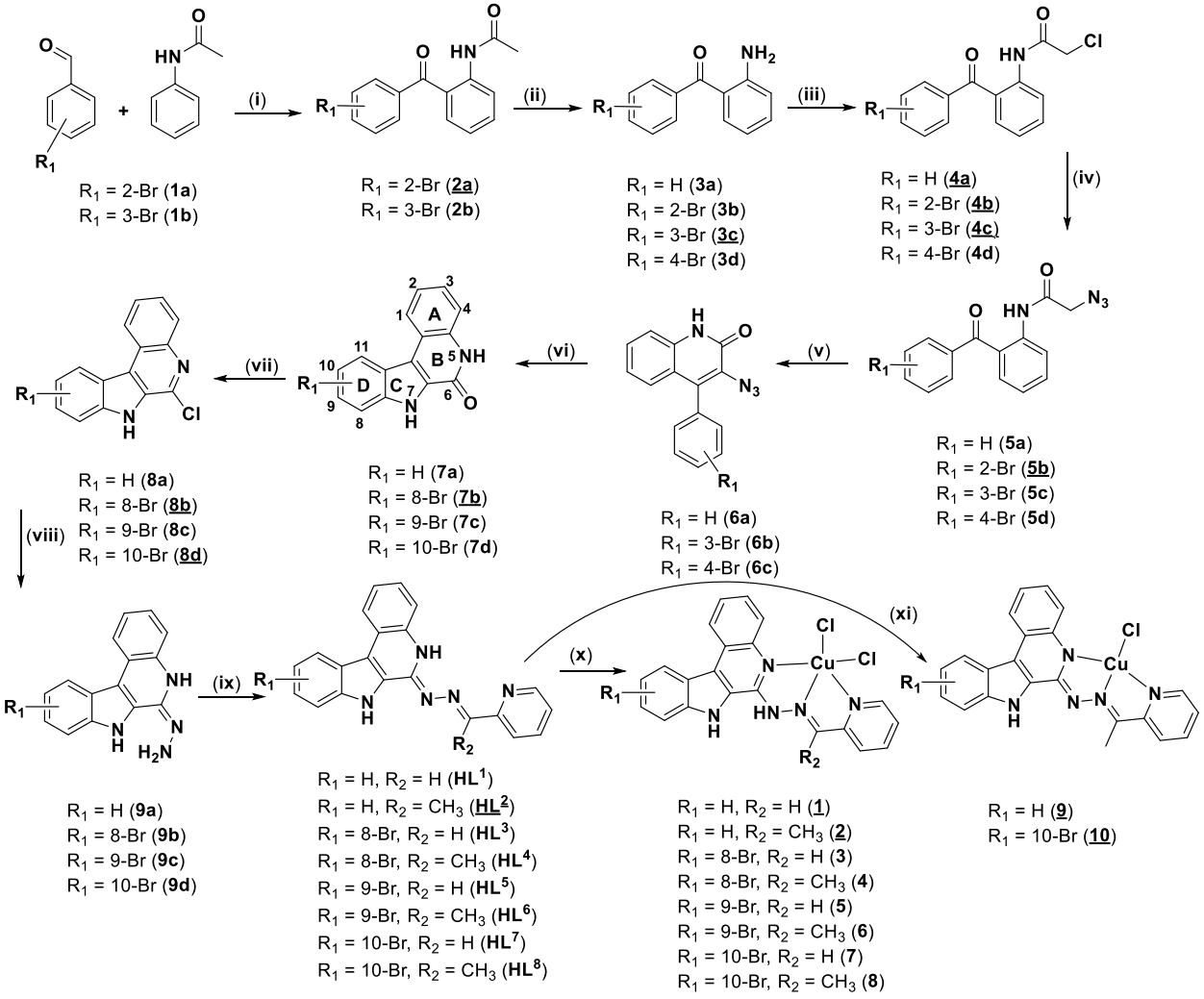

Scheme 1. Underlined numbers indicate compounds studied by X-ray crystallography. Reagents and conditions: (i) water, $Pd(OAc)_2$, sodium dodecyl sulfate, acetanilide, trifluoroacetic acid, *tert*-butyl hydroperoxide and 2-bromo-benzaldehyde (**1a**) or 3-bromo-benzaldehyde (**1b**), room temperature, 25 h; (ii) acetone, hydrochloric acid, 70 °C, 3–5 h; (iii) chloroacetyl chloride, chloroform, reflux, 30 min; (iv) sodium azide, dimethylformamide, water, 60 °C, 30 min; (v) ethanol, aq. sodium hydroxide, 60 °C, 1–6 h; (vi) toluene, reflux, 2 h; (vii) phosphorus oxychloride, reflux, overnight; (viii) hydrazine hydrate, reflux, overnight; (ix) ethanol, 2-formyl- or 2-acetylpyridine, 85 °C, overnight; (x) isopropanol, methanol or dimethylformamide, copper(II) chloride dihydrate, reflux, 15 min; (xi) isopropanol, methanol or dimethylformamide, triethylamine, copper(II) chloride dihydrate, reflux or 80 °C, 15 min.

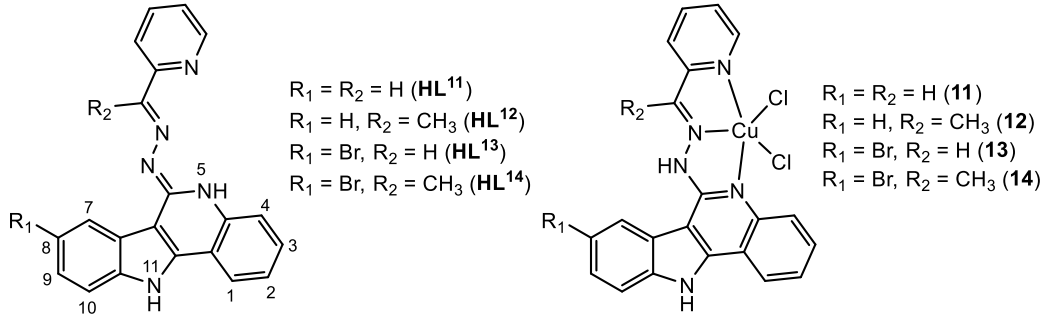

Chart 2. Indolo[3,2-*c*]quinoline based ligands and complexes $\mathbf{HL^{11}}$–$\mathbf{HL^{14}}$ and **11**–**14** [16].

9a–9d in excellent yields (95–99%). ^{1}H NMR spectra of intermediates **2a**−**9d** are shown in Fig. S1−S27, Supplementary Material. Finally, the hydrazin-yl derivatives **9a–9d** were reacted with 2-formyl- or 2-acetyl-pyridine in a Schiff base reaction to give proligands $\mathbf{HL^1}$−$\mathbf{HL^8}$ in 86−97% yields. ^{1}H and ^{13}C-DEPT$_q$ NMR spectra of $\mathbf{HL^1}$−$\mathbf{HL^8}$ are shown in Fig. S28−S43. We note, that these ligands exist as mixtures of tautomers both in solution and in solid state, as also was confirmed by ^{1}H NMR spectroscopy and X-ray crystallography (for $\mathbf{HL^2}$). Two sets of signals were observed in the NMR spectra of free ligands $\mathbf{HL^1}$−$\mathbf{HL^8}$, but the signals were only assigned for the predominant species, containing an exocyclic C=N bond. Low signal intensity along with signal overlapping made assignment of resonances for the minor species

impossible. The ratios between major and minor species in DMSO-d_6 were approximately 1 : 0.25, 1 : 0.10, 1 : 0.25, 1 : 0.10, 1 : 0.15 and 1 : 0.05 for **HL^1**, **HL^2**, **HL^5**, **HL^6**, **HL^7** and **HL^8**, respectively, and 1 : 0.5 and 1 : 1 for **HL^3** and **HL^4**, respectively, in DMF-d_7. The predominant species of **HL^2** crystallized as yellow needles from methanol and showed the presence of an exocyclic C=N bond, where N^5 is protonated (see Scheme 1 and Fig. 1). The minor species crystallized from the same solvent as colorless blocks and contained an endocyclic C=N bond. This species resulted from migration of the proton from N^5 to N^{12} (see Fig. 1b). Positive ion high resolution ESI mass spectra of **HL^1**–**HL^8** showed strong peaks with *m/z* 338.1395, 352.1556, 418.0480, 432.0645, 418.0484, 432.0642, 418.0475 and 432.0639, respectively, attributed to $[M + H^+]^+$ (Fig. S44–S51). The experimental isotopic patterns fitted well the theoretical isotopic distributions. Clearly seen peaks with *m/z* 675.2717, 861.1212, 833.0905, 861.1223 and 861.1225 for **HL^1**, **HL^4**, **HL^5**, **HL^6** and **HL^8** were assigned to ions $[2M + H^+]^+$, indicating formation of dimeric associates in solution under conditions of ESI-MS measurements. The IR spectra of **HL^1**–**HL^8** are shown in Fig. S52–S59 in Supplementary Material). The stretching vibrations ν_{NH} are seen between 3460 and 3310 cm^{-1}, while Schiff base $\nu_{C=N}$ vibrations between 1640 and 1610 cm^{-1}.

Synthesis of Cu(II) complexes. Free ligands **HL^1**–**HL^8** were treated with $CuCl_2{\cdot}2H_2O$ in isopropanol, methanol or DMF to give complexes **1–8** in 69–98% yields. The use of different solvents was necessary due to solubility issues. Additionally, **HL^2** and **HL^8** were treated with $CuCl_2{\cdot}2H_2O$ in methanol in the presence of 2 equiv of triethylamine to afford four-coordinate complexes **9** and **10** in 95 and 97% yield, respectively. It is worth noting, that apart from the separation of **8b** and **8d**, no chromatographic separation was required to obtain the reported compounds in analytically pure form. The synthesis of both free ligands and Cu(II) complexes can be easily upscaled when required. Positive ion high-resolution ESI mass spectra of **1–8** (Fig. S60–S67) showed strong peaks with *m/z* 399.0542, 413.0693, 478.9623, 492.9777, 478.9626, 492.9775, 478.9614 and 492.9776, respectively, attributed to $[M–HCl–Cl^-]^+$, while those of **9** and **10** (Figs. S68 and S69) strong signals with *m/z* 413.0699 and 492.9776 assigned to ions $[M–Cl^-]^+$. Specific peaks with *m/z* 835.0763 and 1269.0985 (for **1**), 863.1064 and 1311.1447 (for **2**) could be attributed to dimeric and trimeric associates, namely $[(Cu^{II}L^1)_2Cl^-]^+$ and $[(Cu^{II}L^1)_3(Cl^-)_2]^+$ (for **1**) and to $[(Cu^{II}L^2)_2Cl^-]^+$ and $[(Cu^{II}L^2)_3(Cl^-)_2]^+$ (for **2**). The experimental isotopic patterns matched well with the theoretical isotopic distributions for the ions observed. The IR spectra of **1–10** are shown in Fig. S70–S79. The stretching vibrations ν_{NH} are seen between 3444 and 3042 cm^{-1}, while Schiff base $\nu_{C=N}$ at 1648–1600 cm^{-1}.

2.2. X-ray crystallography

The results of SC-XRD studies of intermediate species **2a**, **3c**, **4a**, **4b**, **4c**, **5b**, **7b** and **8b**+**8d** are presented in Fig. S80, while those for proligand **HL^2** in two different configurations, **[CuCl$_2$(HL^2)]·DMF** and **[CuCl(L^2)]** are displayed in Fig. 1. Fig. 2 shows the structures of the complexes **1** and **10**. Pertinent metric parameters are quoted in the captions to the figures. Details of data collection and refinement are presented in Tables S1-S3.

Complexes **1** and **2** are five-coordinate. The coordination geometry in both compounds can be described as distorted square-pyramidal (the τ_5-parameter is 0.34 and 0.35, respectively) [42]. This parameter calculated by equation $\tau_5 = \beta-\alpha/60°$, where α and β (β > α) are the two largest valence angles around Cu(II), is 0 for square-pyramidal complexes and 1 for trigonal-bipyramidal coordination geometry. The ligand is neutral tridentate in **1** and **2** and is bound to Cu(II) via nitrogen atoms N5, N13 and N16. The remaining two coordination sites are occupied by two chlorido co-ligands. In contrast, complex **9** is four-coordinate with distorted square-planar coordination geometry. This is in line with the τ_4-parameter calculated by equation $360 - (\alpha+\beta)/141 = 0.263$ [43] and τ'_4-parameter calculated by equation $\beta-\alpha/360-\theta + 180-\beta/180-\theta = 0.228$ [44], where θ is 109°, while α and β the two largest valence angles about Cu(II). These two parameters are 0 for ideal square-planar complexes and 1 for complexes with ideal tetrahedral coordination geometry. Interestingly, complex **10** forms a 1D polymer **[CuCl(L^8)]*n***, a fragment of which is shown in Fig. S81. The coordination geometry of copper(II) in this infinite chain is distorted square-pyramidal (the τ_5-parameter is 0.18). The ligand acts as a monoanion in both complexes **9** and **10** and coordinates to copper(II) via the same three nitrogen atoms.

Comparison of the bond lengths around Cu(II) in five-coordinate complex **2** and four-coordinate complex **9**, as expected, indicates significantly longer Cu–N bonds in **2** in accord with VSEPR theory. The ligand in **2** preserves the configuration of the metal-free ligand shown in Fig. 1a. However, its coordination through N5 is only possible after migration of the H atom at N5 to N12 as in Fig. 1c.

2.3. Solution phase studies indicate low aqueous solubility of Schiff bases, which is increased upon complex formation with Cu(II), and HL and $[Cu(L)]^+$ as predominant species at pH 7.4

First, the thermodynamic solubility (*S*) of the compounds in water was determined. The obtained data showed that the aqueous solubility of the ligands **HL^2**–**HL^8** and **HL^{11}**–**HL^{14}**, but **HL^1** (1.3 μM), was less than 1 μM. The thermodynamic aqueous solubility data for Cu(II) complexes **1**–**8** and **11**–**14** are summarized in Table 1. The collected *S* values clearly indicate an increase of aqueous solubility of the proligands upon complex formation with Cu(II) by factors ≥3 to ≥645 depending on substituents (R_1 and R_2 on indoloquinoline scaffold in Scheme 1). Of note is also the stronger lipophilic character of the metal-free ligands when compared to complexes **1**–**8** and **11**–**14**. The solubility of complexes **11**–**14** is generally higher than that of complexes **1**–**10**. Bromination of the Schiff bases in positions 8, 9 or 10 on indole moiety strongly reduces the aqueous solubility of the corresponding complexes (**3**–**8** and **13**, **14**). Remarkably, the apparent aqueous solubility of **8** improved when human serum albumin (HSA) was present in solution, which is a beneficial feature for both cell culture and *in vivo* applications. More detail about binding of **8** to HSA is given in Supplementary Material (see Fig. S82).

Aqueous stability of the metal-free ligands **HL^1**–**HL^8** and their complexes (**1**–**8**) was followed by UV–vis spectrophotometry for at least 71 h in 50% (*v/v*) DMSO/aqueous HEPES buffer (pH = 7.4) at 298 K and all of the proligands and complexes **1** and **2** showed little changes (Fig. S83). Spectral changes for **6**–**8** are most probably due to partial adsorption onto the cuvette wall. The resulting spectra for **3**–**5**, and their moderate changes suggest that the indolo[2,3-*c*]quinoline-based Schiff bases remain coordinated, while Cu–Cl bonds undergo hydrolysis. This is further confirmed by monitoring the stability of complexes **2** and **8** in 50% (*v/v*) acetonitrile/water and in methanol by HR ESI(+) mass spectrometry over 24 h as shown in Fig. S84–S87. The main peaks with *m/z* 449.0465 (calcd *m/z* 449.0463) and 413.0696 (calcd *m/z* 413.0696) in the mass spectra of **2** and with *m/z* 528.9548 (calcd *m/z* 528.9548) and 492.9783 (calcd *m/z* 492.9783) in the mass spectra of **8** in 50% (*v/v*) acetonitrile/water after 24 h are attributed to $[M–Cl^-]^+$ and $[M–HCl–Cl^-]^+$, respectively. A similar picture is characteristic for spectra of **2** and **8** in methanol after 24 h (see Fig. S85 and S87).

In addition, proton dissociation processes of the selected proligands (**HL^2**, **HL^8** and **HL^{14}**) and formation constants of their Cu(II) complexes **2**, **8** and **14** were investigated, given their stronger antiproliferative activity (*vide infra*), and, the data are summarized in Table 2.

Given the limited aqueous solubility of the proligands, we performed the solution speciation studies in the presence of a less polar co-solvent, namely in a 30% (*v/v*) DMSO/H_2O mixture as in our previous studies on structurally related compounds with aza-containing 6- to 9-membered rings, which also showed low aqueous solubility [37,45,46].

The proton dissociation processes of the free ligands, as well as the formation of complexes, were followed by UV–vis titrations, since this

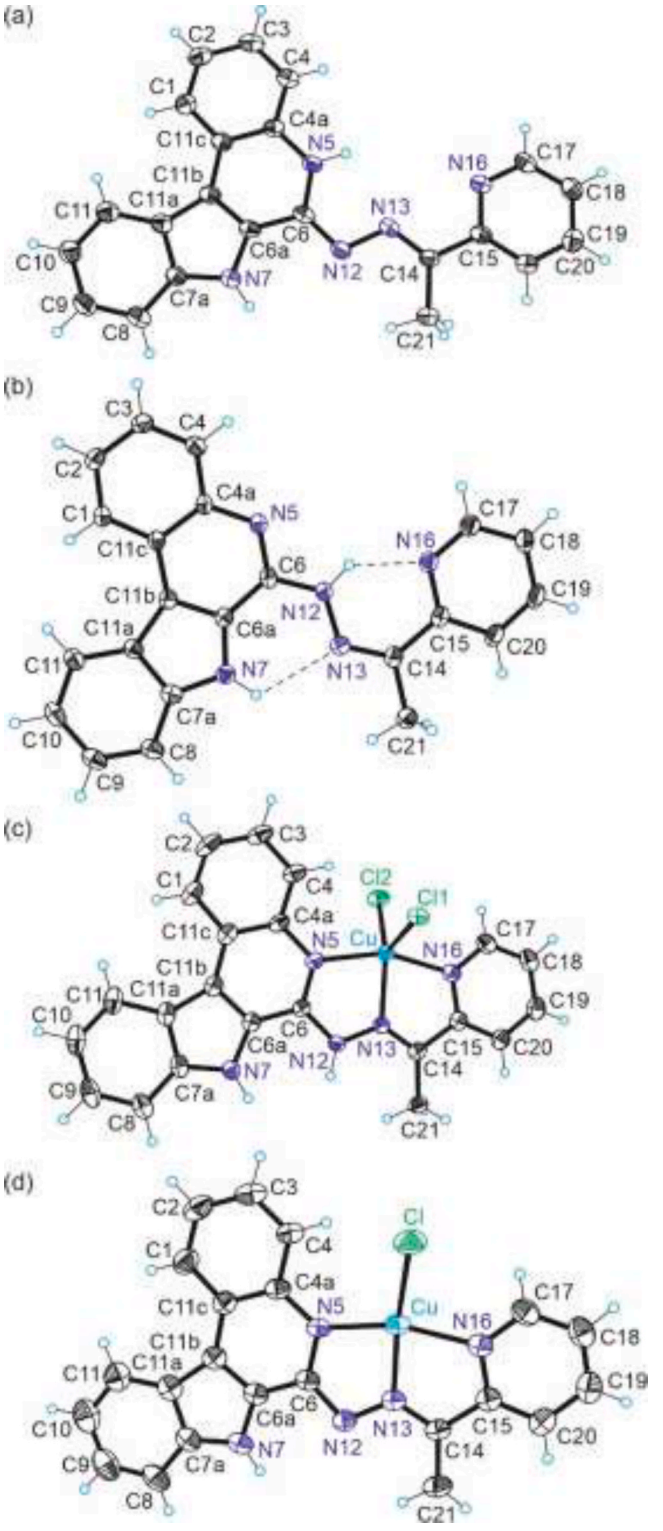

(caption on next column)

Fig. 1. ORTEP views of (a) $\mathbf{HL^2}$ with central six-membered ring with exocyclic C=N bond, (b) $\mathbf{HL^2}$ with central six-membered ring with endocyclic C=N bond, (c) $\mathbf{[CuCl_2(HL^2)]}$ (**2**) and (d) $\mathbf{[CuCl(L^2)]}$ (**9**) with thermal ellipsoids at 50% probability level. Selected bond distances (Å) and H-bonding parameters in (a): N5–C6 1.363(4), C6–N12 1.328(4); in (b): N5–C6 1.314(2), C6–N12 1.3771 (19); H-bonding parameters: N12–H···N16 [N12···N16 = 2.6075(18) Å; ∠N12HN16 = 135.0°] and N7–H···N13 [N7···N13 = 2.8373(18) Å; ∠N7HN13 = 114.9°]. Selected metric parameters in (c): Cu–N5 2.0348(15), Cu–N13 1.9907(14), Cu–N16 2.0211(15), Cu–Cl1 2.4768(5), Cu–Cl2 2.2638(5); N5–C6 1.329(2), C6–N12 1.377(2), N12–N13 1.357(2), N13–C14 1.290(2), C14–C15 1.478(2), C15–N16 1.356(2), N5–Cu–N13 79.64(6), N13–Cu–N16 78.56(6), Cl1–Cu–Cl2 112.643(17)°; in (d): Cu–N5 2.024(3), Cu–N13 1.941(3), Cu–N16 2.029(3), Cu–Cl 2.2090(10); N5–C6 1.359(4), C6–N12 1.351(4), N12–N13 1.342(4), N13–C14 1.297(4), C14–C15 1.465(5), C15–N16 1.353(4), N5–Cu–N13 79.88(11), N13–Cu–N16 79.48(11).

method requires relatively low compound concentrations; representative spectra are shown for $\mathbf{HL^{14}}$ in Fig. 3a. Similarly to the previously studied indolo[2,3-*d*]benzazepine [45,46] and indolo[2,3-*c*]quinoline [37] derivatives, the deprotonation of the free ligands was accompanied by spectral changes. In the case of $\mathbf{HL^2}$, $\mathbf{HL^8}$ and $\mathbf{HL^{14}}$, the increase of the pH to 7.4 led to precipitation of the compounds. Therefore, experimental data were collected at pH < 7 and used for the calculations. The spectral changes of $\mathbf{HL^{14}}$ indicated two processes, as isosbestic points were seen in the pH ranges 1.6 – 3.5 (411, 350, 312 nm) and 3.5 – 6.20 (428, 369 nm), thus two pK_a values were computed (Table 2, Fig. 3b). The suggested deprotonation steps are shown in Fig. 3c. The other two compounds behaved similarly. The species $H_2(\mathbf{HL})^{2+}$ formed at the strongly acidic pH via protonation at the nitrogen atoms of the two pyridine moieties. Most probably the deprotonation started at the pyridinium nitrogen of the 2-acetylpyridine moiety, and this step was accompanied by significant spectral changes, as a strong absorption band was developed at 456 nm. These changes suggest that the deprotonation led to a more extended conjugated electron system, most probably via a tautomeric rearrangement. It is assumed that the $H(\mathbf{HL})^+$ species, in which an exocyclic C=N bond is present and atom N^5 (see Chart 2) is protonated, became the major isomer.

Upon the subsequent deprotonation, the intensity of the strong band decreased, suggesting the presence of the **HL** isomer, in which the endocyclic C=N bond predominated, as the X-ray crystallographic and NMR data also showed for $\mathbf{HL^2}$ (*vide supra*). The obtained pK_a $H_2(\mathbf{HL})^{2+}$ values for $\mathbf{HL^8}$ and $\mathbf{HL^{14}}$ were slightly lower than that of $\mathbf{HL^2}$, most probably due to the electron withdrawing effect of the bromo-substituent at the indolo[2,3-*c*]quinoline backbone, while an opposite trend was seen for the pK_a of the $H(\mathbf{HL})^+$ species. Based on the pK_a values, these compounds became neutral when reaching the neutral pH contributing to their poor aqueous solubility at pH 7.4.

Despite the better aqueous solubility of the complexes, their UV−vis spectra could be recorded only at pH < 6.6 without the appearance of precipitate (see as an example the spectra for complex **14** in Fig. 4a). Formation constants (β) were computed for two kinds of complexes formed in the monitored pH range (Table 2), as was also the case for other related compounds.

In the complex $[Cu(\mathbf{HL})]^{2+}$ the neutral ligand is tridentate (Fig. 4b) with an endocyclic C=N bond as the X-ray crystallographic results showed for **2** (Fig. 3c). Meanwhile, $[Cu(\mathbf{L})]^+$ was formed due to the metal-induced deprotonation of the ligand at N^5 of the isomeric form bearing the exocyclic C=N bond (Fig. 4b) as found in the solid state structures of $\mathbf{[CuCl(L^2)]}$ (**9**) or $\mathbf{[CuCl(L^8)]}$ (**10**). The formation constant and the pK_a value of $[Cu(\mathbf{HL^2})]^{2+}$ was somewhat higher than those of the corresponding complexes of $\mathbf{HL^8}$ and $\mathbf{HL^{14}}$, but in all cases $[Cu(\mathbf{L})]^+$ is assumed to be the predominant species at pH 7.4. For comparison, the equilibrium constants for the analogous compounds of $\mathbf{HL^2}$ and **2**, namely for the indolo[2,3-*d*]benzazepine, the indolo[2,3-*e*]benzazocine and the indolo[2,3-*f*]benzazonine derivatives [37,45,46] with increased 7 to 9-membered central ring size are summarized in Table S4.

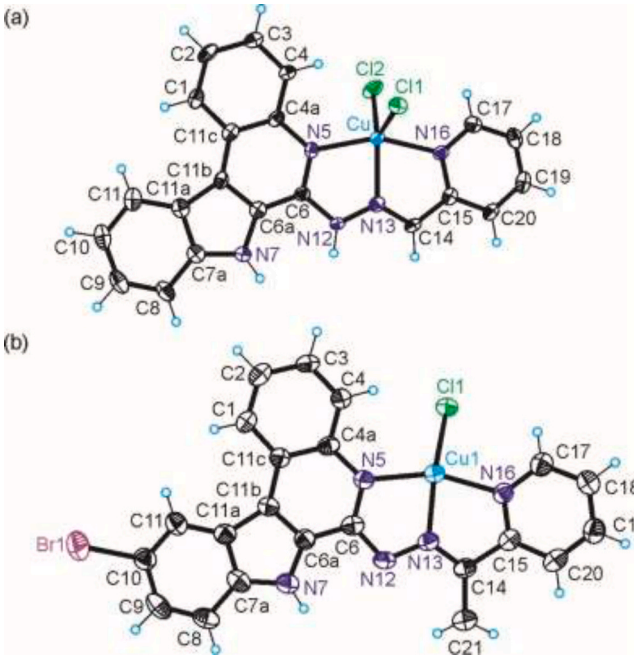

Fig. 2. ORTEP views of (a) **[CuCl$_2$(HL^1)]** (**1**) and (b) **[CuCl(L^8)]** (**10**) with thermal ellipsoids at 50% probability level. Selected bond distances (Å), bond angles (deg) and torsion angles (deg) in (a): Cu–N5 2.039(4), Cu–N13 1.999(4), Cu–N16 2.037(4), Cu–Cl1 2.4227(16), Cu–Cl2 2.2623(16); N5–C6 1.332(7), C6–N12 1.378(6), N12–N13 1.341(6), N13–C14 1.293(7), C14–C15 1.455(7), bite angles N5–Cu–N13 78.62(17) and N13–Cu–N16 77.89(18)°; in (b): Cu–N5 2.018(6), Cu–N13 1.947(7), Cu–N16 2.031(16), Cu–Cl1 2.319(2), Cu–Cl1^i 2.510(2); N5–C6 1.343(10), C6–N12 1.363(11), N12–N13 1.374(10), N13–C14 1.292(10), C14–C15 1.493(12), C15–N16 1.336(10); bite angles N5–Cu–N13 79.9(3) and N13–Cu–N16 79.0(3)°.

The collected data indicate that the indolo[2,3-*d*]benzazepine ligand formed similar or somewhat higher stability complexes with Cu(II) than the compounds reported herein, while the stability of the complexes with the indolo[2,3-*e*]benzazocine and the indolo[2,3-*f*]benzazonine derivatives was significantly lower.

Interaction of **8** with the intracellular reducing agent glutathione (GSH), produced in large amounts in cancer cells, was also studied. Reduction of the metal center accompanied by dissociation of the complex occurred in the presence of 50 equiv GSH (redox potential −0.24 V vs NHE [47]) within 1 h under anaerobic conditions (Fig. S88). Interestingly, reduced nicotinamide adenine dinucleotide (NADH), a more potent intracellular reducing agent (redox potential −0.32 V vs NHE [48]), did not interact with **8** under the same conditions, as the UV−vis spectrum of the complex remained unchanged. ROS generation triggered by **8** and its proligand **HL^8** was investigated by electron paramagnetic resonance (EPR) spin trapping technique. Both compounds induced ROS formation in the presence of H_2O_2 (Fig. S89 and S90). Addition of excess GSH prevented ROS generation by **8**, while this was not the case for ascorbate or NADH. More detail about the nature and amounts of the produced radicals can be found in the Supplementary Material [49,50]. The frozen solution experimental and simulated X-band EPR spectra of **8** in 30% (*v*/*v*) DMSO/H_2O mixture are shown in Fig. S91, while the Spin Hamiltonian parameters are quoted in the legend to figure in the Supplementary Material.

2.4. Comprehensive biological studies of selected compounds

2.4.1. Both free ligands and their Cu(II) complexes showed higher cytotoxicity than cisplatin in various cancer cells

Prior to conducting biological studies, a preliminary toxicity screening was performed using the MTT colorimetric assay. The 72 h cytotoxicity of proligands and their Cu(II) complexes within the two groups (indolo[2,3-*c*]quinoline and indolo[3,2-*c*]quinoline) was evaluated against human breast cancer cell lines (MDA-MB-231, MCF-7), as well as a non-cancerous human fibroblast cell line (MRC-5). The drug selectivity index (SI) for all compounds was calculated by comparing the IC_{50} values between the normal cell line and the cancerous cell lines. The resulting IC_{50} and SI values, with cisplatin as positive control, are presented in Table 3, and the concentration-effect curves are shown in Fig. S92. Overall, all the compounds exhibited potent cytotoxic activity, with significantly lower IC_{50} values compared to cisplatin in both cancer cell lines.

The MDA-MB-231 and MCF-7 cells showed comparable, but sometimes moderately divergent sensitivity to the compounds investigated in this work. The metal-free ligands and the corresponding metal complexes revealed a broad range of activities, with IC_{50} values ranging from low micromolar to nanomolar concentrations, depending on the substituents on four-ring scaffolds from which Schiff bases were derived and on azomethine carbon of the corresponding Schiff base and its protonation state in the Cu(II) complex (Table 3). The most potent in MDA-MB-231 and MCF-7 cancer cells are the R_1 and R_2-substituted **HL^8** and its Cu(II) complex **8**, while the least active are the unsubstituted Schiff base **HL^1** and its Cu(II) complex **1**.

2.4.1.1. Structure-antiproliferative activity relationships. Specific substituents on the proligand framework were installed, and isomerization of the main scaffold was performed, to explore the following structure-activity relationships:

(i) **Flip Effect of the Indole Moiety vs Quinoline Unit**

Comparison of the cytotoxic activity of proligands and copper(II) complexes derived from indolo[2,3-*c*]quinoline, namely **HL^1**, **HL^2**, **HL^7**, **HL^8** and **1**, **2**, **7**, **8** vs those originated from indolo[3,2-*c*]quinoline scaffold, i.e. **HL^{11}**, **HL^{12}**, **HL^{13}**, **HL^{14}** and **11**, **12**, **13**, **14**, respectively (Table 3), indicates that, overall, the 2,3-*c* systems are somewhat more cytotoxic than 3,2-*c* ones against both cancer cell lines (MDA-MB-231 and MCF-7) and non-cancer cells (MRC-5). In contrast, the indolo[3,2-*c*]quinoline-derived Schiff bases and their copper(II) complexes showed slightly superior selectivity towards cancer cell lines with selectivity indices varying from 1.6 to 5.3 vs 1.1−3.5 for MDA-MB-231 cells and 1.3−1.8 vs 0.9−1.5 (MCF-7) for proligands and from 2.6 to 3.0 vs 1.1−1.8 for MDA-MB-231 and 1.7−3.2 vs 1.1−1.6 for MCF-7 for Cu(II)

Table 2
Proton dissociation constants (pK_a) of the proligands and formation constants (logβ) of their Cu(II) complexes determined by UV−vis spectrophotometric titrations in 30% (*v*/*v*) DMSO/H_2O {T = 298 K; I = 0.10 M (KCl)}.

	HL^2	HL^8	HL^{14}
pK_{a1} H_2(**HL**)$^{2+}$	2.60 ± 0.03	2.32 ± 0.03	2.33 ± 0.03
pK_{a2} H(**HL**)$^{+}$	4.86 ± 0.03	5.06 ± 0.03	5.17 ± 0.03
logβ [Cu(**HL**)]$^{2+}$	10.07 ± 0.03	9.40 ± 0.06	9.45 ± 0.03
logβ [Cu(**L**)]$^{+}$	6.33 ± 0.06	6.08 ± 0.06	6.09 ± 0.03
pK_a [Cu(**HL**)]$^{2+}$	3.74	3.32	3.36

Table 1
Thermodynamic solubility (S/μM) of Cu(II) complexes **1**−**14** in water.

1	2	3	4	5	6	7	8	9	10	11	12	13	14
73	10	9	8	11	3	7	14	3	8	645	385	54	15

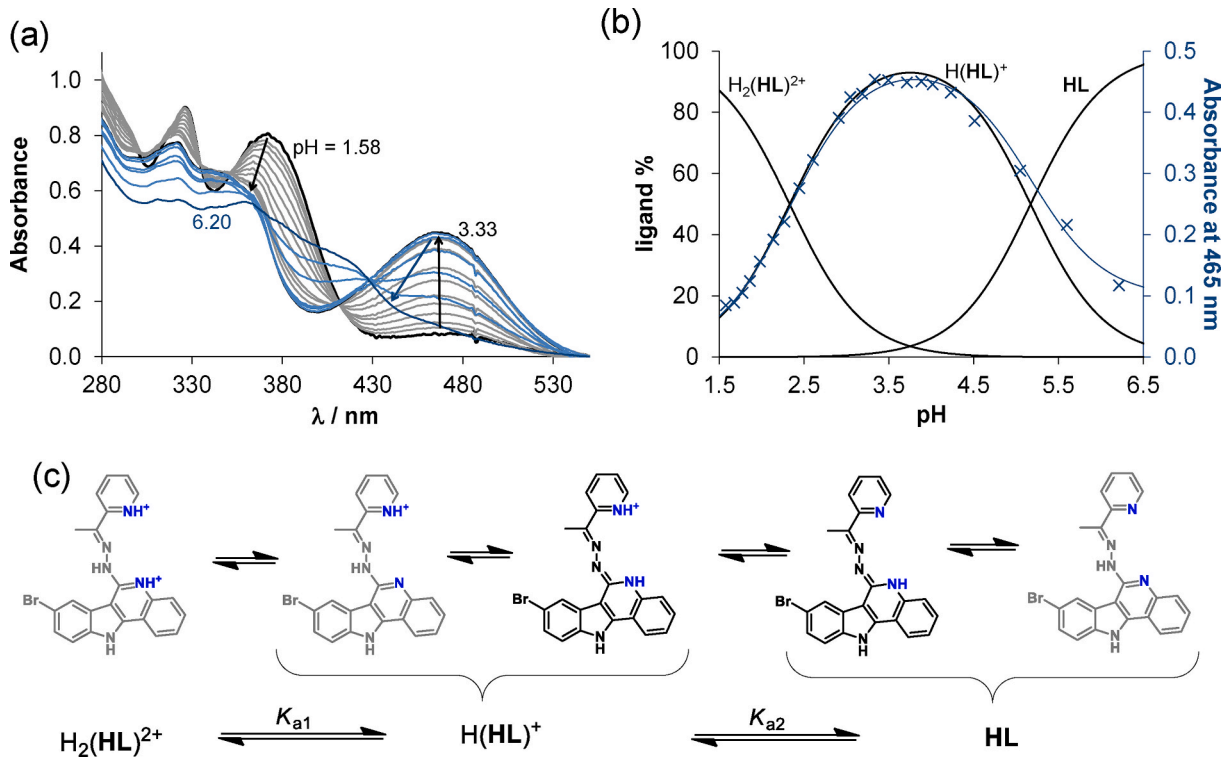

Fig. 3. (a) UV−vis spectra of **HL**[14] measured at different pH values; (b) concentration distribution curves and A_{465} measured (×) together with the fitted line; (c) proton dissociation steps of the diprotonated $H_2(\mathbf{HL})^{2+}$ with the possible tautomeric forms of the $H(\mathbf{HL})^{+}$ and **HL** species {$c_{ligand} = 10\,\mu M$, $T = 298\,K$, $l = 4\,cm$, $I = 0.10\,M$ (KCl), 30% (*v*/*v*) DMSO/H_2O}.

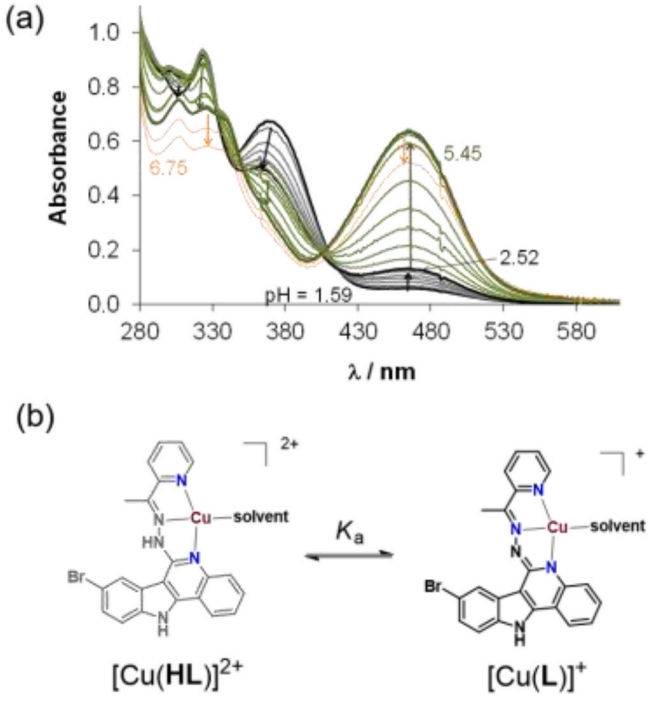

Fig. 4. (a) UV−vis spectra of **14** at different pH values; (b) Proton dissociation steps of the complex $[Cu(\mathbf{HL})]^{2+}$ along with a tautomeric rearrangement {$c_{complex} = 10\,\mu M$, $T = 298\,K$, $l = 4\,cm$, $I = 0.10\,M$ (KCl), 30% (*v*/*v*) DMSO/H_2O}.

complexes, respectively.

(ii) Effect of complex formation of indolo[2,3-*c*]quinoline- and indolo[3,2-*c*]quinoline-derived Schiff bases with Cu(II)

Generally, the Cu(II) complexes showed similar or higher antiproliferative activity than the corresponding proligands in both series of compounds against both cancer cell lines and the normal cells, but the enhancement is overall moderate. The maximal increase of cytotoxicity by factors 2.2 and 3.6 is observed for **6** when compared to **HL**[6] in both MDA-MB-231 and MCF-7 cancer cells, respectively, in the first series of compounds, and, by factors 2.5 and 3.4 for **12** when compared to **HL**[12] in MDA-MB-231 and MCF-7 cells, respectively, in the second series of compounds. The most unfavorable effect of Cu(II) complex formation on antiproliferative activity in normal MRC-5 cells was observed for complexes **3** and **8**. The increase was similar for both compounds (by factors 4.0 and 3.8), when compared to that of Schiff bases **HL**[3] and **HL**[8], respectively.

It is well documented in the literature that the antiproliferative activity of biologically active ligands is often substantially enhanced upon coordination to copper(II) [51–53], due to improved cellular uptake, altered redox activity, or enhanced DNA interaction. The solution speciation studies showed that both the **[Cu(L)]**$^{+}$ species and the neutral Schiff base (**HL**) are predominant in solution at pH 7.4. Given that Cu(II) complexes **2** and **8** are more effective intercalators than **HL**[2] and **HL**[8], and that the Schiff bases **HL**[2] and **HL**[8] are strong chelating agents, we admit that the active species of Schiff bases in cell culture medium with available pool of Cu(II) is likely **[Cu(L)]**$^{+}$. This may lead to comparable cell uptake and antiproliferative activities for complexes and metal-free ligands.

(iii) Effect of bromination in position R_1 of Schiff bases derived from indolo[2,3-*c*]quinoline and indolo[3,2-*c*]quinoline scaffolds and their Cu(II) complexes

The bromination of indolo[2,3-*c*]quinoline-derived Schiff bases was

Table 3
Cytotoxic effects of **HL[1]–HL[8]** and **HL[11]–HL[14]** as well as their Cu(II) complexes **1**–**14** and cisplatin on two human cancer cell lines and on a non-cancerous fibroblast cell line (MRC-5).

Compounds		IC_{50} (μM)[a]				
		MDA-MB-231	MCF-7	MRC-5	SI^{i}	SI^{ii}
HL[1]	2,3-c	0.93 ± 0.40	1.0 ± 0.1	1.5 ± 0.2	1.6	1.5
1	2,3-c	0.89 ± 0.19	1.0 ± 0.04	1.6 ± 0.3	1.8	1.6
HL[2]	**2,3-c**	**0.19 ± 0.07**	**0.55 ± 0.03**	**0.48 ± 0.07**	**2.5**	**0.9**
2	**2,3-c**	**0.22 ± 0.07**	**0.21 ± 0.07**	**0.26 ± 0.06**	**1.2**	**1.2**
HL[3]	2,3-c	0.58 ± 0.08	0.70 ± 0.12	0.72 ± 0.18	1.2	1.0
3	2,3-c	0.51 ± 0.08	0.9 ± 0.1	0.18 ± 0.07	0.4	0.2
HL[4]	2,3-c	0.17 ± 0.03	0.94 ± 0.16	0.45 ± 0.08	2.6	0.5
4	2,3-c	0.12 ± 0.02	0.31 ± 0.06	0.28 ± 0.11	2.3	0.9
HL[5]	2,3-c	0.59 ± 0.17	0.26 ± 0.03	0.92 ± 0.19	1.6	3.5
5	2,3-c	0.41 ± 0.15	0.28 ± 0.04	0.45 ± 0.14	1.1	1.6
HL[6]	2,3-c	0.22 ± 0.04	0.51 ± 0.14	0.65 ± 0.16	3.0	1.3
6	2,3-c	0.10 ± 0.01	0.14 ± 0.02	0.58 ± 0.18	5.8	4.1
HL[7]	2,3-c	0.38 ± 0.08	0.47 ± 0.12	0.41 ± 0.08	1.1	0.9
7	2,3-c	0.32 ± 0.05	0.32 ± 0.05	0.35 ± 0.07	1.1	1.1
HL[8]	**2,3-c**	**0.11 ± 0.01**	**0.25 ± 0.04**	**0.38 ± 0.03**	**3.5**	**1.5**
8	**2,3-c**	**0.07 ± 0.02**	**0.09 ± 0.001**	**0.10 ± 0.03**	**1.4**	**1.1**
9	2,3-c	0.12 ± 0.04	0.19 ± 0.01	0.09 ± 0.03	0.8	0.5
10	2,3-c	4.4 ± 0.4	1.3 ± 0.3	>15	-	-
HL[11]	3,2-c	1.9 ± 0.5	2.5 ± 0.6	4.29 ± 0.85	2.3	1.7
11	3,2-c	2.5 ± 0.5	1.3 ± 0.2	>3.6	-	-
HL[12]	3,2-c	0.37 ± 0.11	0.48 ± 0.11	0.6 ± 0.1	1.6	1.3
12	3,2-c	0.15 ± 0.04	0.14 ± 0.05	0.45 ± 0.08	3.0	3.2
HL[13]	3,2-c	1.7 ± 0.4	1.8 ± 0.3	>30	-	-
13	3,2-c	1.2 ± 0.4	1.6 ± 0.3	>2.3	-	-
HL[14]	**3,2-c**	**0.24 ± 0.06**	**0.7 ± 0.1**	**1.26 ± 0.44**	**5.3**	**1.8**
14	**3,2-c**	**0.17 ± 0.04**	**0.26 ± 0.05**	**0.44 ± 0.16**	**2.6**	**1.7**
Cisplatin		21.4 ± 5.2	9.6 ± 2.5	6.2 ± 1.1	0.3	0.6

[a] 50% inhibitory concentration after 72 h exposure in the MTT assay. Data are represented as mean ± SD (n ≥ 3). $SI^{i} = IC_{50}$ (MRC-5)/IC_{50} (MDA-MB-231); $SI^{ii} = IC_{50}$ (MRC-5)/IC_{50} (MCF-7).

performed in positions 8, 9 and 10 (R_1 in Scheme 1), while bromo-substitution of indolo[3,2-*c*]quinoline-derived Schiff bases in position 10. The favorable effect of bromination in positions 8, 9 and 10 on antiproliferative activity of Schiff bases is evident from comparison of the IC_{50} values of **HL[1]** with those of **HL[3]**, **HL[5]** and **HL[7]** (with R_2=H in Scheme 1), and that of **HL[2]** with those of **HL[4]**, **HL[6]** and **HL[8]** (with R_2=CH_3 in Scheme 1). The same trend is also observed for Cu(II) complexes, where the cytotoxicity of **1** in both cell lines is compared to that of **3**, **5** and **7**, and that of **2** with the activity of **4**, **6** and **8** (see data collected in Table 3). Further inspection of the data shows that bromination in position 10 of the Schiff base with R_2=CH_3 has the most favorable effect on antiproliferative activity of both Schiff base and its Cu(II) complex. A 1.7- and 2.2-fold decrease of the IC_{50} values is evident for **HL[8]** in MDA-MB-231 and MCF-7 cells, respectively, vs **HL[2]** (see Scheme 1 and Table 3), while even stronger decrease by factors 3.1 and 2.3, respectively, was found for complex **8** when compared to **2**.

The effect of bromination of **HL[11]** and **HL[12]** in position 10 is less clear-cut for the two cancer cell lines and even divergent. While **HL[13]** showed similar or slightly higher antiproliferative activity in both cancer cell lines than **HL[11]** (R_2=H in Scheme 1), **HL[14]** revealed slight enhancement of cytotoxicity against MDA-MB-231 cells and decrease of activity against MCF-7 cells when compared to **HL[12]** (R_2=CH_3 in Scheme 1). The situation is different for Cu(II) complexes. A 2-fold enhancement of antiproliferative activity for complex **13** in MDA-MB-231 cell line is observed, while slight decrease against MCF-7 cells when compared to that of **11**. Complex **14** was somewhat less cytotoxic than **12** in both cancer cell lines. Slight decrease of antiproliferative activity was observed against MDA-MB-231 cells and more evident decrease in MCF-7 cells.

(iv) **Effect of methyl substituent at the carbon atom of the azomethine group (R_2)**

A favorable and clear-cut effect of the methyl group in position R_2 (Scheme 1) for both series of the proligands **HL[1]**—**HL[8]** and **HL[11]**—**HL[14]** and their Cu(II) complexes is evident from experiments with MDA-MB-231 cells (Table 3). In particular, a 4.9- and 4.6-fold improvement of cytotoxicity is observed for **HL[2]** (R_2=CH_3) vs **HL[1]** (R_2=H) and for complex **8** vs complex **7**, respectively, while a 7.1-fold increase for both **HL[14]** (R_2=CH_3) vs **HL[13]** (R_2=H) and for **14** vs **13**. In MCF-7 cells the enhancement of antiproliferative activity is clearly seen in the indolo[3,2-*c*]quinoline series of proligands and their Cu(II) complexes, while divergent effects are characteristic for indolo[2,3-*c*]quinoline-derived Schiff bases and their Cu(II) complexes.

(v) **Effect of the original protonation state of the ligand**

Interestingly, despite assuming close antiproliferative activities for complexes **8** (with the ligand in its neutral form **HL[8]**) and **10** (with deprotonated monoanionic ligand **$(L^{8})^{-}$**) as the measurements were performed under the same conditions (pH 7.4), complex **8** exhibited significantly higher cytotoxicity when compared to **10**. This difference in activity may be attributed to variations in their kinetic solubility, resulting in decreased cellular uptake and lower activity for **10**. This is in agreement with the propensity of the latter for association and formation of a polymeric 1D chain (see Fig. S81), which might impart its uptake into the cells by the drop in solubility. Conversely, no similar difference was observed for the pair **2** and **9** as both showed better activities than their proligand **(HL^{2})**. Complex **9** with monoanionic ligand **$(L^{2})^{-}$** is only slightly more active or equally active with complex **2** with the protonated ligand **HL[2]** in MDA-MB-231 and MCF-7 cancer cells, respectively. Based on these findings, complex **8**, the most cytotoxic compound, with its free ligand (**HL[8]**) and their non-substituted counterparts (**2** and **HL[2]**), were selected for further detailed biological investigations from the indolo[2,3-*c*]quinoline series. Similarly, from the indolo[3,2-*c*]quinoline group, compounds **14** and **HL[14]**, which are isomeric analogues of **HL[8]** and **8**, were also included in this more comprehensive study.

Extended antiproliferative activity assays. In order to obtain a broader view on the efficiency and cancer-specificity of the selected ligands and complexes, the compounds were further tested on cancer cells of different origins. For this, besides the drug-sensitive breast cancer MCF-7, the multidrug resistant breast cancer cell line MCF-7 KCR, the prostate adenocarcinoma DU-145, and the lung adenocarcinoma A549 cell lines were used. As the compounds were dissolved in DMSO, vehicle control was included. The final concentration of DMSO never exceeded 1% (*v/v*). DMSO treatment did not influence viability and induced no toxic effect in any of the tested cell lines (Fig. 5).

The toxicity tests revealed that proligand **HL^8** was quite effective on lung, prostate and breast adenocarcinoma cells, as it decreased the cell viability of the A549, DU-145 and MCF-7 cancer cells in a concentration dependent manner. On the other hand, **HL^8** did not affect the MDR MCF-7 KCR cells nor the non-cancerous MRC-5 fibroblasts. Complex **8** significantly decreased the viability of A549, DU-145, MCF-7 cells generally in a concentration dependent manner, as well as of the MDR MCF-7 KCR cells. This implies that complex **8** is capable of overcoming chemotherapy resistant cancer cells and it was more efficient than its ligand. When applied at higher concentrations, **8** decreased the viability of the non-cancerous fibroblasts as well. Importantly, these results imply that the copper(II) complex **8** showed significantly higher toxicity compared to the Schiff base **HL^8** on most tested cells, except for the A549 cell line. **HL^2** decreased the cell viability of all the tested cell lines in a concentration dependent manner, the weakest effect was observed on DU-145 and MRC-5 cells. Surprisingly, this proligand alone was very effective against breast-derived adenocarcinoma cells, as it significantly diminished the viability of the multidrug resistant (MDR) MCF-7 KCR as well as drug-sensitive MCF-7 cell line.

As expected, **2** showed significantly higher toxicity than **HL^2**. At the lowest concentration used, complex **2** reduced the viability of most cell cultures below 10%. The only exception was the MCF-7 KCR cell line, where the complex reduced viability by ca. 50%. Moreover, the free ligand **HL^2** at the highest concentration (10 μM) exhibited a much stronger cytotoxic effect than **2**.

HL^{14} showed significant cytotoxicity on A549 and MCF-7 cells, but only moderate or weak activity was observed on the other tested cell lines (Fig. 5). Complex **14** decreased the viability of A549, MCF-7 and MRC-5 cells, but it was ineffective or just slightly effective for the other two cell types. A significant difference was observed between the effect

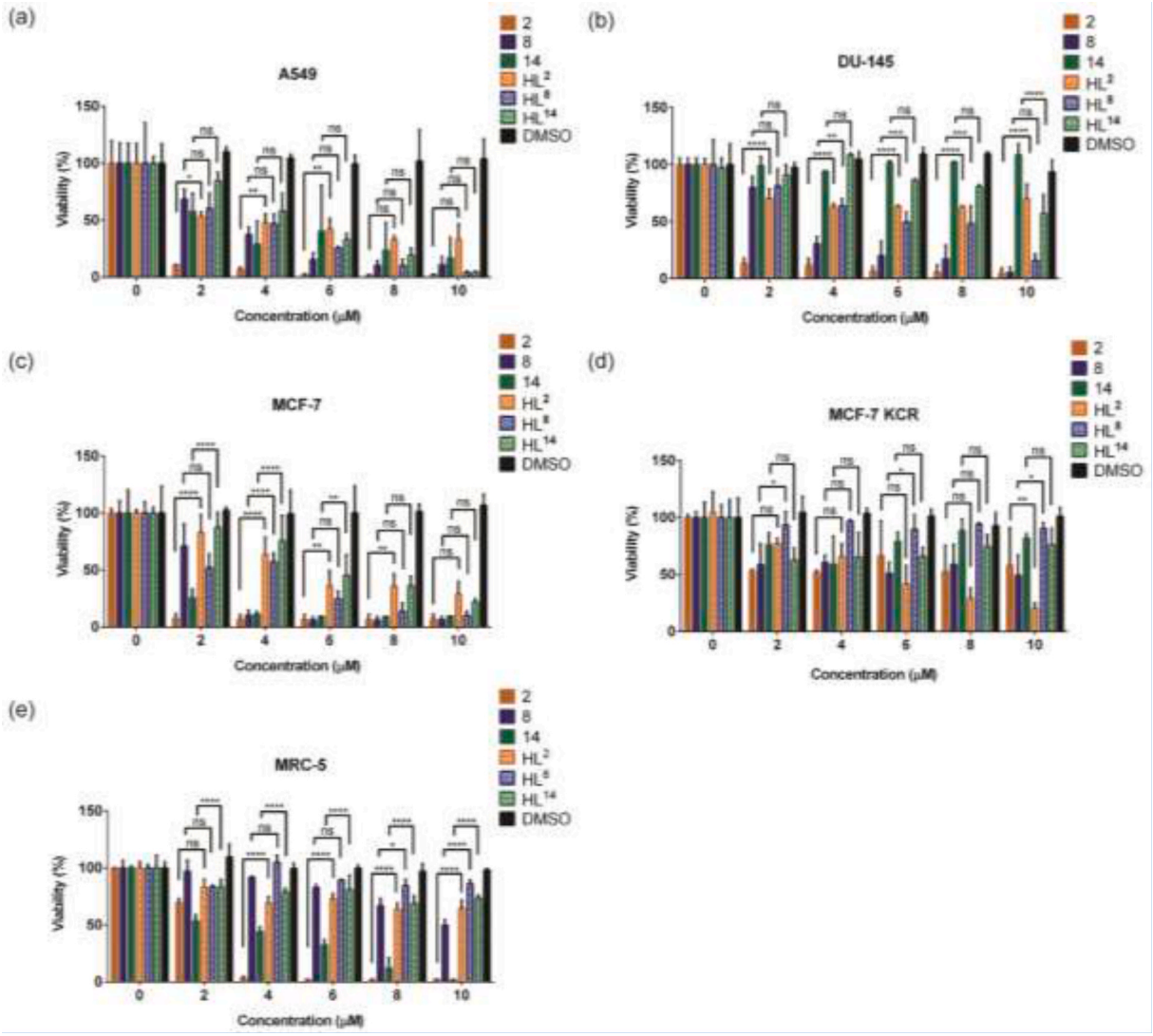

Fig. 5. Toxicity of the selected proligands and their corresponding copper(II) complexes on various cancer and non-cancerous cells. Viability measured by MTT assay on (a) A549, (b) DU-145, (c) MCF-7, (d) MCF-7 KCR and (e) MRC-5 cells following treatment with Cu(II) complexes **2**, **8**, **14** and their corresponding ligands **HL^2**, **HL^8**, **HL^{14}** at various concentrations (2, 4, 6, 8, 10 μM) in addition to the DMSO blank after a 24 h incubation. The viability of the untreated control samples was considered as 100%. The viability (%) of the treated cells was calculated by comparing the obtained absorbance to the absorbance of the untreated control. Data are expressed as the mean ± SD; n ≥ 3. Tukey's multiple comparisons test, *: $P < 0.05$, **: $P < 0.01$, ***: $P < 0.001$, ****: $P < 0.0001$.

of **HL^{14}** and **14** on MCF-7 cancer cells and MRC-5 fibroblast cells, where **14** was more effective in decreasing viability compared to the free ligand. IC_{50} values were calculated from the dose-response curves for each free ligand and corresponding Cu(II) complex on every cell line (Table 4). The differences in the cytotoxicity of the compounds between drug sensitive MCF-7 cell line and MDR MCF-7 KCR cell line are represented by resistance factors (RF). The selectivity to cancer cells over noncancerous cells is represented by selectivity index (SI). These results indicate, that among the studied Cu(II) complexes, **2** showed the highest selectivity for A549 and DU-145 cancer cells. Among the ligands, **HL^{8}** and **HL^{2}** showed the highest selectivity for A549 cancer cells. It is also of note that **HL^{2}** was remarkably effective against both the drug sensitive and the MDR MCF-7 KCR cells, showing a RF value close to 1. In fact, all other compounds including complexes **2**, **8** and **14** were much less potent in growth inhibition of MCF-7 KCR cells, which is reflected by their RF values.

Data from cellular accumulation experiments in A549 lung cancer cells by ICP-MS (Table 5) suggest that methylation at Schiff base azomethine carbon atom is advantageous for cellular uptake of the corresponding complexes, as measured Cu content per cell was by factor 1.9 higher upon exposure to compound **2** compared to **1** and 4.2 times higher upon exposure to **8** compared to **7**. Bromination at position 10, however, was unfavorable for cellular accumulation, as Cu content per cell was 4.8 times lower upon exposure to compound **7** compared to **1** and 2.1 times lower upon exposure to **8** compared to **2**, corresponding to a ten times higher IC_{50} value of **8** compared to **2** in the same cell line.

2.4.2. Fluorescent intercalator displacement assays, circular dichroism (CD) spectroscopy and agarose gel electrophoresis indicate interaction of lead drug candidates with DNA via intercalation

The previously studied Cu(II) complexes of indolo[2,3-*e*]benzazocine and the indolo[2,3-*f*]benzazonine derivatives as well as of indolo[2,3-*c*]quinoline- and indolo[2,3-*d*]benzazepine-morpholine hybrids [37,45] displayed strong binding to calf thymus DNA (ct-DNA) via intercalation. However, different binding strengths were disclosed depending on the substituents and the size of the central *N*-containing ring of the four-ring scaffold. As the binding of the complexes to ct-DNA increased significantly with decreasing the central *N*-containing ring size [45] a strong interaction with the Cu(II) complexes of the indolo[2,3-*c*]quinoline- and indolo[3,2-*c*]quinoline-derived Schiff bases was anticipated.

To find out whether the selected compounds are able to intercalate into DNA, the interaction between ct-DNA and the complexes **2**, **8** and **14** and metal-free ligands **HL^{2}**, **HL^{8}**, and **HL^{14}** was investigated via ethidium (cationic dye used as bromide salt) displacement by spectrofluorometry. Highly diluted conditions (0.5 μM ct-DNA and 0.25 μM ethidium) were applied due to the limited solubility of the compounds. The addition of each of the six selected compounds decreased the high fluorescence of the ct-DNA – ethidium system (Fig. 6).

This decrease was more pronounced for the Cu(II) complexes, reaching a plateau at the emission intensity of the free ethidium cation. Conditional displacement constants determined by the computer program PSEQUAD [54] are listed in Table S5. The actual displacement of ethidium by **8** was confirmed in fluorescence lifetime measurements (see details in Fig. S93). In fact, the complexes replaced ethidium quite effectively; ca. 5 equiv of **8** and **14** were sufficient to completely displace the bound ethidium. For the same effect, 8 equiv of **2** were needed. Interestingly, the respective free ligands also partially replaced the ethidium cation at the concentrations that were used. The most effective competitor of the ethidium cation among the metal-free ligands was indolo[3,2-*c*]quinoline-derived Schiff base **HL^{14}** followed by isomeric indolo[2,3-*c*]quinoline-based ligands **HL^{8}** and **HL^{2}**. The four-ring aromatic scaffold of the free ligands makes them capable of intercalation, although apparently they were not as efficient as ethidium. It is of note that both intercalation and covalent bonding to DNA are possible for the Cu(II) complexes, which, in addition to a more rigid and flat structure contain chlorido co-ligands. However, the fact that the complexes showed a similar binding trend with ct-DNA (**14** ~ **8** > **2**) as the respective free ligands (**HL^{14}** > **HL^{8}** > **HL^{2}**) implies the importance of intercalation of the complexes rather than formation of covalent bond (s).

Next, the interaction with DNA was studied by circular dichroism (CD) spectroscopy. This method provides useful information on the double stranded DNA (dsDNA) structure in solution and its changes upon interaction with various chemical agents. DNA at 25 μM

Table 5
Cellular accumulation (fg Cu per cell) upon 2 h exposure of A549 cells to compounds **1**, **2**, **7** and **8**. Values are means ± standard deviations from three independent experiments.

Compound	**1**	**2**	**7**	**8**
Cellular Accumulation (fg Cu per cell)	181 ± 46	338 ± 15	38 ± 6	158 ± 11

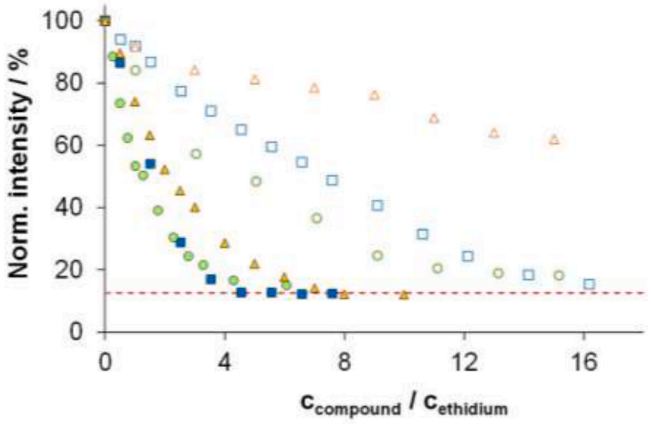

Fig. 6. Fluorescence intensity values of the ct-DNA–ethidium with various compound systems. Symbols denote complexes **2** (▲), **8** (■), and **14** (●) and ligands **HL^{2}** (Δ), **HL^{8}** (□), and **HL^{14}** (○). Red dashed line denotes the emission signal of free ethidium cation. At the indicated ratios, precipitate formation was not observed. {c_{DNA} = 0.5 μM, $c_{ethidium\ bromide}$ = 0.25 μM; λ_{EX} = 510 nm, λ_{EM} = 610 nm; T = 298 K; 10 mM HEPES, pH = 7.40}.

Table 4
IC_{50} values (μM) of the complexes and the free ligands determined on various cancer cell lines and on non-cancerous cells.

Sample	A549	DU-145	MCF-7	MCF-7 KCR	MRC-5	SI^{i}	SI^{ii}	RF^{i}	SI^{iii}
HL^{2}	2.95	>10	5.19	4.87	>10	>3.4	–	0.9	>2.1
2	0. 30	0.15	0.03	9.26	2.29	7.6	15.3	309	0.2
HL^{8}	2.82	5.69	2.69	>10	>10	>3.5	>1.8	>3.7	–
8	2.96	3.27	2.48	>10	>10	>3.4	>3.1	>4.0	–
HL^{14}	4.40	>10	5.92	>10	>10	>2.3	–	>1.7	–
14	2.48	>10	0.58	>10	2.63	1.1	–	>17.2	–
DMSO	>10	>10	>10	>10	>10				

SI^{i} = IC_{50} (MRC-5)/IC_{50} (A549); SI^{ii} = IC_{50} (MRC-5)/IC_{50} (DU-145); RF^{i} = IC_{50} (MCF-7 KCR)/IC_{50} (MCF-7); SI^{iii} = IC_{50} (MRC-5)/IC_{50} (MCF-7 KCR).

deoxynucleotide (dnt) was titrated with the sets of selected free ligands and their Cu(II) complexes, so that the drug/dnt ratios (0, 0.25, 0.5 and 1.0) were varied. As the stock solutions of the potential drugs were prepared in DMSO, the concentration of the DMSO also varied between 0 and 5% (*v/v*) in the final solutions. Therefore, the effect of DMSO on the measurable wavelengths cut-off CD spectra was taken into account. DMSO did not change the shape and intensity of the CD spectra (Fig. S94).

The CD spectra of dsDNA in the presence of $\mathbf{HL}^{2}$, $\mathbf{HL}^{8}$, and $\mathbf{HL}^{14}$ as well as complexes **2**, **8** and **14** are presented in Fig. 7.

The incremental increase of concentration of $\mathbf{HL}^{2}$ (Fig. 7a) had a negligible effect on the DNA spectrum. Only a very slight intensity decrease at the negative band was observed, indicating that DNA conformation remained intact. Notably, this compound exhibited the weakest intercalation ability based on the results of fluorometric experiments (Fig. 6). On the other hand, the CD spectra of dsDNA titrated with $\mathbf{HL}^{8}$ and $\mathbf{HL}^{14}$ (Fig. 7b and c) showed a significant decrease of the intensity of the positive band, while the negative band intensity decreased to a smaller extent. This may be due to a change of DNA conformation from B to a C-like structure [55]. For the latter two compounds, an apparent isodichroic point was observed at ~257 nm, suggesting a continuous change of the DNA conformation between the two states.

The CD spectra of the dsDNA titrated with the Cu(II) complexes (Fig. 7d–f) exhibited a significant and gradual decrease of both the negative and positive band intensities with increasing complex concentration. The complexes **2** and **8** blue-shifted the zero ellipticity value by a few nanometers, thereby changing the shape of the spectra. The strongest effect for **8** was observed at a molar ratio of 1:1, while the shift of the positive band was already achieved at the lowest complex-to-DNA ratio with **2**. These effects can be associated with the change of the DNA conformation, clearly indicating the interaction with Cu(II) complexes. Thus, the Cu(II) complexes **2**, **8**, and **14** and the metal-free ligands $\mathbf{HL}^{8}$ and $\mathbf{HL}^{14}$ caused changes in the CD spectra of a short dsDNA, providing evidence of modifications of DNA conformation, and this effect was more pronounced for the complexes than for the free ligands.

In addition, the interaction of the selected drug candidates with a circular plasmid dsDNA was also studied by agarose gel electrophoresis monitoring the shift of the DNA band upon a binding event or DNA cleavage. As can be seen in Fig. 8, there was no significant change in the band of the DNA in the presence of the added compounds (10 μM) up to a 24 h incubation time with or without the use of the Chelex® 100 (a styrene-divinylbenzene co-polymer containing iminodiacetate groups) metal chelating resin prior to incubation of the reaction mixture.

These experiments were repeated at 20 μM concentrations of the drug candidates without Chelex® 100 treatment (Fig. 9a).

Increasing amounts of the open circular (OC) form of the plasmid DNA were observed upon prolonged incubation times up to 24 h in the presence of **8** and **14**, along with a decrease of the supercoiled (SC) form. The changes in intensity are considered significant in comparison with the control experiment carried out with free Cu(II) ions or with the free ligands. These results suggest that there is a significant effect on the electrophoretic mobility of the plasmid DNA when using the Cu(II) complexes in comparison to metal-free ligands.

The effect of the concentration of tested compounds on the interaction with DNA prompted us to investigate this phenomenon more thoroughly. Therefore, the plasmid DNA was incubated with increasing amounts of **14** (Fig. 9b). This experimental series confirmed the concentration dependence. Furthermore, it revealed that the supercoiled form of the DNA completely disappeared after 24 h in the presence of 50 μM **14**. Although, the supercoiled DNA is converted into the open circular form to almost the same extent by Cu(II) ions under the same conditions, the high stability of the complex did not allow for such high Cu^{2+} concentration in the presence of the free ligand. Thus, the observed effect should be related to the DNA-binding and eventual single strand cleavage by the metal complex.

In conclusion, the selected complexes, which are characterized by high stability in solution, showed significant interactions with DNA, which may underlie their anticancer activity.

2.4.3. Molecular docking further supports the stronger ability of Cu(II) complexes to intercalate into DNA

The metal-free ligands $\mathbf{HL}^{2}$, $\mathbf{HL}^{8}$ and $\mathbf{HL}^{14}$ and their Cu(II) complexes **2**, **8** and **14** were docked into the dsDNA intercalated with the trioxatriangulenium ion ($TOTA^{+}$), i.e., $[d(CGATCG)]_2{\cdot}TOTA_2^{+}$ [56]. The scoring functions GoldScore (GS) [57], ChemScore (CS) [58,59], Piecewise Linear Potential (ChemPLP) [60] and Astex Statistical Potential (ASP) [61] were used with the GOLD (v2024.1) docking algorithm, which is considered an excellent molecular modelling tool [62,63]. The binding scores for the compounds are given in Table 6. For the

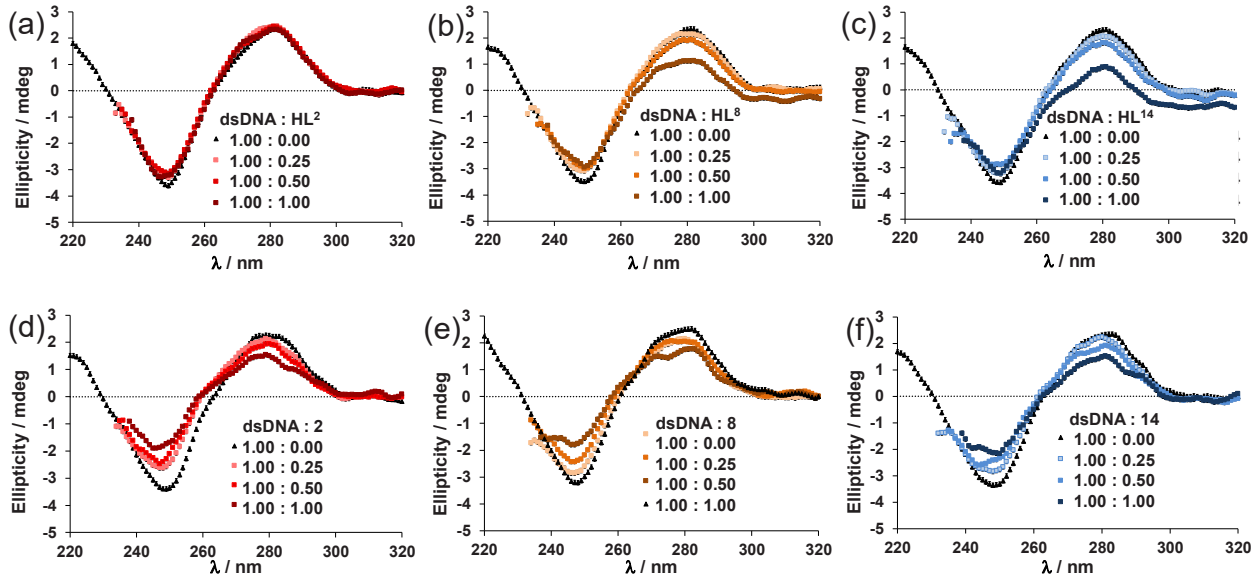

Fig. 7. Circular dichroism spectra of a 42 base pairs (bp) dsDNA with the free ligands and Cu(II) complexes. 25 μM (dnt) of dsDNA was titrated with ligands (a) $\mathbf{HL}^{2}$, (b) $\mathbf{HL}^{8}$ or (c) $\mathbf{HL}^{14}$ or with Cu(II) complexes (d) **2**, (e) **8**, or (f) **14** at M ratios r = *c*(complex or ligand)/*c*(dnt) = 0, 0.25, 0.5, and 1.0. The spectra were recorded with 1 nm spacing. Each symbol represents the average of three scans. The noise level is shown with error bars (and approximately by the size of the symbols).

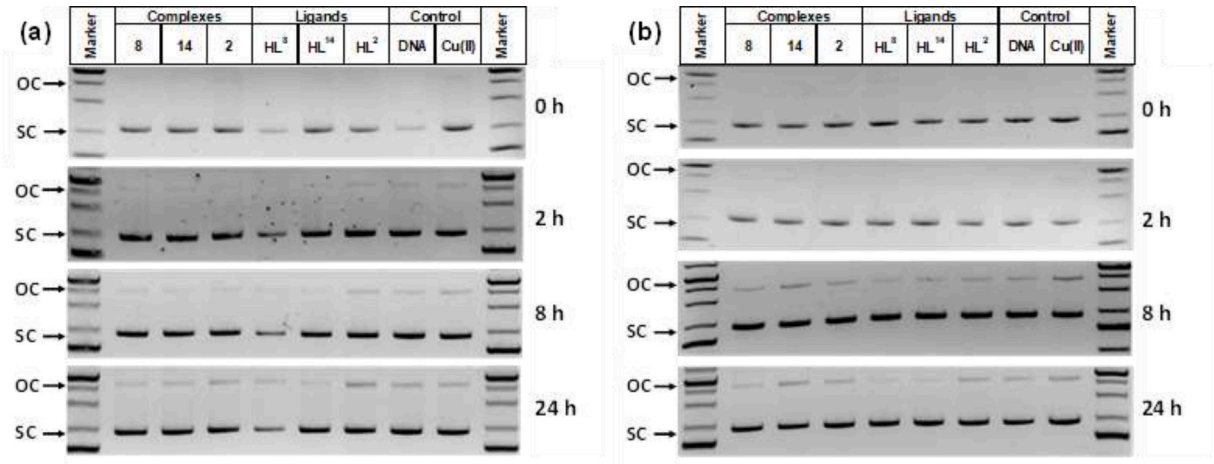

Fig. 8. Nuclease activity of the drug-like molecules monitored by 1% (*w/v*) agarose gel electrophoresis: 10 ng/μL DNA; 10 μM of (a) Chelex® 100-treated and (b) untreated compounds; 30% (*v/v*) DMSO; pH 7.4; incubation was carried out at 37 °C; Marker: 1 kb Gene Ruler Plus.

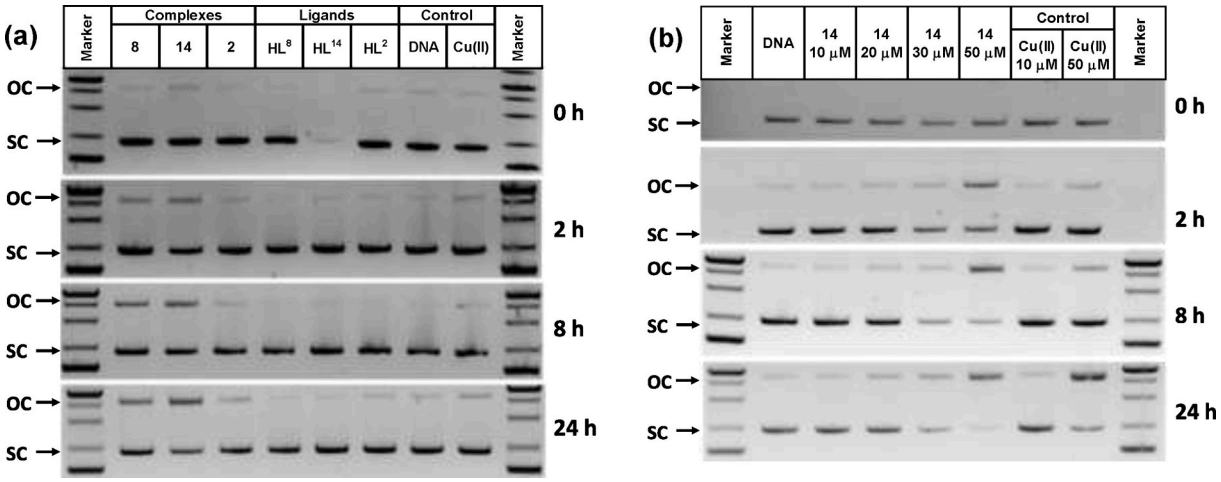

Fig. 9. Nuclease activity of the drug-like molecules monitored by 1 % (*w/v*) agarose gel electrophoresis: (a) 10 ng/μL DNA; 20 μM drug-like molecules and Cu^{2+} in the control experiment; 30% (*v/v*) DMSO; pH 7.4; incubation was carried out at 37 °C; Marker: 1 kb Gene Ruler Plus. It is worth noting that the lack of the band of the supercoiled DNA at the initial point of the **HL^{14}** lane is a mistake of sample loading, since the band is visible at later incubation times. (b) The effect of increasing concentrations of **14** from 10 to 50 μM on plasmid DNA. The further measurement conditions are the same as in (a). The control experiments included 10 and 50 μM Cu^{2+} without the ligand molecule.

Table 6
The binding affinities as predicted by the scoring functions for dsDNA fragment in $[d(CGATCG)]_2{\cdot}TOTA_2^+$. $TOTA^+$, the intercalated co-crystallized ligand cation was re-docked reproducing well the conformation established by protein crystallography with acceptable RMSD values (Root Mean Square Deviation).

Compound	GS	ASP	PLP	CS
HL^2	75.7	58.7	82.9	76.4
2	67.5	-	-	-
HL^8	78.6	57.4	84.7	78.8
8	74.8	-	-	-
HL^{14}	82.3	58.3	82.7	82.1
14	71.9	-	-	-
TOTA	65.9	54.5	77.9	65.7
RMSD (Å)	2.096	0.875	3.294	2.200

metal complexes only GS was used, because it is the only scoring function calibrated for metal complexes.

The GS values were higher for the Cu(II) complexes and the corresponding metal-free ligands than for the co-crystallized $TOTA^+$. Similarly, the other three scoring functions for the **HL^2**, **HL^8** and **HL^{14}** were superior to those for $TOTA^+$, which has a K_d of 24 μM against ct-DNA [56], and also IC_{50} of 0.45 μM against the breast cancer cell line MDA-MB-231 and 0.71 μM for HCT116 (colon) [64].

Fig. 10 shows the binding mode of complex **8** to the DNA fragment. It fits well into the intercalation site, completely overlapping with $TOTA^+$ (Fig. 10b); multiple π-π stacking is predicted between the complex and the DNA bases indicating good binding. Compound **8** is intercalated via the major groove, with the metal center exposed to the water environment. Complexes **2** and **14** have similar binding modes (see Fig. S95); for complex **2** the π – π interactions are predicted as: **2**···G2 3.15 Å; **2**···C5 3.51 Å, **2**···G6 3.6 and 4.2 Å, and for complex **14** only: **14**···G6 3.46 Å; **14**···C5 3.7 Å.

2.4.4. Lead drug candidates induce oxidative stress, mitochondrial dysfunction and potential DNA damage in various cancer cell types

The toxic effect exerted by the free ligands or their Cu(II) complexes might be due to oxidative stress and reactive radical formation. Therefore, the level of reactive oxygen species (ROS) in various cancer cell lines was determined by using 2′,7′-dichlorodihydrofluorescein diacetate (H_2DCF-DA) as a probe (Fig. 11). All treatments of A549 cells triggered the generation of ROS inducing oxidative stress. However,

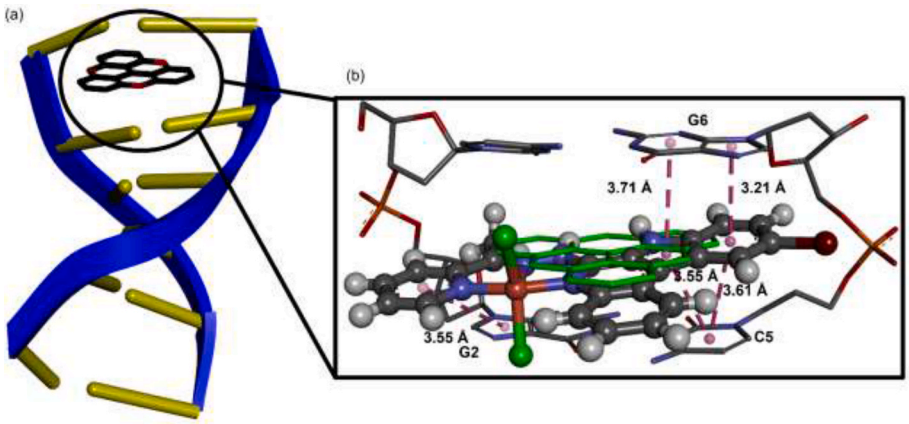

Fig. 10. (a) Co-crystallized $TOTA^+$ in the DNA double stranded hexamer ($[d(CGATCG)]_2 \cdot TOTA^+$) (ref. [54]); (b) The docked conformation of complex **8**, with the adjacent G-C base pairs; π-π stacking is predicted to all the bases except for one cytosine. The co-crystallized cation $TOTA^+$ is shown as green sticks.

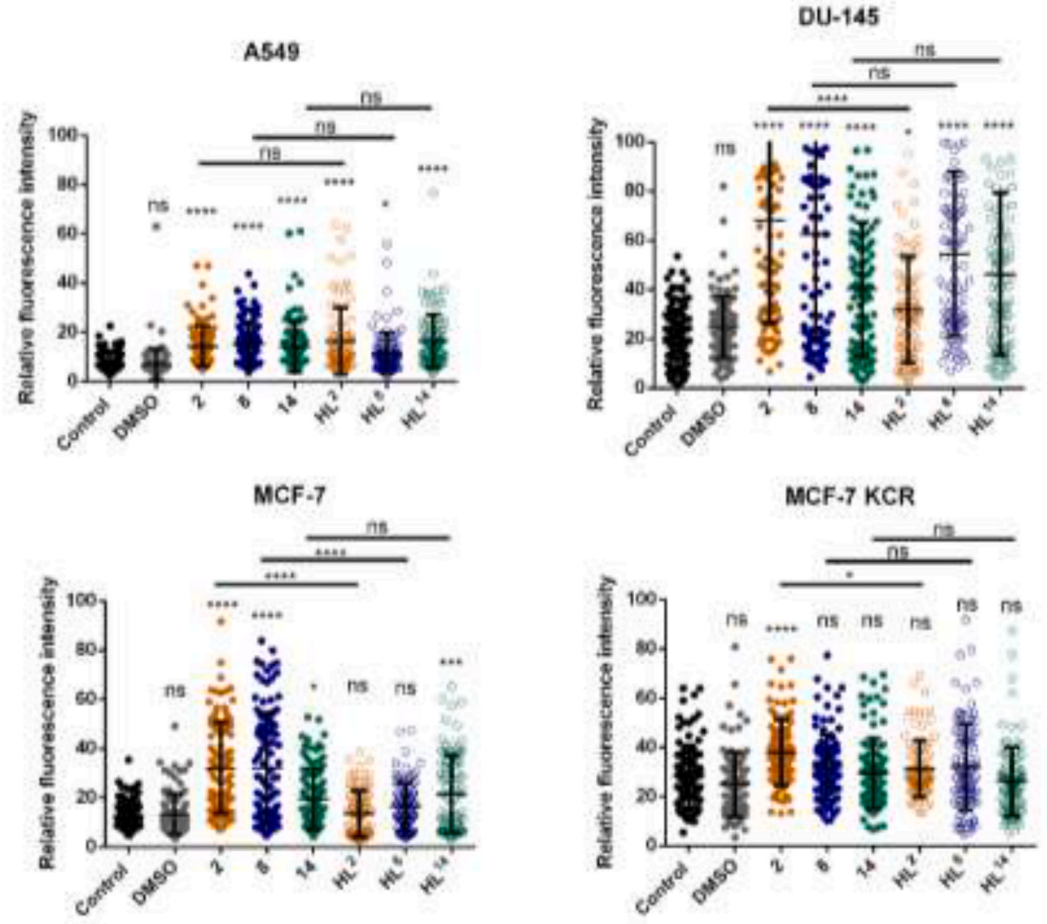

Fig. 11. Generation of reactive oxygen species by the selected free ligands and corresponding Cu(II) complexes on various cancer cell lines. Level of ROS measured by H_2DCF-DA staining on A549, DU-145, MCF-7 and MCF-7 KCR cells upon treatment with Cu(II) complexes **2**, **8**, or **14** and their corresponding proligands $\mathbf{HL^2}$, $\mathbf{HL^8}$, or $\mathbf{HL^{14}}$ (4 μM) following a 3 h incubation and compared to those for a control experiment with DMSO. Data are expressed as the mean ± SD; n ≥ 3. Data were statistically analyzed using Tukey's multiple comparisons test, *: $P < 0.05$, **: $P < 0.01$, ***: $P < 0.001$, ****: $P < 0.0001$.

there was no difference between the effect of the free ligands and the corresponding Cu(II) complexes. This means that the radical formation in these cells is mostly attributed to the presence of the ligand, either added individually or bound to Cu(II) as a complex. A very similar reaction occurred in DU-145 cells, where all compounds administered induced ROS generation. In contrast to A549 cells, complex **2** outperformed the free ligand $\mathbf{HL^2}$ in the ability to produce ROS, suggesting that for a more robust anticancer effect the ligand should be bound in the Cu(II) complex. These findings are in accordance with the toxicity results obtained for complex **2** and ligand $\mathbf{HL^2}$ on DU-145 cells (Fig. 5).

In MCF-7 cells the Cu(II) complexes (**2**, **8** and **14**) and ligand $\mathbf{HL^{14}}$ induced significant oxidative stress, showing an increased 2′, 7′-dichlorofluorescein (DCF) fluorescence intensity compared to the untreated control samples (Fig. 11). Complexes **2** and **8** were significantly

more effective in ROS generation than their ligands, similarly to what was observed during the toxicity screening. As far as the drug-resistant MDR MCF-7 KCR cells are concerned, only one complex, namely **2**, could increase ROS significantly, and it was therefore more effective than its ligand (**HL^2**).

Secondly, mitochondrial damage following the drug treatments was investigated by JC-1 staining, as JC-1 (shows green fluorescence in monomeric and red fluorescence in aggregated form) is a mitochondrial membrane potential indicator. Mitochondrial depolarization is indicated by a decrease in the red/green fluorescence intensity ratio. The red/green fluorescence ratio was significantly decreased upon every treatment in A549 and MCF-7 cells. Only complexes **2**, **14**, and free ligands **HL^8** and **HL^{14}** were effective in DU-145 cells. None of the compounds affected the mitochondrial membrane potential of MCF-7 KCR cells (Fig. 12). In the case of the MDR MCF- KCR cells, verapamil a P-glycoprotein inhibitor was added to the samples before JC-1 staining to avoid dye export due to the overexpressed efflux pumps.

The JC-1 staining results supported the toxicity data, which indicated that A549 and MCF-7 cells were the most sensitive to the cellular effects of the compounds, and, as expected, MCF-7 KCR cells were the most resistant to most of the tested compounds. Moreover, complex **8** outperformed its free ligand **HL^8** in A549 cells in inducing mitochondrial depolarization. Similarly, complex **2** was significantly more detrimental than its free ligand **HL^2** in DU-145 cells. Nevertheless, none of the complexes was able to alter the mitochondrial membrane potential of MCF-7 cells more than its corresponding ligand or could affect the MDR MCF-7 KCR cells.

Since ROS formation might lead to DNA damage, and the complexes as well as the free ligands are able to interact with DNA, we performed γH2AX immunostaining on A549 cells exposed to the drug candidates to detect and quantify the amount of DNA double strand breaks. Such DNA damage appears as bright foci in the nucleus of individual cells. We found that none of the treatments led to serious DNA damage (Fig. S96). The representative images showed that the free ligand- or Cu(II) complex-treated cells stained similarly as the untreated control cells. The number of γH2AX foci was also very low in every sample, indicating that the decrease in cell viability was not due to severe DNA damage but probably due to mitochondrial damage induced by the treatments. Even though, current experiments do not distinguish between nuclear DNA and mitochondrial DNA (mtDNA), the mitochondrial dysfunction (JC-1 staining, Fig. 12) and ROS generation (Fig. 11) are clearly demonstrated. It is well known that mtDNA is particularly susceptible to oxidative damage due to its proximity to the electron transport chain and limited repair capacity [65–67]. Therefore, it is likely that these compounds cause mtDNA damage even without the formation of detectable γH2AX foci in the nucleus.

*2.4.5. Cell cycle analysis and LDH release in the medium indicate that Cu (II) complex **8** inhibits DNA synthesis more effectively than proligand **HL^8**, while both **HL^8** and **8** induce apoptosis in A549 cells*

For metal-based drugs, and, in particular, for Pt(IV), Co(II) or Ru(II) complexes, the effect on the cell cycle and the formation of blocks at single checkpoints is often observed [68–70]. The effect of **HL^8** and **8** on the cell cycle was studied using EdU/FxCycle™ Violet Stain double

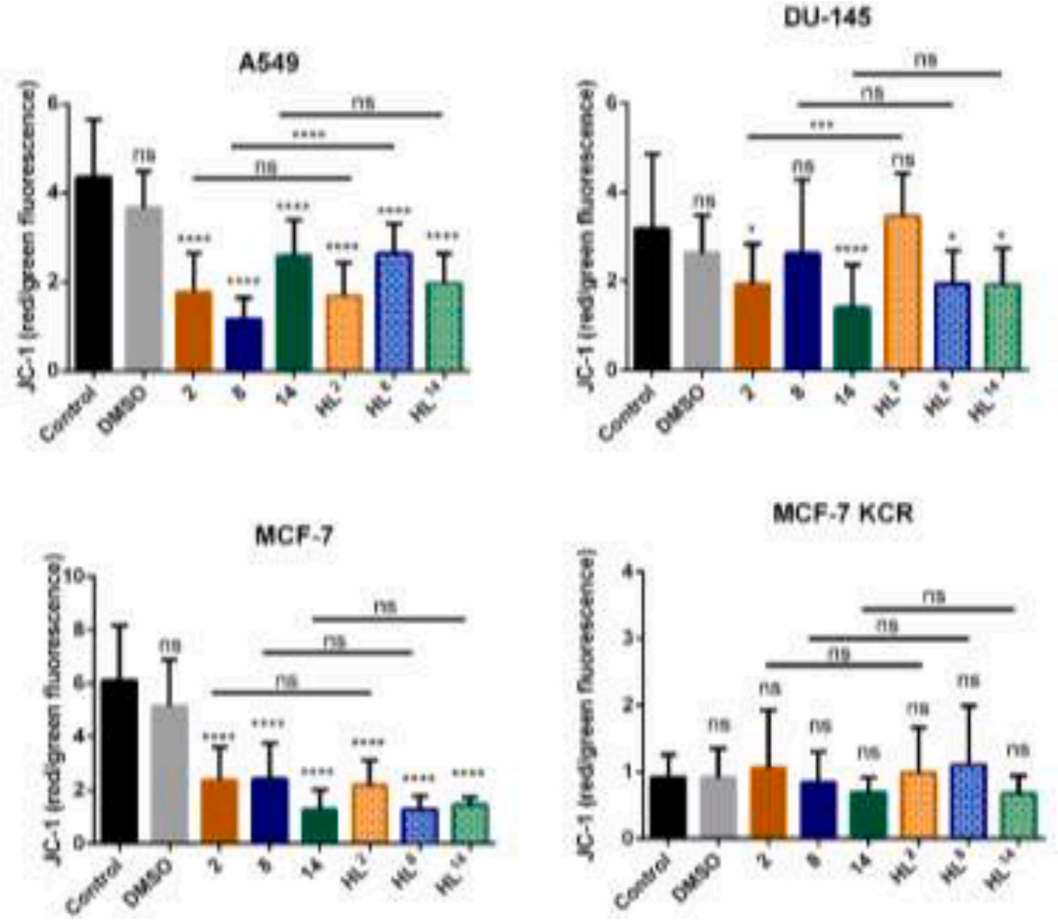

Fig. 12. Mitochondrial dysfunction induced by the selected free ligands and corresponding Cu(II) complexes on various cancer cells. Alterations in mitochondrial membrane potential were detected by JC-1 staining of A549, DU-145, MCF-7 and MCF-7 KCR cells after exposure to Cu(II) complexes **2**, **8**, or **14** and corresponding free ligands **HL^2**, **HL^8**, or **HL^{14}** (4 μM) for 3 h. Red to green fluorescence ratio was determined by fluorescence microscope image analysis. Data are expressed as the mean ± SD; n ≥ 3. Data were statistically analyzed using Tukey's multiple comparisons test, *: P < 0.05, **: P < 0.01, ***: P < 0.001, ****: P < 0.0001.

staining to distinguish cells actively synthesizing DNA. After 48 h of **HL**^{8} exposure, a statistically significant increase in the proportion of A549 cells in G0/G1 phase was observed, as well as a decrease in the proportion of cells in active S phase (Fig. 13). At the same time point, exposure to **8** also caused a significant decrease in the proportion of cells in active S phase, as well as a visible, although not statistically significant, increase in the number of cells in inactive S phase. Although the proportion of cells in the active S phase is similar in cells treated with **HL**^{8} and **8**, the rate of incorporation of EdU into new DNA, and thus the intensity of the fluorescence of the label used to detect it, is significantly lower after exposure to **8** than to **HL**^{8}. This indicates that Cu(II) complex **8** inhibits DNA synthesis with greater efficiency than **HL**^{8}.

Viability of cells. Delays in the cell cycle or cell cycle arrests often lead to cell death. The effect of **HL**^{8} and **8** on viability of A549 cells was measured. Following 48 or 72 h of treatment with IC_{50} concentrations of the compounds the cell number, protein content and lactate dehydrogenase (LDH) release into the medium were analyzed. LDH assay is a well-established and widely used marker of loss of plasma membrane integrity, specifically associated with necrotic or late-stage apoptotic processes [71]. Herein, we studied LDH release to judge whether the observed decrease in cell viability is accompanied by cell membrane damage. Both **HL**^{8} and **8** decreased live cell count after 48 and 72 h of treatment (Fig. 14a). Furthermore, the protein content decreased, indicating that a reduced number of viable cells was present after exposure to both compounds (Fig. 14b). Based on the detection of LDH activity in the medium, a statistically significant increase in the proportion of dead cells in the population was observed after treatment with both compounds. The effect of **8** was more significant (Fig. 14c). These results demonstrate that both **HL**^{8} and **8** decrease cell viability.

Apoptosis of cells. The potential of **HL**^{8} and **8** to induce apoptosis in A549 cells was analyzed by flow cytometry after 48 or 72 h of treatment with IC_{50} concentrations of the compounds, following Annexin V-FITC/propidium iodide (PI) dual staining and compared to DMSO (0.03%) used as vehicle control. The experimental data obtained are presented in Fig. 15 with percentages of early apoptotic cells (Annexin V^{+}/PI^{-}, Q3), late apoptotic and necrotic cells (Annexin V^{+}/PI^{+}, Q2), dead cells (Annexin V^{-}/PI^{+}, Q1) and live cells (Annexin V^{-}/PI^{-}, Q4) in Table S6. By the current test (BD Pharmingen protocol) [72] we cannot reliably distinguish the type of cell death that occurred (i.e., apoptosis or necrosis) in the Q1 (Annexin V $^{-}/PI^{+}$) and Q2 (Annexin V^{+}/PI^{+}) populations, so they are shown together as "late apoptotic + dead" cells.

Compared with the vehicle-treated control cells, the $CuCl_2$-treated cells showed a slight decrease in the percentage of viable cells (87.5%), with no change of the proportion of cells in early apoptosis (2.4%), and a slight increase in the percentage of late apoptotic cells (10.0%), indicating that $CuCl_2$ had only a weak effect on cell survival after 48 h of treatment (Figs. 14a and 15a, Table S6). A slight increase of the percentage of early apoptotic and late apoptotic cells is found after 72 h incubation time (Table S6). The likely reason for the weak effect observed is that the 50 μM concentration of $CuCl_2$ used in A549 cells is too low to significantly induce apoptosis [73–75].

Both **HL**^{8} and **8** induced a substantial rise of early apoptotic cells (18.8 and 15.8%, respectively) compared to 2.5% and 2.4% for DMSO (0.03%) and $CuCl_2$ (50 μM) in A549 cells after 48 h of treatment (Fig. 15a–Table S6). The proportion of late apoptotic and necrotic cells upon the same treatment increased moderately to 13.6% and 14.2% compared to 8.5% and 10.0% for DMSO and $CuCl_2$ treated cells. Prolonged incubation (72 h) led to a further increase of early apoptotic cells (Annexin V^{+}/PI^{-}). A slight increase of late apoptotic/necrotic (Annexin V^{+}/PI^{+}) and dead cells (Annexin V^{-}/PI^{+}) after exposure to **8** was detected as well (Fig. 15a,Table S6). In addition, **8** became more effective than **HL**^{8} in triggering apoptosis (Fig. 15a).

Cleavage of PARP (poly (ADP-ribose) polymerase) is one of the hallmarks of apoptosis [76]. None of the treatments significantly

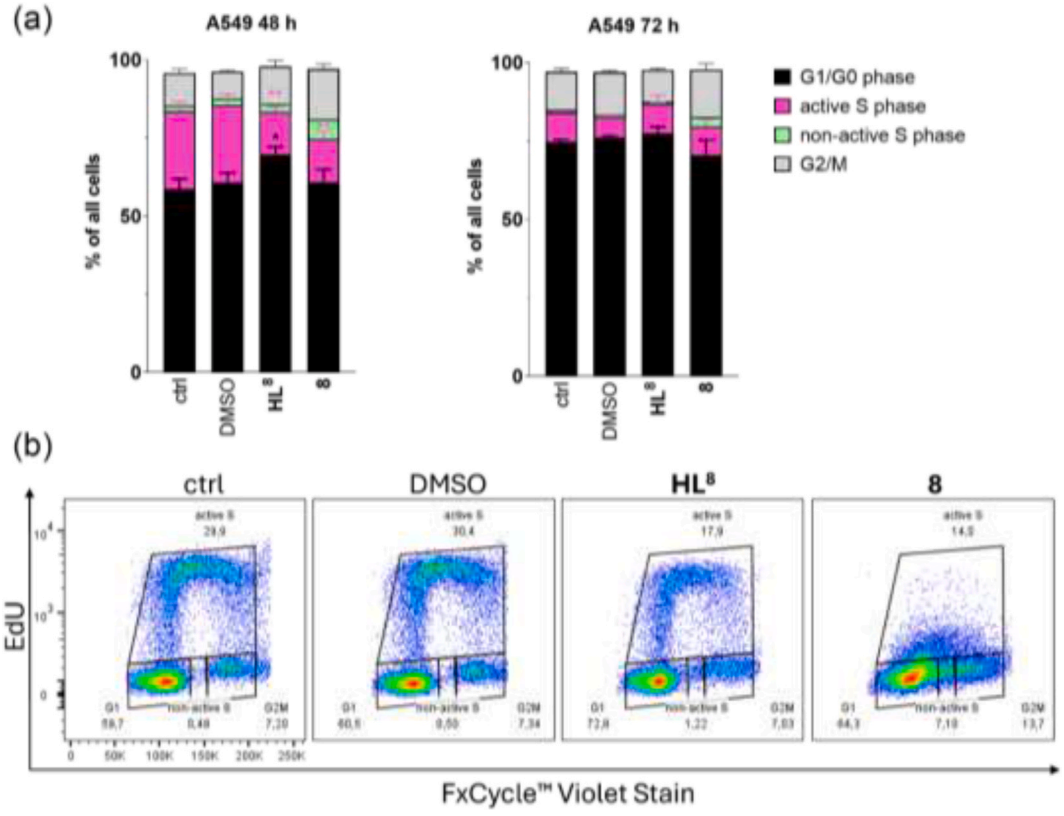

Fig. 13. Inhibition of A549 cell cycle: (a) Cell cycle analysis after 48 and 72 h exposure to **HL**^{8} and **8** by EdU/FxCycle™ Violet Stain double stain of DNA. Data are shown as means ± SEM of percentage of cells in respective cell cycle phase; n = 4; data were analyzed using two way ANOVA followed by Dunnett's test; * = $p < 0.05$, ** = $p < 0.01$; (b) Representative dot plots of cell cycle at 48 h time-point.

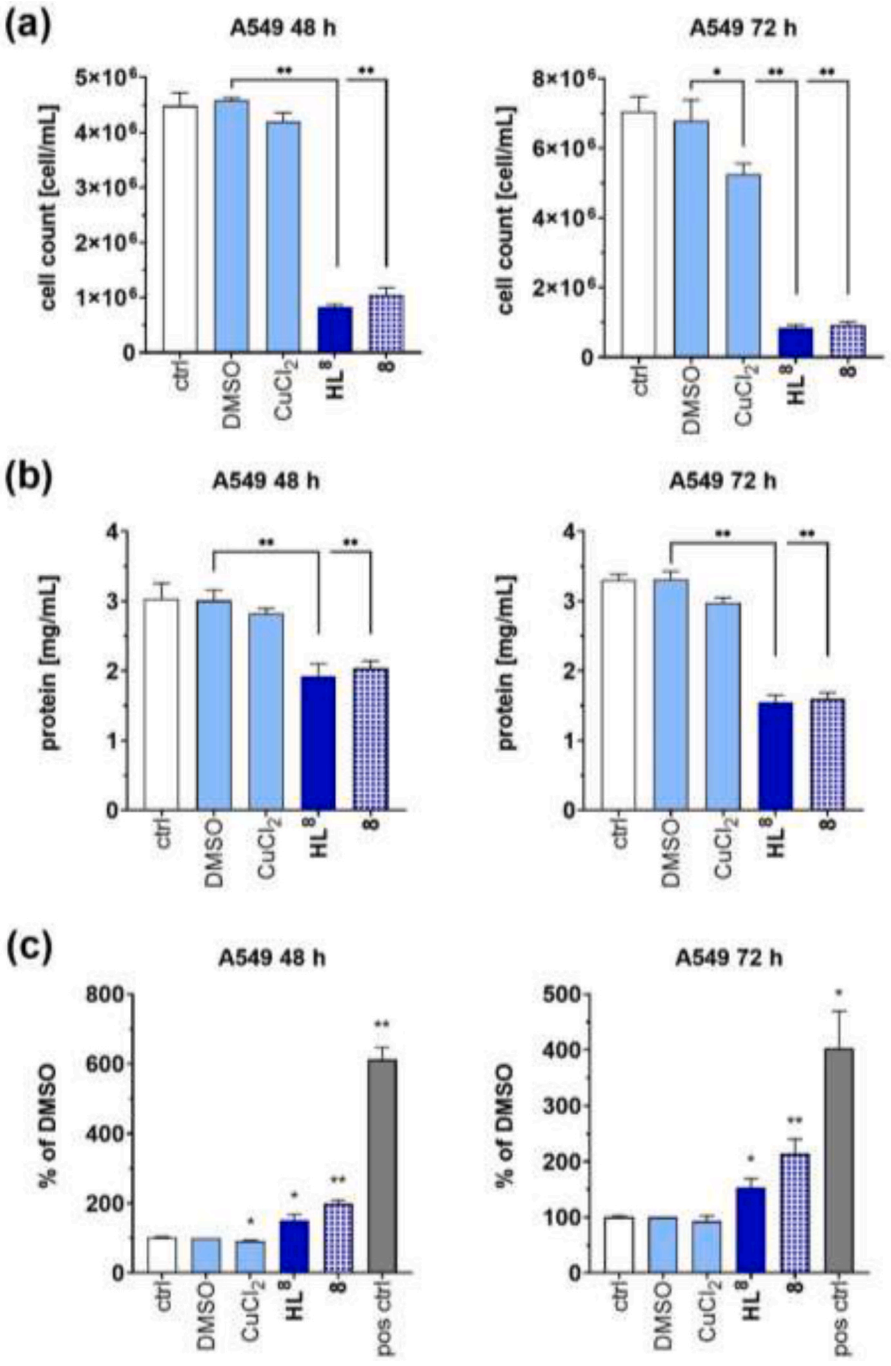

Fig. 14. Viability of A549 cells upon treatment with **HL**^{8} and **8**: (a) Live cell count after 48 and 72 h treatment compared to solvent control (DMSO). Data are shown as means ± SEM; n = 3–5; data were analyzed using one-way ANOVA followed by Dunnett's test; * = $p < 0.05$, ** = $p < 0.01$; (b) Protein content measured using BCA assay after 48 and 72 h exposure. Data are shown as means ± SEM; n = 4–5; data were analyzed using one-way ANOVA followed by Dunnett's test; * = $p < 0.05$, ** = $p < 0.01$; (c) Release of LDH was measured in medium after 48 and 72 h exposure. The results are shown as a mean ± SEM of percentage of solvent control (DMSO); n = 3–7; data were analyzed using one sample *t*-test with a hypothetical value 100; * = $p < 0.05$, ** = $p < 0.01$.

changed PARP expression (Fig. 16a,d). Exposure to both compounds increased cleaved PARP (c-PARP) at 48 h time-point. Higher concentration of the compound resulted in higher PARP cleavage and **8** was more effective in comparison to **HL**^{8} (Fig. 16b). At the 72 h time-point, an increase of c-PARP was observed as well, however because of the variation between experiments only IC_{50} of **8** was statistically significant (Fig. 16e).

H2A is a part of the core histone octamer around which DNA is wrapped. H2AX is one of the variants of H2A and is involved in sensing DNA double strand breaks. When DNA double strand breaks occur H2AX is rapidly phosphorylated on the serine 139 residue resulting in γH2AX [77–80]. During γH2AX immunostaining of A549 cells exposed to the drug candidates the number of γH2AX foci was also very low indicating that the decrease in cell viability was not due to severe DNA damage (Fig. S96). On the contrary, Western blot analysis showed a significant increase of γH2AX after 48 h exposure to both compounds, with **8** being more effective than **HL**^{8} (Fig. 16c). However, at 72 h only higher concentration of **8** remained effective, while the increase observed for the higher concentration of **HL**^{8} was not statistically significant (Fig. 16f). Taken together, both compounds have the capacity to increase the

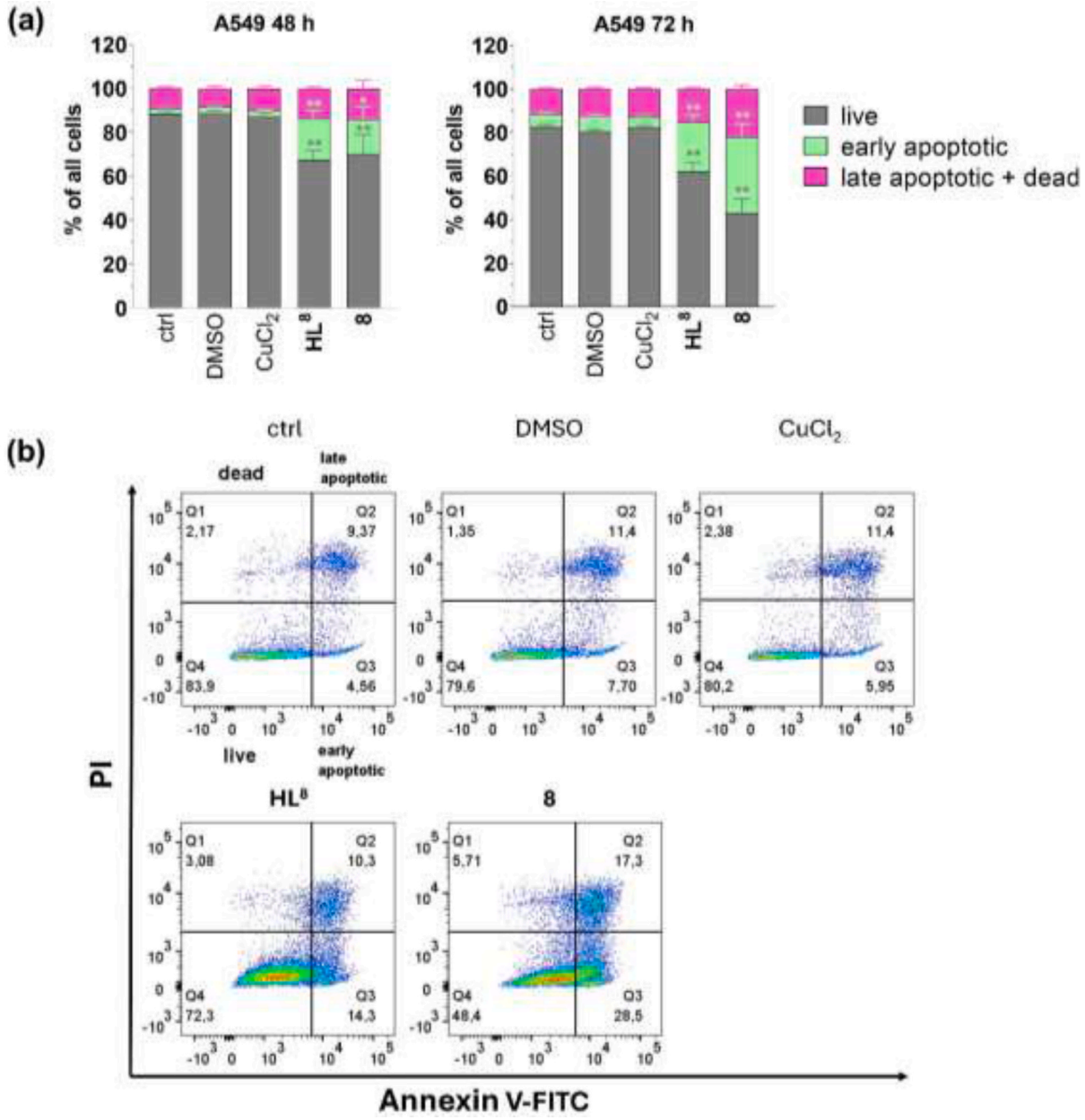

Fig. 15. Induction of apoptosis in A549 cells by **HL^8** and **8** measured by flow-cytometry: (a) percentage of live, early apoptotic, and late apoptotic + dead cells after 48 and 72 h treatment compared to solvent control (DMSO). Data are shown as mean percentage of cells in respective cell death stage ±SEM; data were analyzed using two-way ANOVA followed by Dunnett's test; * = $p < 0.05$, ** = $p < 0.01$ (b) Representative dual parametric dot plots combining Annexin V-FITC and PI of 72 h treatment.

phosphorylation of H2AX, with compound **8** being more potent, particularly at the 48 h time-point, and at higher concentrations. The discrepancy between the immunostaining and Western blot results may be attributed to differences in treatment duration (3 vs 48 h), the antibodies used, and/or the sensitivity of the respective methods.

Collectively, all the above-mentioned results demonstrate that both **HL^8** and **8** may induce cell death through the activation of apoptotic pathways, with compound **8** being more effective.

3. Conclusions

In this study, we synthesized Cu(II) complexes with ligands based on the indolo[2,3-*c*]quinoline scaffold. The new Schiff bases and complexes showed prominent anticancer activity against several cancer cell lines with IC_{50} values in the nanomolar concentration range for the most potent compounds. Ligands and complexes derived from 2-acetylpyridine were significantly more active than those derived from 2-formylpyridine, which is in accordance with data previously reported with isomeric indolo[3,2-*c*]quinolines [16]. Copper(II) complexes showed improved solubility in aqueous media, and, comparable cytotoxicity with that of proligands. Bromo-substitution at different positions of the D-ring revealed that position 10 was favored for maximizing activity, thus making **HL^8** and **8** the lead compounds. Comparison of the indolo[2,3-*c*]quinoline-based compounds with previously studied isomeric indolo[3,2-*c*]quinolines showed that the former were overall more cytotoxic. Interestingly, ligand **HL^2** and the corresponding copper(II) complex **2** showed activity against the MDR breast cancer cell line MCF-7 KCR. Despite being more cytotoxic, the indolo[2,3-*c*]quinolines showed a somewhat weaker affinity towards dsDNA than the isomeric indolo[3,2-*c*]quinolines. Exposure to **8** caused a significant decrease in

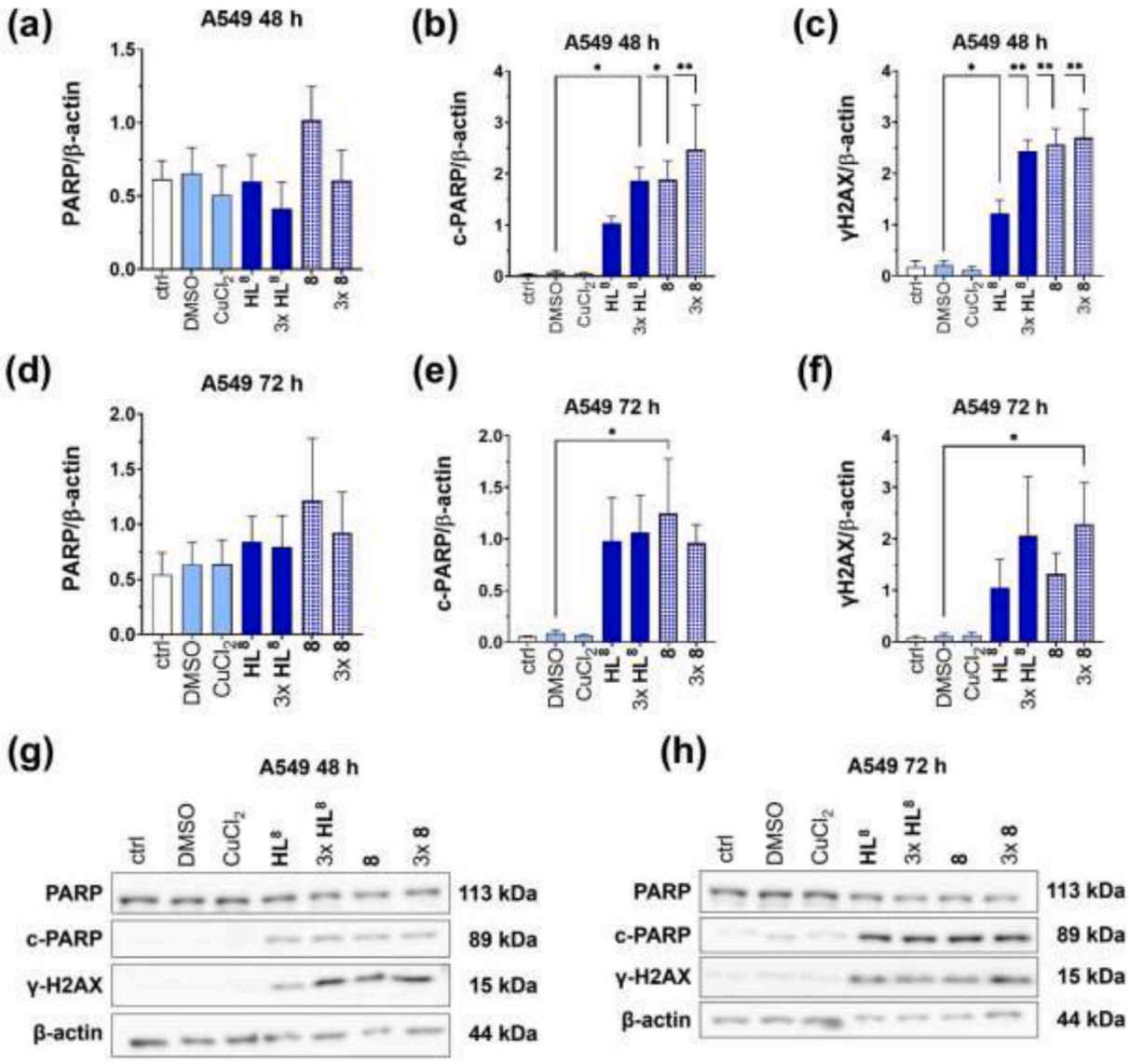

Fig. 16. Induction of apoptosis in A549 cells by $\mathbf{HL^8}$ and **8** measured by Western blot**:** analysis of PARP cleavage and γH2AX phosphorylation in A549 cells after 48 and 72 h exposure to IC_{50} of $\mathbf{HL^8}$ (1.24 μM), 3 × IC_{50} $\mathbf{HL^8}$ (3.72 μM), IC_{50} of **8** (1.61 μM) and 3 × IC_{50} of **8** (4.83 μM) measured by western blotting. (a) PARP after 48 h, (b) cleaved PARP after 48 h, (c) γH2AX after 48 h, (d) PARP after 72 h, (e) cleaved PARP after 72 h, (f) γH2AX after 72 h. As a house-keeping protein, β-actin was used. The results are shown as a mean ± SEM of protein of interest/β-actin ratio; n = 3-4; data were analyzed using one-way ANOVA followed by Dunnett's test; * = $p < 0.05$, ** = $p < 0.01$; (g) representative blots of 48 h treatment, (h) representative blots of 72 h treatment.

the proportion of cells in the active S phase. In addition, the LDH release in the medium caused by **8** in A549 cells was consistent with enhanced ROS production and mitochondrial dysfunction, while a statistically significant increase of the proportion of dead cells after the 48 and 72 h exposures of A549 cells to **8** was also observed. Annexin FITC/PI assay revealed that both $\mathbf{HL^8}$ and **8** induce apoptosis in A549 cells, which is mediated by ROS generation and mitochondrial disfunction. Strong interaction of Cu(II) complexes **2**, **8** and **14** with DNA accompanied by single strand cleavage may also play a role in their anticancer activity.

4. Experimental section

4.1. Chemicals

N-(2-Hydroxyethyl)piperazine-*N*′-(2-ethanesulfonic acid) (HEPES), tris(hydroxymethyl)aminomethane (Tris), calf thymus DNA (ct-DNA, type I, fibers) and ethidium bromide (EB) were purchased from Sigma-Aldrich in puriss quality. DMSO, KCl, KOH, KCl and potassium hydrogen phthalate were obtained from VWR International (Hungary) and used without further purification. Milli-Q water was used for the preparation of all solutions.

4.2. Synthesis of ligands HL^1–HL^8

$HL^1 \cdot 0.5H_2O$. 6-Hydrazin-yl-7*H*-indolo[2,3-*c*]quinoline (**9a**) (1.00 g, 4.03 mmol) was suspended in ethanol (21 mL) in a 50 mL Schlenk tube. The suspension was deoxygenated by bubbling a stream of argon through the reaction mixture for 10 min. Then 2-formylpyridine (422 μL, 4.43 mmol) was added, and the resulting mixture was stirred at 86 °C overnight. The next day, the reaction mixture was allowed to cool to room temperature, and the yellow microcrystalline product was recovered by filtration, washed with cold ethanol and dried in air. Yield: 1.28 g, 94%. Anal. Calcd for $C_{21}H_{15}N_5 \cdot 0.5H_2O$ ($M_r = 346.39$): C, 72.82; H, 4.66; N, 20.22. Found: C, 72.66; H, 4.65; N, 19.99. ^{1}H NMR (600 MHz, DMSO-d_6) δ 12.19 (s, 1H, H^7), 11.08 (s, 1H, H^5), 8.64 – 8.59 (m, 2H, H^{20}, H^{17}), 8.53 (s, 1H, H^{14}), 8.42 (d, $J = 8.2$ Hz, 1H, H^{11}), 8.38

(d, $J = 7.1$ Hz, 1H, H^1), 7.94 – 7.89 (m, 2H, H^{19}, H^4), 7.67 (d, $J = 8.2$ Hz, 1H, H^8), 7.46 – 7.42 (m, 1H, H^9), 7.42 – 7.38 (m, 2H, H^{18}, H^3), 7.32 – 7.28 (m, 2H, H^2, H^{10}). ^{13}C NMR (151 MHz, DMSO) δ 154.55 (Cq, C^{15}), 151.89 (CH, C^{14}), 149.28 (CH, C^{17}), 146.66 (Cq, C^6), 139.28 (Cq, C^{7a}), 136.26 (CH, C^{19}), 134.71 (Cq, C^{4a}), 126.59 (Cq, C^{6a}), 125.95 (CH, C^3), 125.30 (CH, C^9), 123.70 (CH, C^{18}), 122.89 (CH, C^1), 122.30 (Cq, C^{11a}), 122.24 (CH, C^2), 121.67 (CH, C^{11}), 121.18 (CH, C^{20}), 120.66 (CH, C^{10}), 118.83 (Cq, C^{11c}), 116.52 (CH, C^4), 116.13 (Cq, C^{11b}), 112.93 (CH, C^8). ESI-MS (acetonitrile/methanol + 1% water), positive: *m/z* 338.1395 [M + H^+]$^+$; calcd *m/z* 338.1400.

HL^2·0.3MeOH·0.5H_2O. 6-Hydrazin-yl-7*H*-indolo[2,3-*c*]quinoline (**9a**) (1.00 g, 4.03 mmol) was suspended in methanol (17 mL) in a 50 mL Schlenk tube. The mixture was deoxygenated by bubbling argon through the reaction mixture for 10 min. Then 2-acetylpyridine (497 μL, 4.43 mmol) was added, and the resulting mixture was stirred at 76 °C overnight. The next day, the reaction mixture was allowed to cool to room temperature, and the yellow product was removed by filtration, washed with methanol and dried in air. Yield: 1.37 g, 97%. Anal. Calcd for $C_{22}H_{17}N_5$·0.3CH_3OH·0.5H_2O ($M_r = 370.02$): C, 72.38; H, 5.23; N, 18.93. Found: C, 72.24; H, 5.21; N, 18.95. ^{1}H NMR (600 MHz, DMSO-d_6) δ 11.96 (s, 1H, H^7), 10.77 (s, 1H, H^5), 8.73 (dt, $J = 8.1$, 0.9 Hz, 1H, H^{20}), 8.63 (ddd, $J = 4.8$, 1.8, 0.9 Hz, 1H, H^{17}), 8.40 (d, $J = 8.2$ Hz, 1H, H^{11}), 8.33 (d, $J = 7.0$ Hz, 1H, H^1), 7.90 – 7.85 (m, 2H, H^{19}, H^4), 7.70 (d, $J = 8.2$ Hz, 1H, H^8), 7.46 – 7.42 (m, 1H, H^9), 7.41 – 7.34 (m, 2H, H^{18}, H^3), 7.32 – 7.25 (m, 2H, H^2, H^{10}), 2.69 (s, 3H, H^{21}).^{13}C NMR (151 MHz, DMSO-d_6) δ 158.32 (Cq, C^{14}), 156.47 (Cq, C^{15}), 148.47 (CH, C^{17}), 144.78 (Cq, C^6), 139.15 (Cq, C^{7a}), 135.88 (CH, C^{19}), 134.90 (Cq, C^{4a}), 127.40 (Cq, C^{6a}), 125.81 (CH, C^3), 125.09 (CH, C^9), 123.40 (CH, C^{18}), 122.80 (CH, C^1), 122.53 (Cq, C^{11a}), 121.97 (CH, C^2), 121.59 (CH, C^{11}), 121.31 (CH, C^{20}), 120.60 (CH, C^{10}), 118.81 (Cq, C^{11c}), 116.51 (CH, C^4), 115.46 (Cq, C^{11b}), 112.89 (CH, C^8), 13.20 (CH_3, C^{21}). ESI-MS (acetonitrile/methanol + 1% water), positive: *m/z* 352.1556 [M + H^+]$^+$; calcd *m/z* 352.1557. X-ray diffraction quality single crystals were obtained by slow evaporation of methanolic solutions of **HL^2**.

HL^3·0.1H_2O. 8-Bromo-6-hydrazin-yl-7*H*-indolo[2,3-*c*]quinoline (**9b**) (330 mg, 1.01 mmol) was suspended in ethanol (7 mL) in a 25 mL Schlenk tube. The mixture was degassed by bubbling argon through the reaction mixture for 10 min. 2-Formylpyridine (140 μL, 1.46 mmol) was then added, and the reaction mixture was stirred at 86 °C overnight. The reaction mixture was cooled to room temperature and stored at +4 °C overnight. The product was recovered by filtration, washed with cold ethanol and dried in *vacuo*. Yield 320 mg, 93%. Anal. Calcd for $C_{21}H_{14}BrN_5$·0.1H_2O ($M_r = 418.07$): C, 60.33; H, 3.42; N, 16.75. Found: C, 60.19; H, 3.32; N, 16.51. ^{1}H NMR (600 MHz, DMF- d_7) δ 12.13 (s, broad, 1H, H^7), 11.65 (s, broad, 1H, H^{12}), 8.83 (d, $J = 4.1$ Hz, 1H, H^{17}), 8.76 (d, $J = 8.0$ Hz, 1H, H^{11}), 8.72 (d, $J = 6.5$ Hz, 1H, H^1), 8.44 (s, 1H, H^{14}), 8.06 – 8.03 (m, 1H, H^{19} (overlapped DMF peak)), 8.01 – 7.98 (m, 1H, H^{20} (overlapped DMF peak)), 7.92 – 7.86 (m, 2H, H^9, H^4), 7.60 (t, $J = 7.4$ Hz, 1H, H^3), 7.57 – 7.52 (m, 1H, H^2), 7.47 – 7.42 (m, 2H, H^{18}, H^{10}). ^{13}C NMR (151 MHz, DMF- d_7) δ 154.73 (Cq, C^{15}), 153.92 (CH, C^{14}), 151.41 (CH, C^{17}), 147.96 (Cq, C^6), 138.34 (Cq, C^{7a}), 138.10 (CH, C^{19}), 136.71 (Cq, C^{4a}), 129.87 (CH, C^9), 128.97 (Cq, C^{6a}), 127.47 (CH, C^3), 124.84 (CH, C^2), 124.57 (CH, C^{18}), 124.48 (Cq, C^{11a}), 123.99 (CH, C^1), 123.24 (CH, C^{11}), 123.17 (CH, C^{11}), 122.34 (CH, C^{20}), 119.70 (Cq, C^{11c}), 118.78 (Cq, C^{11b}), 117.56 (CH, C^4), 106.40 (Cq, C^8). ESI-MS (acetonitrile/methanol + 1% water), positive: *m/z* 418.0480 [M + H^+]$^+$; calcd *m/z* 418.0487.

HL^4·0.5H_2O. 8-Bromo-6-hydrazin-yl-7*H*-indolo[2,3-*c*]quinoline (**9b**) (225 mg, 0.69 mmol) was suspended in ethanol (5 mL) in a 25 mL Schlenk tube. The mixture was deoxygenated by bubbling argon through the reaction mixture for 10 min. 2-Acetylpyridine (85 μL, 0.76 mmol) was added, and the resulting mixture was stirred at 86 °C overnight. Then the solution was cooled to room temperature and stored at 4 °C overnight. The yellow precipitate was recovered by filtration, washed with cold ethanol and dried *in vacuo*. Yield: 256 mg, 86%. Anal. Calcd for $C_{22}H_{16}BrN_5$•0.5H_2O ($M_r = 438.06$): C, 60.14; H, 3.90; N, 15.94. Found: C, 59.90; H, 3.78; N, 15.58. ^{1}H NMR (600 MHz, DMF-d_7) δ 11.83 (s, broad, 1H, H^7), 11.07 (s, 1H, H^5), 8.69 – 8.62 (m, 1H, H^{17}), 8.60 (d, $J = 8.0$ Hz, 1H, H^{20}), 8.55 (d, $J = 8.0$ Hz, 1H, H^{11}), 8.45 (d, $J = 7.8$ Hz, 1H, H^1), 7.92 (t, $J = 7.1$ Hz, 1H, H^4), 7.87 – 7.82 (m, 1H, H^{19}), 7.73 (d, $J = 7.6$ Hz, 1H, H^9), 7.43 – 7.37 (m, 2H, H^3, H^{18}), 7.35 – 7.28 (m, 2H, H^2, H^{10}), 2.70 – 2.66 (m, 3H, H^{21}). ^{13}C NMR (151 MHz, DMF-d_7) δ 159.57 (Cq, C^{14}) 156.97 (Cq, C^{15}), 148.70 (CH, C^{17}), 145.19 (Cq, C^6), 138.09 (Cq, C^{7a}), 137.12 (CH, C^{19}), 135.95 (Cq, C^{4a}), 129.01 (Cq, C^{6a}), 128.38 (CH, C^9), 126.62 (CH, C^3), 125.02 (Cq, C^{11a}), 123.42 (CH, C^{18}), 123.12 (CH,C^1), 122.19 (CH, C^{10}), 122.08 (CH, C^2), 121.28 (CH, C^{20}, C^{11} (overlapped signals)), 118.68 (Cq, C^{11c}), 117.12 (Cq, C^{11b}), 116.54 (CH, C^4), 105.32 (Cq, C^8), 12.91, (CH_3, C^{21}). ESI-MS (acetonitrile/methanol + 1% water), positive: *m/z* 432.0645 [M + H^+]$^+$; calcd *m/z* 432.0644.

HL^5·0.2H_2O. 9-Bromo-6-hydrazin-yl-7*H*-indolo[2,3-*c*]quinoline (**9c**) (290 mg, 1.01 mmol) was suspended in ethanol (6 mL) in a 25 mL Schlenk tube. The resulting mixture was deoxygenated by bubbling argon through the reaction mixture for 10 min. 2-Formylpyridine (120 μL, 1.72 mmol) was then added, and the reaction mixture was stirred at 86 °C overnight. The reaction mixture was cooled to room temperature and stored at +4 °C overnight. The product was removed by filtration, washed with cold ethanol and dried in *vacuo*. Yield: 350 mg, 96%. Anal. Calcd for $C_{21}H_{14}BrN_5$·0.2H_2O ($M_r = 419.88$): C, 60.07; H, 3.46; N, 16.68. Found: C, 60.11; H, 3.33; N, 16.43. ^{1}H NMR (600 MHz, DMSO-d_6) δ 12.31 (s, 1H, H^7), 11.10 (s, 1H, H^5), 8.64 – 8.59 (m, 2H, H^{17}, H^{20}), 8.53 (s, 1H, H^{14}), 8.39 (d, $J = 8.5$ Hz, 1H, H^{11}), 8.34 (d, $J = 7.7$ Hz, 1H, H^1), 7.95 – 7.88 (m, 2H, H^4, H^{19}), 7.80 (s, 1H, H^8), 7.44 – 7.37 (m, 3H, H^{18}, H^3, H^{10}), 7.30 (t, $J = 7.3$ Hz, 1H, H^2). ^{13}C NMR (151 MHz, DMSO-d_6) δ 154.45 (Cq, C^{15}), 152.26 (CH, C^{14}), 149.29 (CH, C^{17}), 146.40 (Cq, C^6), 140.05 (Cq, C^{7a}), 136.26 (CH, C^{19}), 134.88 (Cq, C^{4a}), 127.28 (Cq, C^{6a}), 126.34 (CH, C^3), 123.79 (CH, C^{11}), 123.52 (CH, C^{18}), 123.48 (CH, C^{10}), 122.94 (CH, C^1), 122.29 (CH, C^2), 121.32 (Cq, C^{11a}), 121.21 (CH, C^{20}), 118.27 (Cq, C^{11c}), 118.13 (Cq, C^9), 116.57 (CH, C^4), 116.10 (Cq, C^{11b}), 115.30 (CH, C^8). ESI-MS (acetonitrile/methanol + 1% water), positive: *m/z* 418.0484 [M + H^+]$^+$; calcd *m/z* 418.0487.

HL^6·0.5H_2O. 9-Bromo-6-hydrazin-yl-7*H*-indolo[2,3-*c*]quinoline (**9c**) (300 mg, 0.92 mmol) was suspended in ethanol (11.5 mL) in a 25 mL Schlenk tube. The resulting mixture was degassed by bubbling an argon stream through the solvent for 10 min. 2-Acetylpyridine (110 μL, 1.18 mmol) was then added, the reaction mixture was stirred at 86 °C overnight, then cooled to room temperature and stored at +4 °C overnight. The product was recovered by filtration, washed with cold ethanol and dried *in vacuo*. Yield: 320 mg, 80%. Anal. Calcd for $C_{22}H_{16}BrN_5$·0.5H_2O ($M_r = 439.31$): C, 60.15; H, 3.90; N, 15.94. Found: C, 60.50; H, 3.68; N, 15.82. ^{1}H NMR (600 MHz, DMSO-d_6) δ 12.06 (s, 1H, H^7), 10.79 (s, 1H, H^5), 8.72 (d, $J = 8.0$ Hz, 1H, H^{20}), 8.63 (d, $J = 4.6$ Hz, 1H, H^{17}), 8.37 (d, $J = 8.6$ Hz, 1H, H^{11}), 8.31 (d, $J = 7.8$ Hz, 1H, H^1), 7.90 – 7.82 (m, 3H, H^4, H^{19}, H^8), 7.44 – 7.34 (m, 3H, H^{18}, H^{10}, H^3), 7.26 (t, $J = 7.5$ Hz, 1H, H^2), 2.68 (s, 3H, H^{21}). ^{13}C NMR (151 MHz, DMSO-d_6) δ 158.64 (Cq, C^{14}), 156.34 (Cq, C^{15}), 148.47 (CH, C^{17}), 144.49 (Cq, C^6), 139.93 (Cq, C^{7a}), 135.89 (CH, C^{19}), 135.05 (Cq, C^{4a}), 128.04 (Cq, C^{6a}), 126.19 (CH, C^3), 123.47 (CH, C^{18}), 123.46 (CH, C^{10}), 123.36 (CH, C^{11}), 122.84 (CH, C^1), 122.01 (CH, C^2), 121.53 (Cq, C^{11a}), 121.33 (CH, C^{20}), 118.22 (Cq, C^{11c}), 117.87 (Cq, C^9), 116.55 (CH, C^4), 115.43 (Cq, C^{11b}), 115.28 (CH, C^8), 13.21 (CH_3, C^{21}). ESI-MS (acetonitrile/methanol + 1% water), positive: *m/z* 432.0642 [M + H^+]$^+$; *m/z* 432.0662.

HL^7·0.2EtOH. 10-Bromo-6-hydrazin-yl-7*H*-indolo[2,3-*c*]quinoline (**9d**) (0.30 g, 0.92 mmol) was suspended in ethanol (10.0 mL) in a 25 mL Schlenk tube. The mixture was deoxygenated by bubbling argon through the reaction mixture for 10 min. 2-Formylpyridine (96 μL, 1.01 mmol) was added, and the reaction mixture was stirred at 85 °C overnight. The reaction mixture was cooled to room temperature, and the yellow precipitate was recovered by filtration, washed with ethanol and dried *in vacuo*. Yield: 0.36 g, 93%. Anal. Calcd for $C_{21}H_{14}BrN_5$·0.2C_2H_6O ($M_r = 425.49$): C, 60.41; H, 3.60; N, 16.46. Found: C, 60.42; H, 3.33; N, 16.37. ^{1}H NMR (600 MHz, DMSO-d_6) δ 12.39 (s, 1H, H^7), 11.09 (s, 1H,

H^5), 8.64 – 8.56 (m, 3H, H^{20}, H^{17}, H^{11}), 8.52 (s, 1H, H^{14}), 8.37 (d, $J = 7.6$ Hz, 1H, H^1), 7.94 – 7.91 (m, 1H, H^{19}), 7.89 (dd, $J = 8.2$, 0.8 Hz, 1H, H^4), 7.61 (d, $J = 8.7$ Hz, 1H, H^8), 7.57 (dd, $J = 8.7$, 1.8 Hz, 1H, H^9), 7.43 – 7.39 (m, 2H, H^{18}, H^3), 7.32 – 7.27 (m, 1H, H^2). ^{13}C NMR (151 MHz, DMSO-d_6) δ 154.45 (Cq, C^{15}), 152.37 (CH, C^{14}), 149.32 (CH, C^{17}), 146.42 (Cq, C^6), 137.92 (Cq, C^{7a}), 136.29 (CH, C^{19}), 134.78 (Cq, C^{4a}), 127.94 (CH, C^9), 127.64 (Cq, C^{6a}), 126.28 (CH, C^3), 123.86 (CH, C^{11}), 123.83 (CH, C^{18}), 123.72 (Cq^{11a}), 123.15 (CH, C^1), 122.38 (CH, C^2), 121.25 (CH, H^{20}), 118.27 (Cq, C^{11c}), 116.51 (CH, C^4), 115.47 (Cq, C^{11b}), 114.84 (CH, C^8), 113.15 (Cq, C^{10}). ESI-MS (acetonitrile/methanol + 1% water), positive: *m/z* 418.0475 $[M + H^+]^+$; calcd *m/z* 418.0487.

HL^8. 10-Bromo-6-chloro-7*H*-indolo[2,3-*c*]quinoline (**9d**) (0.30 g, 0.92 mmol) was suspended in ethanol (10.0 mL) in a 25 mL Schlenk tube. The suspension was deoxygenated by bubbling argon through the reaction mixture for 10 min. 2-Acetylpyridine (114 µL, 1.01 mmol) was then added, and the reaction mixture was stirred at 85 °C overnight. The reaction mixture was cooled to room temperature, and the yellow-orange precipitate was recovered by filtration, washed with ethanol and dried in *vacuo*. Yield: 0.34 g, 86%. Anal. Calcd for $C_{22}H_{16}BrN_5$ ($M_r = 430.31$): C, 61.41; H, 3.74; N, 16.28. Found: C, 61.11; H, 3.47; N, 15.94. ^{1}H NMR (600 MHz, DMSO-d_6) δ 12.14 (s, 1H, H^7), 10.78 (s, 1H, H^5), 8.72 (d, $J = 8.0$ Hz, 1H, H^{20}), 8.63 (ddd, $J = 4.8$, 1.7, 0.9 Hz, 1H, H^{17}), 8.58 (d, $J = 1.7$ Hz, 1H, H^{11}), 8.33 (d, $J = 7.2$ Hz, 1H, H^1), 7.91 – 7.82 (m, 2H, H^4, H^{19}), 7.65 (d, $J = 8.7$ Hz, 1H, H^8), 7.56 (dd, $J = 8.7$, 1.8 Hz, 1H, H^9), 7.42 – 7.33 (m, 2H, H^3, H^{18}), 7.30 – 7.21 (m, 1H, H^2), 2.68 (s, 3H, H^{21}). ^{13}C NMR (151 MHz, DMSO-d_6) δ 158.78 (Cq, C^{14}), 156.36 (Cq, C^{15}), 148.49 (CH, C^{17}), 144.47 (Cq, C^6), 137.80 (Cq, C^{7a}), 135.91 (CH, C^{19}), 134.96 (Cq, C^{4a}), 128.45 (Cq, C^{6a}), 127.69 (CH, C^9), 126.12 (CH, C^3), 124.08 (Cq, C^{11a}), 123.62 (CH, C^{11}), 123.50 (CH, C^1), 123.03 (CH, C^{18}), 122.09 (CH, C^2), 121.36 (CH, C^{20}), 118.22 (Cq, C^{11c}), 116.49 (CH, C^4), 114.80 (2C, (Cq, C^{11b}), (CH, C^8), signals overlapped), 113.09 (Cq, C^{10}), 13.22 (CH_3, C^{21}). ESI-MS (acetonitrile/methanol + 1% water), positive: *m/z* 432.0639 $[M + H^+]^+$; calcd *m/z* 432.0641.

4.3. Synthesis of copper(II) complexes 1–10

Complex 1·0.2^{i}PrOH·0.3H$_2$O. To a solution of **HL^1** (150 mg, 0.44 mmol) in hot isopropanol (105 mL) $CuCl_2{\cdot}2H_2O$ (76 mg, 0.44 mmol) in methanol (1 mL) was added. The color of the solution changed from yellow to red, and the mixture was refluxed for 15 min. Then the mixture was allowed to cool to room temperature and stored at +4 °C overnight. The red product was recovered by filtration and washed with isopropanol. Yield: 204 mg, 98%. Anal. Calcd for $C_{21}H_{15}Cl_2CuN_5{\cdot}0.2C_3H_8O{\cdot}0.3H_2O$ (M_r = 489.25): C, 53.03, H, 3.54; N, 14.31. Found: C, 53.18; H, 3.43; N, 14.03. ESI-MS (acetonitrile/methanol + 1% water), positive: *m/z* 399.0542 $[M - Cl^- - HCl]^+$; calcd *m/z* 399.0540. X-ray diffraction quality single crystals were obtained by slow diffusion of diethyl ether into a DMF solution of **1** (c ≈ 3 mg/mL).

Complex 2·0.8H$_2$O. To a solution of **HL^2** (300 mg, 0.85 mmol) in boiling methanol (70 mL) $CuCl_2{\cdot}2H_2O$ (146 mg, 0.85 mmol) in methanol (5 mL) was added. The color of the solution changed from yellow to orange-red, and the mixture was refluxed for 15 min. The mixture was allowed to cool to room temperature, and the orange-red precipitate was recovered by filtration, washed with methanol and dried in air. Yield: 392 mg, 95%. Anal. Calcd for $C_{22}H_{17}Cl_2CuN_5{\cdot}0.8H_2O$ (M_r = 500.27): C, 52.82; H, 3.75; N, 14.00. Found: C, 52.80; H, 3.46; N, 13.88. ESI-MS (acetonitrile/methanol + 1% water), positive: *m/z* 449.0458 $[M - Cl^-]^+$; calcd *m/z* 449.0463. X-ray diffraction quality single crystals were obtained by slow diffusion of diethyl ether into a DMF solution of **2** (c ≈ 3 mg/mL).

Complex 3·H$_2$O. To a solution of **HL^3** (150 mg, 0.36 mmol) in boiling methanol (35 mL) $CuCl_2{\cdot}2H_2O$ (70 mg, 0.43 mmol) in methanol (1 mL) was added. The color of the solution changed from yellow to dark red, and the mixture was refluxed for 15 min. Then the mixture was cooled to room temperature and stored at +4 °C overnight. The product was recovered by filtration, washed with a small amount of methanol and dried *in vacuo*. Yield 180 mg, 90%. Anal. Calcd for $C_{21}H_{14}BrCl_2CuN_5{\cdot}H_2O$ (M_r = 568.74): C, 44.35; H, 2.84; N, 12.31. Found: C, 44.51; H, 2.60; N, 12.07. ESI-MS (acetonitrile/methanol + 1% water), positive: *m/z* 478.9623 $[M - Cl^- - HCl]^+$; calcd *m/z* 478.9627.

Complex 4·MeOH. To a solution of **HL^4** (130 mg, 0.36 mmol) in boiling methanol (30.0 mL) $CuCl_2{\cdot}2H_2O$ (60 mg, 0.37 mmol) in methanol (1 mL) was added. The color changed from yellow to dark red, and the mixture was refluxed for 15 min. Then the solution was cooled to room temperature and stored at +4 °C overnight. The red product was removed by filtration, washed with methanol (3 mL) and dried *in vacuo* for 3 days. The product was obtained as a dark red powder. Yield 190 mg, 92%. Anal. Calcd for $C_{22}H_{16}BrCl_2CuN_5{\cdot}CH_3OH$ (M_r = 596.79): C, 46.29; H, 3.38; N, 11.74. Found: C, 46.39; H, 3.40; N, 11.50. ESI-MS (acetonitrile/methanol + 1% water), positive: *m/z* 492.9777 $[M - Cl^- - HCl]^+$; calcd *m/z* 492.9783.

Complex 5. To a solution of **HL^5** (150 mg, 0.36 mmol) in boiling methanol (60 mL) $CuCl_2{\cdot}2H_2O$ (70 mg, 0.43 mmol) in methanol (1 mL) was added. The color changed from yellow to dark red, and the mixture was refluxed for 25 min. Then the mixture was cooled to room temperature and stored at +4 °C overnight. The precipitated product was recovered by filtration, washed with methanol (2 mL) and dried *in vacuo*. Yield 190 mg, 93%. Anal. Calcd for $C_{21}H_{14}BrCl_2CuN_5$ (M_r = 550.72): C, 45.80; H, 2.56; N, 12.72. Found: C, 45.60; H, 2.51; N, 12.45. ESI-MS (acetonitrile/methanol + 1% water), positive: *m/z* 478.9626 $[M - Cl^- - HCl]^+$; calcd *m/z* 478.9627.

Complex 6·0.8H$_2$O. To a solution of **HL^6** (150 mg, 0.35 mmol) in boiling methanol (60 mL) $CuCl_2{\cdot}2H_2O$ (70 mg, 0.43 mmol) in methanol (1 mL) was added. The color changed from yellow to dark red, and the mixture was refluxed for 15 min. Then the mixture was cooled to room temperature and stored at +4 °C overnight. The precipitated product was recovered by filtration, washed with cold methanol and dried *in vacuo*. Yield 190 mg, 94%. Anal. Calcd for $C_{22}H_{16}BrCl_2CuN_5{\cdot}0.8H_2O$ (M_r = 579.16), %: C, 45.62; H, 3.06; N, 12.09. Found, %: C, 45.91; H, 2.72; N, 11.82. ESI-MS (acetonitrile/methanol + 1% water), positive: *m/z* 492.9775 $[M - Cl^- - HCl]^+$; calcd *m/z* 492.9783.

Complex 7·0.2DMF. To a solution of **HL^7** (100 mg, 0.24 mmol) in DMF (10 mL) $CuCl_2{\cdot}2H_2O$ (41 mg, 0.24 mmol) in methanol was added. The mixture was stirred at 80 °C for 5 min and then cooled to room temperature and stored at 4 °C overnight. The red-purple precipitate was recovered by filtration, washed with methanol and crystallized from DMF. Yield: 91 mg, 69%. Anal. Calcd for $C_{21}H_{14}BrCl_2CuN_5{\cdot}0.2C_3H_7NO$ (M_r = 565.34): C, 45.89; H, 2.74; N, 12.88. Found: C, 46.28; H, 2.62; N, 12.59. ESI-MS (acetonitrile/methanol + 1% water), positive: *m/z* 478.9614 $[M - Cl^- - HCl]^+$; calcd *m/z* 478.9627.

Complex 8·H$_2$O. To a solution of **HL^8** (150 mg, 0.35 mmol) in boiling methanol (135 mL) $CuCl_2{\cdot}2H_2O$ (60 mg, 0.35 mmol) in methanol (10 mL) was added. The mixture was refluxed for 15 min, and, after cooling to room temperature, the red precipitate was recovered by filtration and washed with methanol and dried in air. Yield: 194 mg, 98%. Anal. Calcd for $C_{22}H_{16}BrCl_2CuN_5{\cdot}H_2O$ (M_r = 582.77): C, 45.34; H, 3.11; N, 12.02. Found: C, 45.44; H, 2.94, N, 11.84. ESI-MS (acetonitrile/methanol + 1% water), positive: *m/z* 492.9776 $[M - Cl^- - HCl]^+$; calcd *m/z* 492.9783.

Complex 9·0.8H$_2$O. To a solution of **HL^2** (100 mg, 0.28 mmol) and triethylamine (79 µL, 0.56 mmol) in boiling methanol (30 mL) $CuCl_2{\cdot}2H_2O$ (48 mg, 0.28 mmol) in methanol (5 mL) was added. The color of the solution changed from yellow to red, and the mixture was refluxed for 15 min. Then the mixture was allowed to cool to room temperature and the red precipitate was recovered by filtration, washed with methanol and dried in air. Yield: 119 mg, 95%. Anal. Calcd for $C_{22}H_{17}ClCuN_5{\cdot}0.8H_2O$ (M_r = 463.81): C, 56.97; H, 3.82; N, 15.10. Found: C, 57.05; H, 3.66; N, 15.04. ESI-MS (acetonitrile/methanol + 1% water), positive: *m/z* 413.0699 $[M - Cl^-]^+$; calcd *m/z* 413.0696.

Complex 10. To a solution of **HL^8** (100 mg, 0.23 mmol) and triethylamine (64 µL, 0.46 mmol) in boiling methanol (75 ml) $CuCl_2{\cdot}2H_2O$ (40 mg, 0.23 mmol) in methanol (5 mL) was added. The mixture was

refluxed for 15 min. After cooling to room temperature, the red precipitate was recovered by filtration, washed with methanol and dried in air. Yield: 118 mg, 97%. Anal. Calcd for $C_{22}H_{15}BrClCuN_5$ ($M_r = 528.29$): C, 50.02; H, 2.86; N, 13.26. Found: C, 49.81; H, 2.84; N, 13.01. ESI-MS (acetonitrile/methanol + 1% water), positive: *m/z* 492.9776 $[M - Cl^-]^+$; calcd *m/z* 492.9783.

4.4. Physical measurements

All compounds reported are >95% pure by elemental analysis. Elemental analysis was carried out in a Carlo-Erba microanalyzer at the Microanalytical Laboratory at the Faculty of Chemistry of the University of Vienna. The samples for low resolution electrospray ionization mass spectrometry (ESI-MS) were measured on an amaZon speed ETD Bruker instrument. Expected and experimental isotope distributions were compared. 1D (^{1}H, ^{13}C) and 2D (^{1}H–^{1}H COSY, ^{1}H–^{13}C HSQC, ^{1}H–^{13}C HMBC) NMR spectra were acquired on a Bruker AV NEO 500 or AV III 600 spectrometers in DMSO-d_6 or DMF-d_7 at 25 °C.

4.5. Crystallographic structure determinations

The measurements were performed on Bruker D8 Venture and Bruker X8 APEX-II CCD diffractometers. Single crystals were positioned at 30, 30, 27, 35, 30, 27, 30, 30, 27, 25, 27, 30, 30 and 30 mm from the detector, and 939, 360, 486, 1826, 345, 972, 325, 180, 1200, 1164, 1200, 2990, 360 and 412 frames were measured, each for 8, 3, 20, 5.5, 5, 7, 60, 8, 20, 2, 25, 15, 5 and 20 s over 1, 0.5, 1, 0.38, 1, 0.5, 1, 1, 0.5, 0.4, 0.5, 0.5, 0.5 and −0.7° scan width for species **2a**, **3c**, **4a**, **4b**, **4c, 5b**, **7b**, **8b+8d**, **HL^{2}·1.5MeOH**, **HL$^{2\prime}$·MeOH**, **1·DMF**, **2·1.5DMF**, **9** and **10·0.75DMF·0.9H$_2$O**, respectively. Crystal data, data collection parameters, and structure refinement details are given in Tables 1–3. The structures were solved by direct methods and refined by full-matrix least-squares techniques. Non-H atoms were refined with anisotropic displacement parameters. H atoms were inserted in calculated positions and refined with a riding model. The following computer programs and hardware were used: structure solution, *SHELXS-2014* and refinement, *SHELXL-2014* [81]; molecular diagrams, ORTEP [82]; computer, Intel CoreDuo. CCDC 2364792 (**2a**), 2364793 (**3c**), 2364794 (**4a**), 2364795 (**4b**), 2364796 (**4c**), 2364797 (**5b**), 2364798 (**7b**), 2364799 (**8b+8d**), 2364800 (**HL^{2}·1.5MeOH**), 2364801 (**HL$^{2\prime}$·MeOH**), 2364802 (**1·DMF**), 2364803 (**2·1.5DMF**) and 2364804 (**9**) and 2364805 (**10·0.75DMF·0.9H$_2$O**).

4.6. Spectrophotometric titrations, stability and solubility tests

Aqueous stability of **HL^{2}** – **HL^{8}** and complexes **1**–**8** were followed by UV−vis spectrophotometry on a Peltier controlled (298 K) 8-channel Agilent Cary 3500 photometer at 5 μM concentration over at least 71 h in 50% (*v/v*) DMSO/aqueous HEPES buffer (pH = 7.4, 10 mM). The UV−vis spectra for the ligands (**HL^{2}**, **HL^{8}**, and **HL^{14}**) and complexes (**2**, **8**, and **14**) were recorded using an Agilent Cary 8454 diode array spectrophotometer. The path length was 4 cm. The samples containing the ligands or the complexes at 10 μM in 30% (*v/v*) DMSO/H_2O were titrated by a KOH solution (with 30% (*v/v*) DMSO) at 25.0 ± 0.1 °C in the pH range from 1.5 to 10.0 using 0.1 M KCl ionic strength. An Orion 710A pH-meter equipped with a Metrohm combined electrode (type 6.0234.100) and a Metrohm 665 Dosimat burette were applied for the pH measurements and titrations. The electrode system was calibrated to the pH = −log[H+] scale in the DMSO/H_2O solvent mixture according to the Irving method [83] as described in our previous studies [37,45,84]. The average water ionization constant (pK_w) was 14.52 ± 0.05. During the titrations, argon gas was passed over the solutions. Proton dissociation constants (pK_a) of the ligands, overall stability constants ($\log\beta$) of the Cu(II) complexes and the individual spectra of the various species present in solution were computed by the computer program PSEQUAD [54]. $\beta(M_pL_qH_r)$ is defined for the general equilibrium pM + qL + rH ⇌ $M_pL_qH_r$ as $\beta\ (M_pL_qH_r) = [M_pL_qH_r]/[M]^p[L]^q[H]^r$, where M denotes the Cu(II) ion and L the completely deprotonated ligand. The calculations were always made from the experimental titration data measured in the absence of any precipitate in the solution.

The thermodynamic solubility (*S*) of the compounds was determined for the saturated solutions by using samples containing 0.5 mg of compound in 1 mL water after sonication for 6 min, followed by standing at 298 K for 2 h and centrifugation for 15 min. The concentration of the saturated solutions was determined by UV−vis spectrophotometry using stock solutions of the compounds of known concentration dissolved in 100% DMSO and 50% (*v/v*) DMSO/water for the calibration.

The human serum albumin (essentially globulin free, Sigma Aldrich) binding studies were carried out in 10 mM HEPES pH = 7.4 buffer at 298 K; the maximal DMSO content was 2% (*v/v*). UV-vis spectra were recorded in 1 cm quarz cells, the complex concentration varied between 5 and 22 μM or it was kept constant at 5 μM and the albumin concentration was varied (1−50 μM). The fluorometric measurements were done at 0.25 μM albumin concentration and 0−10 μM complex concentration at $\lambda_{EX} = 295$ nm.

4.7. Interaction with intracellular reducing agents and ROS generation

Interaction with reduced glutathione and NADH was followed by UV−vis spectroscopy, in 50% (*v/v*) DMSO/aqueous buffer (pH = 7.4, 10 mM HEPES); samples contained 10 μM **8** and 500 μM reducing agent under air-free conditions, $T = 298$ K. In the ROS generation experiments the spin trapping agent 5,5-dimethyl-1-pyrroline-*N*-oxide (DMPO, Sigma-Aldrich) was distilled before use (70 Pa; 80−90 °C). Standard settings during EPR spin trapping experiments were microwave frequency ~9.448 GHz; power of the microwave radiation 2 mW; sweep width 200 G; center field 3350 G; modulation amplitude 2 G; time constant 20.5 ms; and sweep time 42 s, series of 10 spectra with 3 scans for each measurement. Optical spectra were measured on a Shimadzu 3600 UV−vis−NIR spectrometer (Japan). EPR measurements were performed using an X-band Bruker EMX spectrometer (Germany).

4.8. MTT assay

Two sets of MTT assays (a and b) were performed in this work.

(a) All compounds were tested against MDA-MB-231, MCF-7 and MRC-5 cell lines.

The cytotoxicity of the compounds was determined using the MTT colorimetric test. The cells were harvested from culture flasks by trypsinization and seeded into 96-well microculture plates at a seeding density of 6000 cells per well (6×10^4 cells/mL). After the cells were allowed to resume exponential growth for 24 h, they were exposed to drugs at different concentrations in media for 72 h. The drugs were diluted in a complete medium at the desired concentration and added to each well (100 μL) and serially diluted to other wells. After exposure for 72 h, the media was replaced with MTT in media (5 mg/mL, 100 μL/well) and incubated for an additional 50 min. Subsequently, the medium was aspirated, and the purple formazan crystals formed in viable cells were dissolved in DMSO (100 μL/well). Optical densities were measured at 570 nm using the BioTekH1 Synergy microplate reader. The quantity of viable cells was expressed in terms of treated/control (T/C) values by comparison to untreated control cells, and 50% inhibitory concentrations (IC_{50}) were calculated from concentration−effect curves by interpolation. The evaluation was based on means from at least three independent experiments, each comprising three replicates per concentration level.

(b) Selected compounds **HL^{2}**, **HL^{8}**, **HL^{14}**, **2**, **8**, and **14** were further investigated.

The biological effect of Cu(II) complexes and their proligands were investigated in A549 lung adenocarcinoma (ATCC), DU-145 prostate cancer (ATCC), MCF-7 sensitive (ATCC) and and MCF-7 KCR multidrug-resistant breast cancer cell lines (gift kindly provided by Eva Balint (HUN-REN)), and on MRC-5 non-cancerous human fibroblast cells (ATCC). Human cancer cell lines were maintained in RPMI-1640 cell culture media (Biosera, Nuaille, France) complemented with 10% fetal bovine serum (FBS, Biosera, Nuaille, France), 2 mM L-glutamine (Biosera, Nuaille, France), 0.01% streptomycin and 0.005% penicillin (Biosera, Nuaille, France), and were cultured in a 37 °C incubator with 5% CO_2 and 95% humidity.

The viability of human cancer cells was assessed by the MTT assay after the treatments with Cu(II) complexes and with their ligands. For this, 10,000 cells/well (A549, DU-145, MCF-7, MCF-7 KCR and MRC-5) were seeded into 96-well plates and left to grow. On the following day cells were exposed to 0, 2, 4, 6, 8 or 10 μM compound. After 24 h, cells were washed with PBS and were incubated with 0.5 mg/mL MTT reagent (Sigma-Aldrich, St Louis, MO, USA) for 1 h at 37 °C. Then the formazan crystals were solubilized in DMSO (Molar Chemicals, Halásztelek, Hungary), and the absorbance of samples was measured at 570 nm using a Synergy HTX plate reader (BioTek, Winooski, VT, USA). IC_{50} values were calculated in GraphPad Prism 6 software. The viability measurements were repeated three times using 3 independent biological replicates.

4.9. Cellular accumulation

A549 cells were seeded at densities of 2.1×10^5 cells/well in 1 mL of minimum essential medium (MEM) supplemented with 1 mM sodium pyruvate, 4 mM L-glutamine, 1% (v/v) nonessential amino acids from 100-fold stock (all purchased from Sigma-Aldrich) and 10% fetal bovine serum (FBS, purchased from Serana, Pessin, Germany) per well into 12-well plates (CytoOne™, Starlab, Hamburg, Germany). After 24 h, compounds dissolved in DMSO and diluted in MEM were added to the wells to a final concentration of 10 μM, and plates were incubated at 37 °C for 2 h. During incubation, the cell number was determined from three control wells of a plate seeded in parallel to the treatment plates. After the 2-h incubation, the medium was removed and all wells were washed with 3 × 1 mL PBS, and cells were lysed by adding 400 μL HNO_3 per well for 1 h at room temperature. 300 μL of each lysate were added to 7.7 mL MilliQ water to obtain a total volume of 8 mL, and determination of copper content was carried out by an Agilent 7800 ICP-MS instrument (Agilent Technologies). Data from three independent experiments were normalized to the corresponding cell number and are given in fg Cu per cell.

4.10. DNA binding studies: fluorescence spectroscopy

Fluorescence measurements were carried out on a Fluoromax (Horiba Jobin Yvon) fluorometer. Stock solutions of the metal complexes and proligands were made in pure DMSO ($c = 1$ or 0.5 mM). Stock solution of ct-DNA was prepared as described previously [45]. The sample volume was 20.0 mL that contained 0.5 μM ct-DNA expressed in base pairs, 0.25 μM ethidium bromide and different concentrations of complexes or ligands in 10 mM HEPES buffer (pH 7.40). DMSO content of the samples varied between 0 and 1% (*v/v*). The excitation wavelength was 510 nm, and the fluorescence emission was measured in the wavelength range of 530–750 nm. Corrections for self-absorbance and inner filter effect were done as previously described [45]. Conditional binding constants were calculated for the compound-(ct-DNA) adduct (*K'*) as described recently [85].

4.11. DNA binding studies: circular dichroism spectroscopy

Circular dichroism (CD) spectra were recorded on a Jasco J-1500 CD spectrometer at room temperature (298 K). The measurement parameters were adjusted as follows: wavelength range, 320 – 220 nm; path length, 1.0 cm (Jasco cuvette); D.I.T., 2 s; bandwidth, 1.0 nm; scanning speed, 50 nm/min (continuous scanning mode). Each spectrum is the average of three accumulated scans. The concentration of deoxynucleotide (dnt) units in the solution of the dsDNA formed from two 42 dnt long deoxyoligonucleotides (Ars-N-F: 5′-CTAGCATCCACGAATATTTCTTGCAGT ATTGACAAGATATCG-3′ and Ars-N-R 5′-CTAGCGATATCTTGTCAA-TACTGCAAGAAATATTCGTGGATG-3′) (Life Technologies Japan LTD. Tokyo Japan) was adjusted to 25 μM (dnt) in 10 mM Tris-HCl (pH 7.5), 5 mM NaCl. For the investigation of the effect of the ligands and metal complexes, 25 μM (dnt) concentration of the dsDNA was mixed with Cu(II) complexes (**2**, **8**, or **14**), or ligands ($\mathbf{HL^2}$, $\mathbf{HL^8}$, or $\mathbf{HL^{14}}$) to adjust molar ratios $r = c(\text{complex or ligand})/c(\text{dnt}) = 0.00$, 0.25, 0.50, and 1.00. The Cu(II) complexes as well as the ligands were dissolved in DMSO. The final concentration of DMSO in the buffered solution was 1.25% (*v/v*) for $r = 0.25$, 2.5% (*v/v*) for $r = 0.5$, and 5% (*v/v*) for $r = 1$.

The dsDNA was prepared by hybridization of the above two single strand DNAs (ssDNA). 50 μL of 200 μM aqueous solution from both deoxy oligonucleotides in the presence of ~10 mM NaCl was mixed and incubated in a programmed thermocycler. The hybridization was carried out using the following conditions: step 1, denaturation at 95 °C for 2 min; step 2, decrease the temperature by 1 °C each, 1 min, 85 times; step 3, keep at 10 °C. Then the diluted solution of the dsDNA for the CD experiment was prepared in 10 mM Tris-HCl (pH 7.5) adjusting the NaCl concentration to 5 mM.

4.12. Agarose gel electrophoretic mobility shift assays (EMSA)

Electrophoretic mobility of circular plasmid DNA in the presence or absence of the studied ligands or the metal complexes was studied. The DNA bands of the superhelical, relaxed open circular, and linear forms were separated in 1% (*m/v*) agarose gels containing 500 ng/mL ethidium bromide (EtBr) at 100 V for 45 min using a Cleaver Scientific MultiSUB Wide Midi tank combined with a Biorad PowerPac 300 power supply. GeneRuler™ 1 kb Plus DNA Ladder (Thermo Scientific) served as a reference. Gel images were photographed by a Uvitec BTS 20MS gel documentation system.

Each 40 μL reaction mixture contained 400 ng plasmid DNA, one of the investigated compounds at 10 – 50 μM concentrations in a 30% (*v/v*) DMSO/H_2O solvent mixture. Control experiments were carried out under the same conditions with the plasmid DNA itself, as well as in the presence of Cu(II) provided at equal concentrations to those of the drug-like molecules. The pH was adjusted to 7.4 by HEPES so that the buffer concentration was 10 mM. The mixtures were incubated at 37 °C up to 24 h. At each investigated time point 10 μL aliquots were taken, flash frozen in liquid N_2 and stored at −80 °C until the gel electrophoresis experiment was performed.

4.13. Molecular docking

The metal-free ligands and Cu(II) complexes were docked against the DNA double strand intercalated with the trioxatriangulenium ion ($TOTA^+$), {[d(CGATCG)]$_2$·$TOTA_2^+$} [56]. The GOLD (v2024.1) software suite was used to prepare the crystal structures for docking, i.e., the hydrogen atoms were added, water molecules deleted and the co-crystallized $TOTA^+$ ions identified. The docking centre for the binding pocket was defined as the position of the co-crystallized ligand with a 10 Å radius. Fifty docking runs were allowed for each ligand with default search efficiency (100%). The scoring functions GoldScore (GS) [57], ChemScore (CS) [58,59], Piecewise Linear Potential (ChemPLP) [60] and Astex Statistical Potential (ASP) [61] were used in the GOLD (v2024.1) docking algorithm. The complexes were built in the HyperChem8.0.7 software (Hypercube, Inc. Copyright 1995-2009), and the geometries were optimized with the MM + force field [86].

4.14. ROS generation

The level of intracellular reactive oxygen species (ROS) generated upon the treatments with **HL^2**, **HL^8**, **HL^{14}**, **2**, **8** or **14** was measured by DCFDA staining on A549, DU-145, MCF-7 and MCF-7 KCR cells. For this, 1×10^5 cells/well were seeded onto glass coverslips (VWR International, Radnor, PA, USA) placed in 24-well plates and left to grow. On the following day, the cells were treated with 4 μM of copper complexes and of their ligands or with equivalent amounts of DMSO (Thermo Fisher Scientific, Waltham, MA, USA) for 3 h. After treatments, cells were washed twice with PBS then incubated for 30 min with 10 μM DCFDA solution (Thermo Fisher Scientific, Waltham, MA, USA) diluted in PBS. After the incubation, the cells were washed 3 times with PBS, and the fluorescence of the samples was visualized with an OLYMPUS BX51 microscope with an Olympus DP70 camera (Olympus Corporation, Shinjuku, Tokyo, Japan). The fluorescence intensity was quantified using ImageJ software.

4.15. JC-1 staining

The mitochondria damaging effect of the compounds was verified using JC-1 staining on A549, DU-145, MCF-7 and MCF-7 KCR cells following treatments with **HL^2**, **HL^8**, **HL^{14}**, **2**, **8** or **14.** For this, 1×10^5 cells/well were seeded onto glass coverslips (VWR International, Radnor, PA, USA) placed in 24-well plates and left to grow. Next day the cells were treated with 4 μM of each compound for 3 h. After the treatments, the cells were washed twice in PBS, and JC-1 dye (Thermo Fisher Scientific, Waltham, MA, USA) was added in a 10 μg/mL final concentration diluted in cell culture media for 10 min. In case of MCF- KCR cells, 1 h prior to JC-1 staining 20 μM verapamil, a P-glycoprotein (Pgp) inhibitor was added to the samples, since JC-1 dye is a Pgp substrate, and the Pgp efflux pump is overexpressed by MCF-7 KCR cells. Then the fluorescence of the samples was detected using an OLYMPUS BX51 microscope with an Olympus DP70 camera (Olympus Corporation, Shinjuku, Tokyo, Japan), and the red and green fluorescence intensity was quantified using ImageJ software.

4.16. γH2AX immunostaining

To determine the degree of DNA damage induced by the treatments, DNA double strand breaks were visualized by γH2AX immunostaining. For this, 1×10^5 A549 cells/well were seeded onto glass coverslips in 24-well plates. On the following day, the samples were treated for 3 h with 4 μM of copper complexes or with their ligands or with equivalent amounts of DMSO. Then the cells were fixed with 4% formaldehyde (Molar Chemicals, Halásztelek, Hungary), permeabilized with 0.3% Triton-X-100 (Calbiochem, Merck Millipore, Darmstadt, Germany) and were blocked using 5% BSA diluted in PBS (Sigma-Aldrich, St. Louis, MO, USA). Then the samples were incubated with anti-γH2AX primary antibody (Thermo Fisher Scientific, Waltham, MA, USA) in 1:300 dilution followed by Alexa 488 fluorophore-conjugated goat anti-mouse secondary antibody (Abcam, Cambridge, UK) in a 1:600 dilution. The fluorescence intensity of the stained samples was detected with an Olympus FV10i confocal microscope Olympus Corporation, Shinjuku, Tokyo, Japan).

4.17. Cell culture

A549 cells were grown in high glucose Dulbecco's Modified Eagle Medium (DMEM; Gibco – Thermo Fisher Scientific) supplemented with 10% heat-inactivated low endotoxin fetal bovine serum (LE FBS; v/v, PAA – GE HealthCare), 2 mM L-glutamine (Gibco) and 100 U/ml of penicillin and 100 μg/mL of streptomycin (Sigma-Aldrich). Cells were sub-cultured three times per week (until approximately 80% confluency was reached). Cells were maintained at 37 °C in an atmosphere of 5% CO_2 and 95% air. Cells were seeded onto 6-well tissue culture plates (TPP) at a density of 5.5×10^4 cells/cm^2 (5×10^5 cells/well) in 2 mL of cultivation media. For Western blot assay cells were seeded onto 24-well tissue culture plates (TPP) at a density of 5.5×10^4 cells/cm^2 (1×10^5 cells/well) in 0.5 mL of cultivation media. Cells were allowed to attach to the bottom of the plate overnight. The next day, the cultivation media was changed to a fresh one containing IC_{50} of **HL^8** (1.24 μM), $3 \times IC_{50}$ of **HL^8** (3.72 μM), **8** (1.61 μM) or $3 \times IC_{50}$ of **8** (4.83 μM). Note these IC_{50} values differ slightly from those quoted in Table 4 because MTT assays were performed in different laboratories. Cultivation media containing the respective amount of DMSO was used as the negative control. Cells were collected after 48 h and 72 h exposure and used for cell cycle, Western blot and apoptosis Annexin V/PI analyses. The methods are described below.

4.18. LDH assay

The potential cytotoxic effect was determined by measuring the activity of lactate dehydrogenase (LDH) released from the cytosol of dying cells in a culture medium using the Cytotoxicity Detection KitPLUS (Roche). Briefly, 80 μL of the medium was mixed with the reaction mixture in a ratio of 1:1 and incubated at room temperature. A_{490} was measured using a SPECTRA Sunrise microplate reader (Tecan). A positive control was prepared by applying supplier-provided lysis buffer to untreated cells for 30 min before media collection.

4.19. Cell cycle

2 h before collection, EdU (5-ethynyl-2′-deoxyuridine, a nucleoside analog of thymidine) was added to cells for a final concentration of 10 μM. Cells were harvested, and 5×10^5 cells/sample were used for staining. Incorporation of EdU was determined using Click-iT™ EdU Alexa Fluor™ 488 Flow Cytometry Assay Kit (Thermo Fisher Scientific). Total DNA was stained using FxCycle™ Violet Stain (Thermo Fisher Scientific). Briefly, cells were washed with 1% BSA in PBS and fixed using Click-iT™ fixative. After washing, cells were permeabilized using Click-iT™ saponin-based permeabilization and wash reagent and stained by Click-iT™ EdU reaction cocktail (PBS, $CuSO_4$, Alexa Fluor488™ azide and Click-iT™ EdU buffer additive). After washing, cells were resuspended in 1 μg/mL FxCycle™ Violet Stain in PBS and incubated for 30 min at 4 °C in the dark. Cells were visualized using BD FACSVerse™, and the results were analyzed using FlowJo™ v10.10.0 Software (BD Life Sciences).

4.20. Western blot

Cells were lysed in lysis buffer (1% sodium dodecyl sulfate (SDS); 100 mM Tris, pH 7.4; 10% glycerol; phenylmethanesulfonyl fluoride. The samples were heated at 95 °C for 10 min, and the protein concentration was determined using the BCA™ protein assay (Pierce, Rockford, IL, USA), with BSA used as a standard. The expression of target proteins was quantified by Western blot. Briefly, cell lysates were supplemented with 5 × Laemmli buffer (200 mM Tris–HCl (pH 6.8), 3% SDS, 30% glycerol, 0.03% bromophenol blue, 3% 2-mercaptoethanol, and 200 mM dithiothreitol). 10 μg of protein per sample was loaded on a 10% acrylamide gel. To ensure equal protein loading, β-actin protein was used as a housekeeping loading control. After the SDS-polyacrylamide gel electrophoresis, proteins were transferred on polyvinylidene difluoride membrane (Immobilon-P, Millipore), blocked in 5% non-fat dry milk in 1 × Tris-buffered saline supplemented with 0.1% Tween for 1 h. The membranes were incubated at 4 °C overnight with the primary antibodies for the targeted proteins PARP 113 kDa (1:1000, #ab191217, Abcam), cleaved PARP 89 kDa (1:1000, #9541, Cell Signalling), γH2AX (phospho S139) 15 kDa (1:2000, #ab11174, Abcam) and ß-actin (1:5000, #A5441, Sigma Aldrich). After that, they were counterstained using the horseradish peroxidase-conjugated anti-mouse or anti-rabbit IgG secondary antibodies (both from Cell Signalling

Technology, 1:5000) at room temperature for 1 h. Proteins were visualized by the SuperSignal West Pico/Femto Chemiluminescent Substrate (Pierce) using Amersham Imager 680 (GE HealthCare). Relative protein levels were quantified by ImageJ software. The level of the protein of interest was normalized to the respective β-actin level.

4.21. Annexin V/PI assay

A549 cells were harvested and 1×10^5 cells/sample were used for staining. Culture medium, 0.03% DMSO and 50 μM $CuCl_2$ were used as control treatments. The cells were also treated with IC_{50} of **HL**[8] (1.24 μM) or **8** (1.61 μM). Apoptosis was determined using ApoFlowEx FITC Kit (Exbio). Briefly, cells were washed twice with cold PBS and pellet was resuspended in Annexin V Binding Buffer. Then cells were stained with Annexin V-FITC and Propidium Iodide (PI) for 15 min at room temperature in the dark. After incubation cells were centrifuged. Pellet was resuspended in Annexin V Binding Buffer and samples were kept on ice in the dark. Cells were visualized using BD FACSVerse™, and the results were analyzed using FlowJo™ v10.10.0 Software (BD Life Sciences).

Disclaimer

This research was supported in part by the Developmental Therapeutics Program in the Division of Cancer Treatment and Diagnosis of the National Cancer Institute, which includes federal funds under Contract No. HHSN261200800001E. The content of this publication does not necessarily reflect the views or policies of the Department of Health and Human Services, nor does mention of trade names, commercial products, or organizations imply endorsement by the U.S. Government.

CRediT authorship contribution statement

Felix Bacher: Conceptualization, Formal analysis, Investigation, Supervision, Writing – original draft. **Christian Madejski:** Data curation, Investigation. **Irina Kuznetcova:** Investigation, Methodology. **Orsolya Dömötör:** Data curation, Investigation, Methodology. **Béla Gyurcsik:** Investigation, Supervision, Writing – original draft. **Zeyad H. Nafaee:** Investigation, Methodology. **Nóra Igaz:** Data curation, Investigation, Methodology, Visualization. **Csenge Bocz:** Investigation, Methodology. **Bálint Péntek:** Investigation, Methodology. **Mónika Kiricsi:** Investigation, Supervision, Validation, Writing – original draft. **Petra Raptova:** Data curation, Investigation, Methodology, Visualization. **Alexandru-Constantin Stoica:** Data curation, Formal analysis, Investigation, Methodology, Software. **Michaela Hejl:** Investigation, Methodology. **Michael A. Jakupec:** Investigation, Supervision, Writing – original draft. **Samah Mutasim Alfadul:** Investigation, Methodology. **Maria V. Babak:** Investigation, Methodology, Supervision, Validation. **Peter Rapta:** Conceptualization, Investigation, Methodology. **Jóhannes Reynisson:** Investigation, Methodology, Supervision, Validation, Visualization. **Lenka Sindlerova:** Investigation, Methodology, Supervision, Validation. **Éva A. Enyedy:** Conceptualization, Funding acquisition, Investigation, Methodology, Project administration, Supervision, Writing – original draft, Writing – review & editing. **Ernest Hamel:** Formal analysis, Investigation, Writing – review & editing. **Vladimir B. Arion:** Conceptualization, Funding acquisition, Project administration, Resources, Supervision, Writing – original draft, Writing – review & editing.

Declaration of competing interest

The authors declare no competing financial interest.

Acknowledgments

This work was funded by the Austrian Science Fund (FWF) grant no. P31293, by a grant from the Romanian National Authority for Research, project no. PNRR–III–C9-2023-I8-99 within the National Recovery and Resilience Plan, by the Slovak Research and Development Agency under contract nos APVV-23-0195, SK-HU-24-0003 (P. R.) and the grant agency VEGA (contract no. 1/0392/24), as well as by the National Research, Development and Innovation Office-NKFIA (Hungary) through projects TKP2021-EGA-32, K138318 and PharmaLab (RRF-2.3.1.-21-2022-00015). MTT experiments were performed using support from the City University of Hong Kong (Project No. 7005829).

Appendix A. Supplementary data

Supplementary data to this article can be found online at https://doi.org/10.1016/j.ejmech.2026.118882.

Abbreviations

ASP	Astex Statistical Potential
BSA	bovine serum albumin
CD	circular dichroism
^{13}C-DEPT$_q$	^{13}C quantitative distortionless enhancement by polarization transfer
ChemPLP	Piecewise Linear Potential
CS	ChemScore
ct-DNA	calf thymus DNA
H_2DCF-DA	2′,7′-dichlorofluorescein diacetate
DMEM	Dulbecco's Modified Eagle Medium
dsDNA	double stranded DNA
dnt	deoxynucleotide;
EdU	5-ethynyl-2′-deoxyuridine;
EPR	electron paramagnetic resonance
FBS	fetal bovine serum
GS	GoldScore
GSH	glutathione
HEPES	*N*-(2-hydroxyethyl)piperazine-*N*′-(2-ethanesulfonic acid)
ICP-MS	induced coupled plasma mass spectrometry
LDH	lactate dehydrogenase
MDR	multidrug resistant
MTT	3-(4,5-dimethylthiazol-2-yl)-2,5-diphenyltetrazolium bromide;
NADH	nicotinamide adenine dinucleotide, reduced
PBS	phosphate-buffered saline;
Pgp,	P-glycoprotein
ROS	reactive oxygen species
SC-XRD	single crystal X-ray diffraction
SDS	sodium dodecyl sulfate
SI	selectivity index
$TOTA^+$	trioxatriangulenium ion
Tris	tris(hydroxymethyl)aminomethane

Data availability

Data will be made available on request.

References

[1] D. Laryea, A. Isaksson, C.W. Wright, R. Larsson, P. Nygren, Characterization of the cytotoxic activity of the indoloquinoline alkaloid cryptolepine in human tumour cell lines and primary cultures of tumour cells from patients, Invest. N. Drugs 27 (2009) 402–411.
[2] G.C. Kirby, A. Paine, D.C. Warhurst, B.K. Noamese, J.D. Phillipson, *In vitro* and *in vivo* antimalarial activity of cryptolepine, a plant-derived indoloquinoline, Phytother Res. 9 (1995) 359–363.
[3] F. Riechert-Krause, K. Weisz, Indoloquinolines as DNA binding ligands, Heterocycl. Commun. 19 (2013) 145–166.
[4] J. Lavrado, R. Moreira, A. Paulo, Indoloquinolines as scaffolds for drug discovery, Curr. Med. Chem. 17 (2010) 2348–2370.

[5] P.T. Parvatkar, P.S. Parameswaran, S.G. Tilve, Isolation, biological activities and synthesis of indoloquinoline alkaloids: cryptolepine, isocryptolepine and neocryptolepine, Curr. Org. Chem. 15 (2011) 1036–1057.

[6] S. Hostyn, B.U.W. Maes, L. Pieters, G.L.F. Lemière, P. Mátyus, G. Hajós, R. A. Dommisse, Synthesis of the benzo-β-carboline isoneocryptolepine: the missing indoloquinoline isomer in the alkaloid series cryptolepine, neocryptolepine and isocryptolepine, Tetrahedron 61 (2005) 1571–1577.

[7] K. Bonjean, M.C. De Pauw-Gillet, M.P. Defresne, P. Colson, C. Houssier, L. Dassonneville, C. Bailly, R. Greimers, C. Wright, J. Quetin-Leclercq, M. Tits, L. Angenot, The DNA intercalating alkaloid cryptolepine interferes with topoisomerase II and inhibits primarily DNA synthesis in B16 melanoma cells, Biochemistry 37 (1998) 5136–5146.

[8] W. Peczynska-Czoch, F. Pognan, L. Kaczmarek, J. Boratynski, Synthesis and structure-activity relationship of methyl-substituted indolo[2,3-*b*]quinolines: novel cytotoxic, DNA topoisomerase II inhibitors, J. Med. Chem. 37 (1994) 3503–3510.

[9] F. Pognan, J.-M. Saucier, C. Paoletti, L. Kaczmarek, P. Nantka-Namirski, M. Mordarski, W. Peczynska-Czoch, A carboline derivative as a novel mammalian DNA topoisomerase II targeting agent, Biochem. Pharmacol. 44 (1992) 2149–2155.

[10] Ł. Kaczmarek, R. Balicki, P. Nantka-Namirski, W. Peczyńska-Czoch, M. Mordarski, Cancerostatics, VI. Synthesis and antineoplastic properties of some benzo-iso-α-carbolines, Arch. Pharm. 321 (1988) 463–467.

[11] A. Jaromin, A. Kozubek, K. Suchoszek-Lukaniuk, M. Malicka-Blaszkiewicz, W. Peczynska-Czoch, L. Kaczmarek, Liposomal formulation of DIMIQ, potential antitumor indolo[2,3-*b*]quinoline agent and its cytotoxicity on hepatoma morris 5123 cells, Drug Deliv. 15 (2008) 49–56.

[12] K. Sidoryk, L. Kaczmarek, W.J. Szczepek, J. Wietrzyk, M. Switalska, W. Peczynska-Czoch, New amino acid derivatives of 6*H*-indolo[2,3-*b*]quinolines, Pol. J. Chem. 82 (2008) 2095–2105.

[13] K. Sidoryk, M. Świtalska, J. Wietrzyk, A. Jaromin, M. Piętka-Ottlik, P. Cmoch, J. Zagrodzka, W. Szczepek, Ł. Kaczmarek, W. Peczyńska-Czoch, Synthesis and biological evaluation of new amino acid and dipeptide derivatives of neocryptolepine as anticancer agents, J. Med. Chem. 55 (2012) 5077–5087.

[14] K. Sidoryk, A. Jaromin, J.A. Edward, M. Świtalska, J. Stefańska, P. Cmoch, J. Zagrodzka, W. Szczepek, W. Peczyńska-Czoch, J. Wietrzyk, A. Kozubek, R. Zarnowski, D.R. Andes, Ł. Kaczmarek, Searching for new derivatives of neocryptolepine: synthesis, antiproliferative, antimicrobial and antifungal activities, Eur. J. Med. Chem. 78 (2014) 304–313.

[15] K. Sidoryk, M. Świtalska, A. Jaromin, P. Cmoch, I. Bujak, M. Kaczmarska, J. Wietrzyk, E.G. Dominguez, R. Żarnowski, D.R. Andes, K. Bańkowski, M. Cybulski, Ł. Kaczmarek, The synthesis of indolo[2,3-*b*]quinoline derivatives with a guanidine group: highly selective cytotoxic agents, Eur. J. Med. Chem. 105 (2015) 208–219.

[16] M.F. Primik, S. Göschl, M.A. Jakupec, A. Roller, B.K. Keppler, V.B. Arion, Structure−activity relationships of highly cytotoxic copper(II) complexes with modified indolo[3,2-*c*]quinoline ligands, Inorg. Chem. 49 (2010) 11084–11095.

[17] L.K. Filak, G. Mühlgassner, M.A. Jakupec, P. Heffeter, W. Berger, V.B. Arion, B. K. Keppler, Organometallic indolo[3,2-*c*]quinolines versus indolo[3,2-*d*] benzazepines: synthesis, structural and spectroscopic characterization, and biological efficacy, J. Biol. Inorg. Chem. 15 (2010) 903–918.

[18] L.K. Filak, G. Mühlgassner, F. Bacher, A. Roller, M.S. Galanski, M.A. Jakupec, B. K. Keppler, V.B. Arion, Ruthenium− and osmium−arene complexes of 2-substituted indolo[3,2-*c*]quinolines: synthesis, structure, spectroscopic properties, and antiproliferative activity, Organomet. 30 (2011) 273–283.

[19] L.K. Filak, S. Göschl, S. Hackl, M.A. Jakupec, V.B. Arion, Ruthenium- and osmium-arene complexes of 8-substituted indolo[3,2-*c*]quinolines: synthesis, X-ray diffraction structures, spectroscopic properties, and antiproliferative activity, Inorg. Chim. Acta. 393 (2012) 252–260.

[20] L.K. Filak, S. Göschl, P. Heffeter, K. Ghannadzadeh Samper, A.E. Egger, M. A. Jakupec, B.K. Keppler, W. Berger, V.B. Arion, Metal–arene complexes with indolo[3,2-*c*]quinolines: effects of ruthenium vs osmium and modifications of the lactam unit on intermolecular interactions, anticancer activity, cell cycle, and cellular accumulation, Organomet. 32 (2013) 903–914.

[21] L.K. Filak, D.S. Kalinowski, T.J. Bauer, D.R. Richardson, V.B. Arion, Effect of the piperazine unit and metal-binding site position on the solubility and anti-proliferative activity of ruthenium(II)- and osmium(II)-arene complexes of isomeric indolo[3,2-*c*]quinoline−piperazine hybrids, Inorg. Chem. 53 (2014) 6934–6943.

[22] S.M. Emam, I.E.T. El Sayed, N. Nassar, Transition metal complexes of neocryptolepine analogues. Part I: synthesis, spectroscopic characterization, and in vitro anticancer activity of copper(II) complexes, Spectrochim. Acta, Part A Mol. Biomol. Spectrosc. 138 (2015) 942–953.

[23] M.F. Primik, S. Göschl, S.M. Meier, N. Eberherr, M.A. Jakupec, É.A. Enyedy, G. Novitchi, V.B. Arion, Dicopper(II) and dizinc(II) complexes with nonsymmetric dinucleating ligands based on indolo[3,2-*c*]quinolines: synthesis, structure, cytotoxicity, and intracellular distribution, Inorg. Chem. 52 (2013) 10137–10146.

[24] C. Santini, M. Pellei, V. Gandin, M. Porchia, F. Tisato, C. Marzano, Advances in copper complexes as anticancer agents, Chem. Rev. 114 (2014) 815–862.

[25] J. Rani, Roy, Recent development of copper(II) complexes of polypyridyl ligands in chemotherapy and photodynamic therapy, ChemMedChem 18 (2023) e202200652.

[26] B. Rogalewicz, A. Czylkowska, Recent advances in the discovery of copper(II) complexes as potential anticancer drugs, Eur. J. Med. Chem. 292 (2025) 117702.

[27] S. Abdolmaleki, A. Aliabadi, S. Khaksar, Unveiling promising anticancer effect of copper-based compounds: a comprehensive review, J. Cancer Res. Clin. Oncol. 150 (2024) 213.

[28] A.C. Hangan, L.S. Oprean, L.M. Procopciuc, L. Dican, S. Gog-Bogdan, R.L. Lucaciu, Copper complexes: main mechanisms as anticancer agents, Molecules 31 (2026) 874.

[29] J. Serment-Guerrero, P. Cano-Sanchez, E. Reyes-Perez, F. Velasquez-Garcia, M. E. Bravo- Gomez, L. Ruiz-Azuara, Genotoxicity of the copper antineoplastic coordination complexes casiopeinas, Toxicol. In Vitro 25 (2011) 1376–1384.

[30] S.G. Davila-Manzanilla, Y. Figueroa-de-Paz, C. Megia, L. Ruiz-Azuara, Synergistic effects between a copper-based metal Cassiopeina III-ia and cisplatin, Eur. J. Med. Chem. 129 (2017) 266–274.

[31] P. Zheng, C. Zhou, L. Lu, B. Liu, Y. Ding, Elesclomol: a copper ionophore targeting mitochondrial metabolism for cancer therapy, J. Exp. Clin. Cancer Res. 41 (2022) 271.

[32] X. Fang, W. Weijun, [^{64}Cu]Cu-ATSM: an emerging theranostic agent for cancer and neuroinflammation, Eur. J. Nucl. Med. Mol. Imag. 49 (2022) 3964–3972.

[33] H. Matsumoto, Y. Yoshii, A. Baden, E. Kaneko, H. Hashimoto, H. Suzuki, K. Kawamura, M.-R. Zhang, T. Higashi, H. Kurihara, Preclinical pharmacokinetic and safety studies of copper-diacetyl-bis(*N*4-methylthiosemicarbazone) (Cu-ATSM): translational studies for internal radiotherapy, Transl. Oncol. 12 (2019) 1206–1212.

[34] E. Grunberg, M.J. Kramer, M. Buck, P.W. Trown, Activity of 10-chloro-5-(2-dimethylaminoethyl)-7*H*-indolo[2,3-*c*]quinolin-6(5*H*)-one hydrochloride against experimental tumors in mice and rats, Chemother 24 (1978) 77–80.

[35] K. Fukushima, M.N. Teller, I.M. Mountain, G.S. Tarnowski, C.C. Stock, Predictive relationship of phagocytic activity to tumor regression in Indoloquinolinone derivative-treated mice, J. Reticuloendothel. Soc. 26 (1979) 187–195.

[36] P. Srihari, B. Padmabhavani, S. Ramesh, Y. Bharath Kumar, A. Singh, R. Ummanni, PMA-SiO_2 catalyzed synthesis of indolo[2,3-*c*]quinolines as potent anti cancer agents, Bioorg. Med. Chem. Lett 25 (2015) 2360–2365.

[37] C. Wittmann, F. Bacher, E.A. Enyedy, O. Dömötör, G. Spengler, C. Madejski, J. Reynisson, V.B. Arion, Highly antiproliferative latonduine and indolo[2,3-*c*] quinoline derivatives: complex formation with copper(II) markedly changes the kinase inhibitory profile, J. Med. Chem. 65 (2022) 2238–2261.

[38] C. Wittmann, I. Besleaga, S. Mahmoudi, O. Palamarciuc, M. Balan-Porcarasu, M. Dascalu, S. Shova, M. Cazacu, M. Kiricsi, N. Igaz, O. Dömötör, E.A. Enyedy, D. Dvoranová, P. Rapta, V.B. Arion, Physical properties and cytotoxicity of Cu(II) and Zn(II) complexes with a TMS-substituted indolo[2,3-*c*]quinoline-derived Schiff base, Dalton Trans. 54 (2025) 7882–7898.

[39] J.B. Petersen, K.H. Lakowitz, New methods for the preparation of 1,4-benzodiazepinones, carbostyrils and indolo(2,3-*c*)quinolones, Acta Chem. Scand. 23 (1969) 971–974.

[40] F. Szabó, J. Daru, D. Simkó, T. Zs Nagy, A. Stirling, Z. Novák, Mild palladium-catalyzed oxidative direct *ortho*-C−H acylation of anilides under aqueous conditions, Adv. Synth. Catal. 355 (2013) 685–691.

[41] J. Han, J.L. Aceña, N. Yasuda, H. Uekusa, T. Ono, V.A. Soloshonok, K.D. Klika, Carbonyl group coordination preferences in square-planar Ni^{II} and Pd^{II} complexes of pentadentate ligands by electron-withdrawing/donating substituents, Inorg. Chim. Acta. 433 (2015) 3–12.

[42] A.W. Addison, T.N. Rao, J. Reedijk, J. van Rijn, G.C. Verschoor, Synthesis, structure, and spectroscopic properties of copper(II) compounds containing nitrogen–sulphur donor ligands; the crystal and molecular structure of aqua[1,7-bis(*N*-methylbenzimidazol-2′-yl)-2,6-dithiaheptane]copper(II) perchlorate, J. Chem. Soc. Dalton Trans. (1984) 1349–1356.

[43] L. Yang, D.R. Powell, R.P. Houser, Structural variation in copper(I) complexes with pyridylmethylamide ligands: structural analysis with a new four-coordinate geometry index, τ_4, Dalton Trans. (9) (2007) 955–964.

[44] A. Okuniewski, D. Rosiak, J. Chojnacki, B. Becker, Coordination polymers and molecular structures among complexes of mercury(II) halides with selected 1-benzoylthioureas, Polyhedron 90 (2015) 47–57.

[45] C. Wittmann, O. Dömötör, I. Kuznetcova, G. Spengler, J. Reynisson, L. Holder, G. J. Miller, E.A. Enyedy, R. Bai, E. Hamel, V.B. Arion, Indolo[2,3-*e*]benzazocines and indolo[2,3-*f*]benzazonines and their copper(II) complexes as microtubule destabilizing agents, Dalton Trans. 52 (2023) 9964–9982.

[46] F. Bacher, C. Wittmann, M. Nové, G. Spengler, M.A. Marć, E.A. Enyedy, D. Darvasiová, P. Rapta, T. Reiner, V.B. Arion, Novel latonduine derived proligands and their copper(II) complexes show cytotoxicity in the nanomolar range in human colon adenocarcinoma cells and *in vitro* cancer selectivity, Dalton Trans. 48 (2019) 10464–10478.

[47] H. Zhang, W.C. Lau, P.F. Hollenberg, Formation of the thiol conjugates and active metabolite by human liver microsomes, Mol. Pharmacol. 82 (2012) 302–309.

[48] D. Voet, J.G. Voet, C. Pratt, Fundamentals of Biochemistry: Life at the Molecular Level, fifth ed., Wiley, 2016.

[49] D. Dvoranová, Z. Barbieriková, V. Brezová, Radical intermediates in photoinduced reactions on TiO_2 (an EPR spin trapping study), Molecules 19 (2014) 17279–17304.

[50] K. Valachová, P. Rapta, N.M.M. Moura, I. Batinic-Haberle, L. Šoltés, Ortho isomeric Mn(III) *N*-alkyl- and alkoxyalkylpyridylporphyrins-enhancers of hyaluronan degradation induced by ascorbate and cupric ions, Int. J. Mol. Sci. 22 (2021) 8608.

[51] S. Tardito, A. Barilli, I. Bassanetti, M. Tegoni, O. Bussolati, R. Franchi-Gazzola, C. Mucchino, L. Marchio, Copper-dependent cytotoxicity of 8-hydroxyquinoline derivatives correlates with their hydrophobicity and does not require caspase activation, J. Med. Chem. 55 (2012) 10448–10459.

[52] F. Bacher, O. Dömötör, A. Chugunova, N. May, L. Filipović, S. Radulović, É. A. Enyedy, V.B. Arion, Strong effect of copper(II) coordination on antiproliferative activity of thiosemicarbazone-piperazine and thiosemicarbazone-morpholine hybrids, Dalton Trans. 44 (2015) 9071–9090.

[53] D.B. Lovejoy, P.J. Jansson, U.T. Brunk, J. Wong, P. Ponka, D.R. Richardson, Antitumor activity of metal-chelating compound Dp44mT is mediated by formation of a redox-active complex that accumulates in lysosomes, Cancer Res. 71 (2011) 5871–5880.
[54] L. Zekany, I. Nagypal, PSEQUAD: a comprehensive program for the evaluation of potentiometric and/or spectrophotometric equilibrium data using analytical derivatives, in: D.J. Leggett (Ed.), Computational Methods for the Determination of Formation Constants, Springer US, Boston, MA, 1985, pp. 291–353.
[55] V.I. Ivanov, L.E. Minchenkova, A.K. Shchelkina, A.I. Poletaev, Different conformations of double-stranded nucleic acid in solution as revealed by circular dichroism, Biopolymers 12 (1973) 89–110.
[56] J. Reynisson, G.B. Schuster, S.B. Howerton, L.D. Williams, R.N. Barnett, C. L. Cleveland, U. Landman, N. Harrit, J.B. Chaires, Intercalation of trioxatriangulenium ion in DNA: binding, electron transfer, X-ray crystallography, and electronic structure, J. Am. Chem. Soc. 125 (2003) 2072–2083.
[57] G. Jones, P. Willett, R.C. Glen, A.R. Leach, R. Taylor, Development and validation of a genetic algorithm for flexible docking, J. Mol. Biol. 267 (1997) 727–748.
[58] M.D. Eldridge, C.W. Murray, T.R. Auton, G.V. Paolini, R.P. Mee, Empirical scoring functions: I. The development of a fast empirical scoring function to estimate the binding affinity of ligands in receptor complexes, J. Comp.-Aid. Mol. Des. 11 (1997) 425–445.
[59] M.L. Verdonk, J.C. Cole, M.J. Hartshorn, C.W. Murray, R.D. Taylor, Improved protein–ligand docking using GOLD, Proteins 52 (2003) 609–623.
[60] O. Korb, T. Stützle, T.E. Exner, Empirical scoring functions for advanced protein−ligand docking with PLANTS, J. Chem. Inf. Model. 49 (2009) 84–96.
[61] W.T.M. Mooij, M.L. Verdonk, General and targeted statistical potentials for protein–ligand interactions, Proteins 61 (2005) 272–287.
[62] Z. Wang, H. Sun, X. Yao, D. Li, L. Xu, Y. Li, S. Tian, T. Hou, Comprehensive evaluation of ten docking programs on a diverse set of protein–ligand complexes: the prediction accuracy of sampling power and scoring power, Phys. Chem. Chem. Phys. 18 (2016) 12964–12975.
[63] C. Bissantz, G. Folkers, D. Rognan, Protein-based virtual screening of chemical databases. 1. Evaluation of different docking/scoring combinations, J. Med. Chem. 43 (2000) 4759–4767.
[64] E. Leung, L.I. Pilkington, M.M. Naiya, D. Barker, A. Zafar, C. Eurtivong, J. Reynisson, The cytotoxic potential of cationic triangulenes against tumour cells, Med. Chem. Commun. 10 (2019) 1881–1891.
[65] Z. Rong, P. Tu, P. Xu, Y. Sun, F. Yu, N. Tu, L. Guo, Y. Yang, The mitochondrial response to DNA damage, Front. Cell Dev. Biol. 9 (2021) 669379.
[66] F.M. Yakes, B. Van Houten, Mitochondrial DNA damage is more extensive and persists longer than nuclear DNA damage in human cells following oxidative stress, Proc. Natl. Acad. Sci. USA 94 (1997) 514–519.
[67] I. Shokolenko, M. Alexeyev, Mitochondrial DNA: consensuses and controversies, DNA (N. Y.) 2 (2022) 131–148.
[68] L. Svihálková-Sindlerová, V. Foltinová, A. Vaculová, V. Horváth, K. Soucek, P. Sova, J. Hofmanová, A. Kozubík, LA-12 overcomes confluence-dependent resistance of HT-29 colon cancer cells to Pt(II) compounds, Anticancer Res. 30 (2010) 1183–1188.
[69] H. Song, H. Kostrhunova, J. Cervinka, J. Macpherson, J. Malina, T. Rajan, R. Phillips, M. Postings, S. Shepherd, X. Zhang, V. Brabec, N.J. Rogers, P. Scott, Dicobalt(II) helices kill colon cancer cells *via* enantiomer-specific mechanisms; DNA damage or microtubule disruption, Chem. Sci. 15 (2024) 11029–11037.
[70] J. Chen, Y. Deng, J. Wang, S. Chen, F. Peng, X. He, M. Liu, H. Luo, J. Zhang, L. Chen, Cyclometalated Ru(II) β-carboline complexes induce cell cycle arrest and apoptosis in human HeLa cervical cancer cells via suppressing ERK and Akt signaling, J. Biol. Inorg. Chem. 26 (2021) 793–808.
[71] B. Méry, J.-B. Guy, A. Vallard, S. Espinol, D. Ardail, C. Rodriguez-Lafrasse, C. Rancoule, N. Magné, In vitro cell death determination for drug discovery: a landscape of real issues, J. Cell Death 10 (2017) 1–8.
[72] https://www.bdbiosciences.com/en-dk/products/reagents/flow-cytometry-reagents/research-reagents/panels-multicolor-cocktails-ruo/fitc-annexin-v-apoptosis-detection-kit-i.556547?tab=product_details.
[73] B. Li, J. Qiu, X. Bai, ROS-mediated apoptosis induction by a cationic pyridoxal benzoylhydrazone copper complex in oral cancer cells, ACS Omega 11 (2026) 11890–11897.
[74] I. Hassan, Khan A. Ali, S. Aman, W. Qamar, H. Ebaid, J. Al-Tamimi, I.M. Alhazza, A.M. Rady, Restrained management of copper level enhances the antineoplastic activity of imatinib in vitro and in vivo, Sci. Rep. 8 (2018) 1682.
[75] L. Zhong, L. Wang, L. Xu, Q. Liu, L. Jiang, Y. Zhi, W. Lu, P. Zhou, The role of NOS-mediated ROS accumulation in an early phase Cu-induced acute cytotoxicity in MCF-7 cells, Biometals 28 (2015) 113–122.
[76] Q. Chen, K. Ma, X. Liu, S.-H. Chen, P. Li, Y. Yu, X. Yu, Truncated PARP1 mediates ADP-ribosylation of RNA polymerase III for apoptosis, Cell Discov. 8 (2022) 3.
[77] L.-J. Mah, A. El-Osta, T.C. Karagiannis, gammaH2AX: a sensitive molecular marker of DNA damage and repair, Leukemia 24 (2010) 679–686.
[78] P. Oberdoerffer, K.M. Miller, Histone H2A variants: diversifying chromatin to ensure genome integrity, Semin. Cell Dev. Biol. 135 (2023) 59–72.
[79] V.-V. Palla, G. Karaolanis, I. Katafigiotis, I. Anastasiou, P. Patapis, D. Dimitroulis, D. Perrea, gamma-H2AX: can it be established as a classical cancer prognostic factor? Tumour Biol 39 (2017) 1010428317695931.
[80] E.P. Rogakou, D.R. Pilch, A.H. Orr, V.S. Ivanova, W.M. Bonner, DNA double-stranded breaks induce histone H2AX phosphorylation on serine 139, J. Biol. Chem. 273 (1998) 5858–5868.
[81] G.M. Sheldrick, Crystal structure refinement with *SHELXL*. Acta Crystallogr. C, Struct. Chem. 71 (2015) 3–8.
[82] M.N. Burnett, C.K. Johnson, ORTEP-III: Oak Ridge Thermal Ellipsoid Plot Program for Crystal Structure Illustrations, ORNL–6895, 369685, 1996.
[83] H.M. Irving, M.G. Miles, L.D. Pettit, A study of some problems in determining the stoicheiometric proton dissociation constants of complexes by potentiometric titrations using a glass electrode, Anal. Chim. Acta 38 (1967) 475–488.
[84] É.A. Enyedy, N.V. Nagy, É. Zsigó, C.R. Kowol, V.B. Arion, B.K. Keppler, T. Kiss, Comparative solution equilibrium study of the interactions of copper(II), iron(II) and zinc(II) with triapine (3-aminopyridine-2-carbaldehyde thiosemicarbazone) and related ligands, Eur. J. Inorg. Chem. (2010) 1717–1728.
[85] O. Dömötör, R.F.M. De Almeida, L. Côrte-Real, C.P. Matos, F. Marques, A. Matos, C. Real, T. Kiss, É.A. Enyedy, M. Helena Garcia, A.I. Tomaz, Studies on the mechanism of action of antitumor bis(aminophenolate) ruthenium(III) complexes, J. Inorg. Biochem. 168 (2017) 27–37.
[86] A. Hocquet, M. Langgård, An evaluation of the MM+ force field, J. Mol. Model. 4 (1998) 94–112.